EXPERIMENTAL STUDY AND COMPUTER

MODELING OF HYDRATION-RELATED BEHAVIOR

OF L-TYROSINE-DERIVED POLYARYLATES

by

LORETO M. VALENZUELA

A Dissertation submitted to the

Graduate School-New Brunswick

Rutgers, the State University of New Jersey

and

The Graduate School of Biomedical Sciences

University of Medicine and Dentistry of New Jersey

in partial fulfillment of the requirements

for the degree of

Doctor of Philosophy

Graduate Program in Biomedical Engineering

written under the direction of:

Dr. Joachim Kohn

and approved by

_____

_____

_____

_____

New Brunswick, New Jersey

May 2009

ABSTRACT OF THE DISSERTATION

Experimental study and computer modeling of hydration-related behavior of L-tyrosine-derived polyarylates

By LORETO M. VALENZUELA

Dissertation Director:

Dr. Joachim Kohn

Water uptake influences many properties of polymers and has been widely studied. In the context of polymeric biomaterials, several recent publications reported an unusual high variability of analytical results of water uptake. In the current investigation, two possible causes for the high variability of water uptake data are studied: (1) variations in the initial molecular weight of the polymer samples and (2) variations in the processing conditions used during sample preparation. Using model polymers from the combinatorial library of L-tyrosine-derived polyarylates, it was shown that the water uptake variability could be reduced significantly by annealing the film specimens after pressing. With the introduction of an annealing step, accurate and reproducible results (relative SD < 11 %) could be obtained using a ^{3}H-radiolabeled water method that

ii

enables parallel measurements required for the efficient screening of multiple polymer samples.

Water uptake from a subset of 23 polymers from this library could not be predicted using a single parameter such as glass transition temperature or hydrophobicity. Thus, a semi-empirical model using artificial neural networks was developed to predict with high accuracy (Pearson coefficient > 0.6) the water uptake, represented by the Weibull equation. Accurate predictions (within experimental error) of water uptake were obtained for 10 of the 18 polymers used in this study, with only one polymer for which predictions were very inaccurate. The model was evaluated in an external polymer set and showed high accuracy. A semi-empirical model was also obtained for degradation kinetic parameters, with accurate predictions (Pearson coefficient $= 0.7$) for the kinetic coefficient of the first order model, suggesting a first order mechanism.

Predictions of water uptake and degradation kinetics were obtained for the rest of the library. These predictions may be used to select a group of polymers that satisfy certain design criteria, and eventually find a lead polymer for a specific medical application. However, modeling does not eliminate the need to run experiments, it only reduces the space of polymers that should be tested to find that lead polymer.

Acknowledgements

Dedication

To my parents Sergio and Margarita, my brothers Sergio and Mauricio, and my grandmother Graciela, and the ones who are not with us anymore, I love you.

Table of Contents

List of Tables

List of Illustrations

List of Abbreviations

3D-MoRSE	3D-MOlecule Representation of Structures based on Electron diffraction descriptors
^3H_2O	Radiolabeled water
ANN	Artificial Neural Network
ANOVA	Analysis of variance
CCM	Combinatorial-Computational Method
CFS	Correlation based feature selection
Cp	Heat capacity
DP	Degree of polymerization
DSC	Differential scanning calorimetry
DTR	Desaminotyrosyl tyrosine alkyl ester: R = methyl (M), ethyl (E), iso-propyl (iP), butyl (B), iso-butyl (iB), sec-butyl (sB), hexyl (H), octyl (O), dodecyl (D), benzyl (Bn), 2-(2-ethoxyethoxy)ethyl (G)
E	Expectation step of the expectation-maximization cluster analysis
EM	Expectation-maximization cluster analysis
GETAWAY	GEometry, Topology and Atom-Weights AssemblY descriptors
GPC	Gel permeation chromatography
HPC	Hydroxypropyl cellulose
HPLC	High performance liquid chromatography
HPMC	Hydroxypropyl methylcellulose
HTR	Hydroxyacetic acid-tyrosine alkyl ester: R = ethyl (E), hexyl (H), octyl (O)
LSC	Liquid scintillation cocktail
M	Maximization step of the expectation-maximization cluster analysis

Mn	Number average molecular weight
MOE	Molecular Operating Environment
MPD-I	Poly(m-phenylenediamineisophthyl)amide
Mw	Molecular weight
PBS	Phosphate buffer saline
PCL	Poly(ε-caprolactone)
PEG	Poly(ethylene glycol)
PEOE	Partial Equalization of Orbital Electronegativities method
PGA	Poly(glycolic acid)
PLA	Poly(lactic acid)
PLGA	Poly(lactic-co-glycolic acid)
PTMC	Poly(1,3-trimethylene carbonate)
PVA	Poly(vinlyl acetate)
PVP	Polyvinylpyrrolidone
QSPR	Quantitative Structure-Property Relationships
SD	Standard deviation
rms	Root mean squared error
rsd	Relative standard deviation
Tg	Glass transition temperature
TGA	Thermogravimetrical analysis
THF	Tetrahydroduran
WEKA	Waikato Environment for Knowledge Analysis
WHIM	Weighted Holistic Invariant Molecular descriptors

Nomenclature

A	Constant of the Berens -Hopfengerg equation
b	Shape parameter on the Weibull equation
b_k	Bias function of a neuron (k) on an Artificial Neural Network
C	Concentration
C_j	Cluster j on a Cluster analysis
c_j	Class j on a Decision Tree
d	Distance of a sample from the center of the film
D	Diffusion coefficient
De	Deborah number
$freq(c_js)$	Frequency of class c_j in a node at the attribute s, on a Decision Tree
$gain$	Information gain function on a Decision Tree
$info$	Information function on a Decision Tree
$\overline{info}$	Information average over all attributes on a Decision Tree
k	Kinetic parameter of the power law equation
k_0	Kinetic parameter of degradation of zero order
k_1	Kinetic parameter of degradation of first order
k_2	Kinetic parameter of degradation of second order
k_{BH}	Kinetic parameter of the Berens -Hopfengerg equation
k_D	Kinetic parameter associated with diffusion
k_{eq}	Kinetic parameter associated with the equilibration water uptake
k_I	Kinetic parameter associated with a specific interaction
k_{P1} , k_{P2}	Kinetic parameters of the Peleg equation
k_R	Kinetic parameter associated with relaxation

L	Thickness of a film
m	Exponent of diffusion-relaxation equation
$M_{^3H_2O}$	Mass of radiolabeled water on a sample
M_{dry}	Dry mass of a sample
M_{loss}	Change in mass of a sample the TGA
M_{sample}	Mass of a sample
n	Exponent parameter of the power law equation
p_j	Proportion of a certain instance in cluster j,
$P_R[x_i|C_j]$	Probability of cluster j on a Cluster analysis
r	Pearson correlation coefficient
R^2	Squared correlation coefficient
S	Sample
s	Attribute on a Decision Tree
s_X	Standard deviation of experimental values of a certain parameter over all polymers
s_Y	Standard deviation of predicted values of a certain parameter over all polymers
t	Time
t_{scale}	Time scale of the release or uptake process on the Weibull equation
w_{kj}	Weight for each neuron (k) and each synapse (j) on an Artificial Neural Network
WU	Water uptake
WU_0	Initial water content

WU_{eq}	Equilibrium water uptake
x	Distance
x_j	Input signals of a synapse (j) on an Artificial Neural Network
X_i	Experimental value of a certain parameter for polymer i
$\overline{X}$	Average of experimental values of a certain parameter over all polymers
y_k	Output of a node (k) on an Artificial Neural Network
Y_i	Predicted value of a certain parameter for polymer i
$\overline{Y}$	Average of predicted values of a certain parameter over all polymers
α	Probability that a water molecule become mobile at a given time and place on the Langmuir equation
γ	Probability that a water molecule become linked or trapped in the polymer at a given time and place on the Langmuir equation
φ	Activation function on an Artificial Neural Network
λ	Characteristic stress-relaxation time of a polymer/solvent system
θ	Characteristic diffusion time of a solvent

1   Opening

1.1   Scope

A library of L-tyrosine-derived polyarylates has been studied for water uptake and degradation. Previous studies have shown very high variability in the water uptake of certain polymers. A reproducible, fast and parallel method to measure water uptake was developed using radiolabeled water. A semi-empirical approach was used to model and predict the water uptake for a subset of the library, using only 18 polymers to train the model.

1.2   Hypotheses

Water uptake for a library of polymers can be accurately modeled using only a small subset of experimental data (the "training set") and molecular descriptors for all the polymers in the library. Accurate predictions for the rest of the library can be obtained using this model.

1.3   Goals of the dissertation

I. To validate an appropriate method to measure water uptake for a large number of samples in parallel.

II. To develop a method to produce films for which water uptake is homogeneous throughout each film.

III. To select a subset of polymers from the L-tyrosine-derived polyarylates in which water uptake and degradation can be measured, as a representative sample of the entire library.

IV. To measure water uptake and degradation of the selected subset of polymers, using the aforementioned methods.

V. To extract kinetic parameters from the obtained water uptake and degradation data.

VI. To build semi-empirical models for the water uptake of the subset of polymers for which water uptake and degradation was measured.

VII. To predict water uptake and degradation for the rest of the polymer library.

1.4   *Thesis overview*

Chapter 2 presents the introduction and background regarding the L-tyrosine-derived polyarylate library; water uptake, degradation and erosion processes; and semi-empirical modeling used in polymer sets and libraries.

Chapter 3 presents the experimental water uptake studies. The effects of quenching and annealing after compression molding, and the effect of initial molecular weight on the water uptake are evaluated. After validating a method to measure water uptake that uses radiolabeled water, it was used to measure water uptake for a subset 24 polymers from the library (subset selection is further discussed in Chapter 5).

Chapter 4 presents a kinetic analysis of the previously obtained water uptake measurements. Fick's diffusion, power law, Weibull and Peleg equations were used to model the water uptake behavior.

Chapter 5 presents the application of the Combinatorial-Computational Method, developed by Kohn et al. in the New Jersey Center for Biomaterials [1], to select the subset of polymers for which water uptake was measured. In three iterations, starting from six polymers selected randomly, 23 polymers were selected.

Chapter 6 presents the semi-empirical model for water uptake of the L-tyrosine-derived polyarylate library, using a small number of descriptors from an initial large set of descriptors developed previously in the New Jersey Center for Biomaterials. Descriptors were selected using a cluster analysis, decision tree analysis and linear regression, while the model was built using artificial neural networks. Predictions were built for the rest of the polymer library.

Chapter 7 presents the experimental and computational study of polymer degradation of the library of L-tyrosine-derived polyarylates. Degradation was measured by means of molecular weight reduction in a one-year study. Different kinetic equations (zero, first, and second order) were applied to the degradation data. A semi-empirical model was built for kinetic parameters of degradation. Predictions were built for the rest of the polymer library.

Chapter 8 presents the conclusions and future directions of this study.

2   Introduction and Background

For short-term applications, non-degradable implantable biomaterials may need to be removed surgically after they accomplish their objective. Alternatively, degradable biomaterials do not need to be removed, since they will eventually disappear. During this process, the implanted polymeric device undergoes water uptake, degradation, and erosion (Figure 2-1). Water uptake is an important parameter in the characterization of biodegradable polymers [2, 3]. It affects degradation, swelling and changes in mechanical properties [4, 5], as well as the biological response [6] and drug release behavior [7, 8].
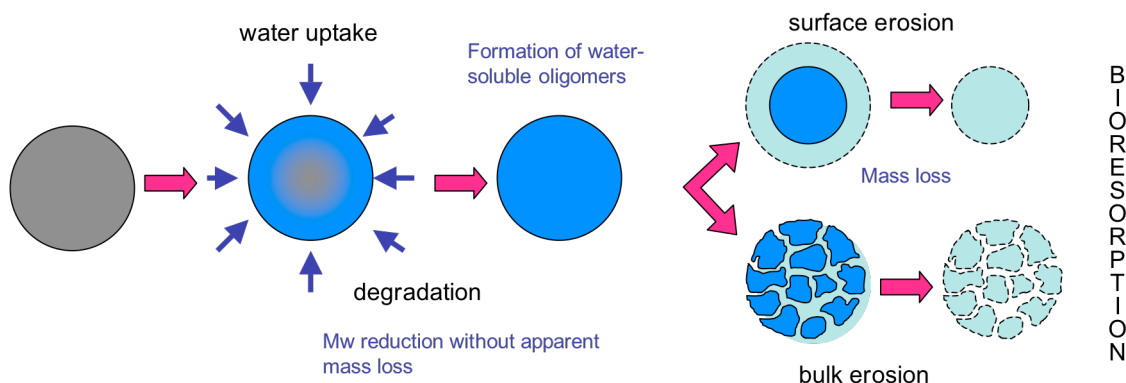
Figure 2-1: Schematic representation of the process of bioresorption.

Previously, the L-tyrosine-derived polyarylate library (Figure 2-2) was synthesized and characterized by Kohn and coworkers [9-11]. Hooper et al. [12] showed that bone pins made from tyrosine-derived polyarylates are resorbed in vivo without a significant inflammatory response. Currently, a tyrosine-derived polyarylate is used in a FDA approved device for hernia repair [13].
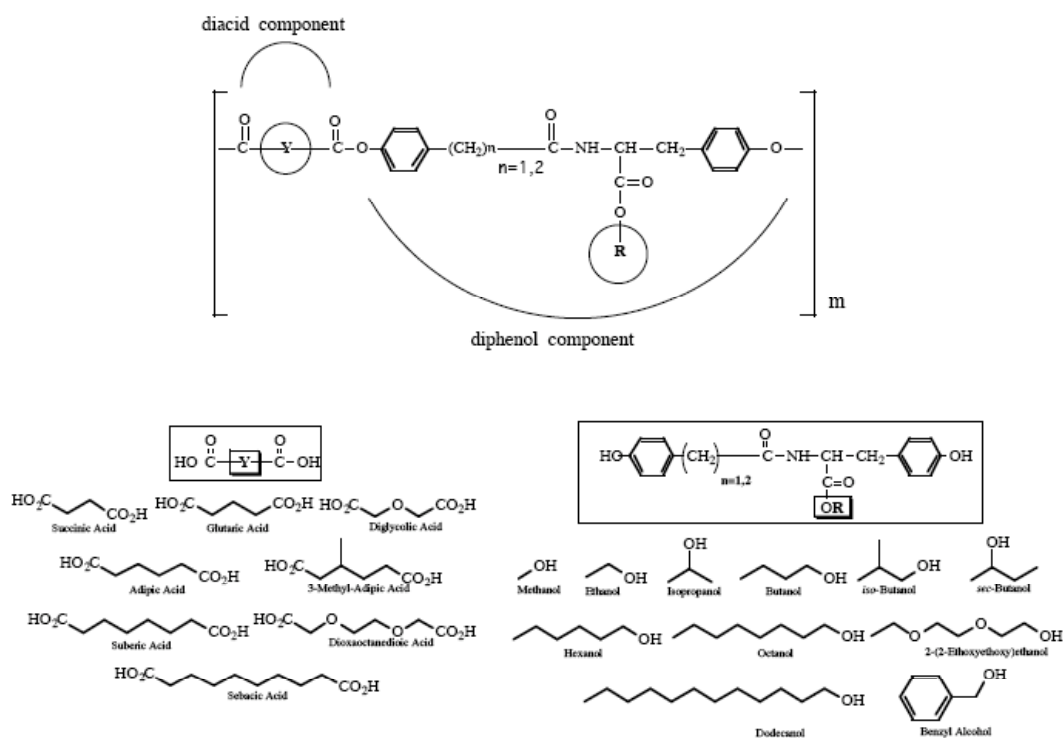
Figure 2-2: General structure of L-tyrosine-derived polyarylates. Symbol Y stands for 8 diacids (shown on the left side) and symbol R stands for 14 tyrosine-derived diphenols (shown on the right side).

2.1 Degradation and erosion

Degradation is the chemical transformation of a high molecular weight (Mw) polymer into lower Mw polymers and oligomers. This process involves the cleavage of chemical bonds and can be driven by hydrolysis, enzymes, radiation, or temperature. Degradation is influenced by many materials/device properties such as (i) ability of water to penetrate the matrix, (ii) distribution of hydrophilic and hydrophobic chemical groups along the backbone chain, (iii) degree of swelling, (iv) rigidity of the backbone chain, (v) solubility of oligomers determined by pH, ionic strength, temperature and buffering capacity, and (vi) device geometry in terms of size and shape.

No comprehensive degradation study has been conducted for the L-tyrosine-derived polyarylates. However, Tangpasuthadol et al. [14, 15] studied and modeled

degradation for a similar polymer library, the L-tyrosine-derived polycarbonates (Figure 2-3). Polycarbonates have three potentially hydrolyzable bonds (i.e., amide, carbonate, and ester), from which the backbone carbonate bond is randomly hydrolyzed at a faster rate than the pendent chain ester bond, thereby reducing the Mw, while the amide bond is stable to hydrolysis in an aqueous buffer solution without enzymes.

R = alkyl group; -(CH$_2$)$_n$CH$_3$
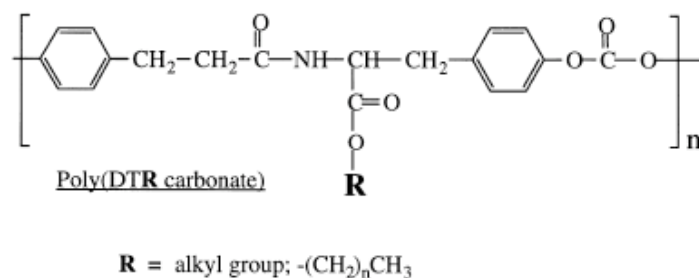
Figure 2-3: General chemical structure of tyrosine-derived polycarbonates [14].

From the polyarylate library, poly(DTE adipate) has higher *in vivo* degradation than the equivalent polycarbonate (i.e., poly(DTE carbonate)). Both polymers show random hydrolytic chain cleavage and a very small amount of acidic degradation products [12], in contrast with other polymers like poly(lactic acid) (PLA) (Figure 2-4) that releases carboxylic end groups, provoking autocatalysis of other bonds and acidic degradation by-product generation [16].
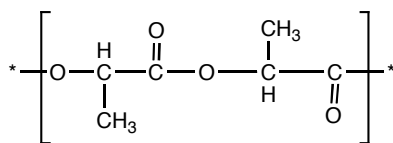
Figure 2-4: Chemical structure of poly(lactic acid) (PLA).

Finally, oligomers are released depending on their solubility in the media, and this process drives erosion, which correspond to the mass loss of the polymer. The erosion is

determined by both water diffusion and degradation rates. When water diffusion into the water-insoluble bulk polymer occurs faster than degradation, the matrix undergoes bulk erosion. However, if water diffusion is slower than degradation, the polymer matrix undergoes surface erosion. Erosion also depends on environmental conditions, such as temperature and pH, as well as matrix dimension and geometry [17].

2.2 Water uptake

Water uptake is the first event after device implantation. It depends on polymer chemistry and structure (e.g., Mw, macromolecular structure, and rigidity), matrix size and geometry (e.g., surface area over volume ratio and porosity), swelling of the matrix, environmental conditions (e.g., ions, pH, and temperature), processing induced properties (e.g., residual stresses), and the presence of other molecules besides the polymer (e.g., water, drugs and additives).

In previous studies, Small et al. [18] observed a variability up to 100% in the water uptake of polyacid-modified composite resins, Jeong et al. [19] observed over 80% of variability in the water uptake of poly(D,L-lactic-co-glycolic acid)/poly(ethylene glycol) (PLGA/PEG) di-block polymer blend films, Bajpai et al. [20] observed water uptake variability over 30% for calcium alginate/chitosan bi-polymeric beads, and Lyu et al. [21] observed very high variability in the water uptake of PLA. In our laboratory, we observed that some tyrosine-derived polyarylates exhibited highly reproducible water uptake profiles, while others showed great variability, despite the fact that analyses were performed by the same operator using identical methods. The published reports as well as our own experience convinced us that the occasionally observed high variability of water uptake is poorly understood. Given the importance of water uptake studies and the

frequency by which such studies are performed in many different laboratories, this phenomenon warrants further investigation and an explanation.

Water uptake by a polymer matrix is affected by the polymer's free volume, which depends on the density, the physical state, and the glass transition temperature (Tg) of the polymer [14]. Akbari et al. [22] showed that those parameters also depend on the fabrication technique. In polyanhydride matrices, they showed that solvent-cast devices present a less packed morphology associated with higher initial water uptake, in comparison with compression-molded devices that have a more densely packed morphology associated with lower water uptake.

It was further shown that water uptake is influenced by polymer mobility and relaxation [23, 24]. It seems, therefore, reasonable to assume that the degree of physical ageing experienced by the test specimen, as well as its thermal history, especially the degree to which the test specimen was either quenched or annealed, are additional fabrication-dependent parameters that may contribute to variability during water uptake studies. Again, the published data are inconsistent: while Akele et al. [25] have shown that physical ageing does not affect the water diffusion behavior into polycarbonate films, Surana et al. [26] have shown that physical aging decreases the rate and extent of water uptake by trehalose samples, and Loo et al. [27] observed that long annealing periods increase the water uptake of PLGA films. Likewise, the effect of the Mw of the polymer specimens used for water uptake studies is not fully understood. The few published studies examining the effect of polymer Mw on water uptake indicate that that the effect of variations in the Mw of test specimens is unpredictable, i.e., reducing the Mw of the test polymer can result in either higher [28, 29] or lower water uptake [30, 31].

In the past, only a limited number of experimental methods were used to measure water uptake, the most common being gravimetric analysis [32] and thermogravimetrical analysis (TGA). In addition, the use of ^{3}H-radiolabeled water ([3]H$_2$O) had been explored for both polymers [18, 33] and other materials such as concrete and proton exchange membranes [34, 35]. After incubation, the radioactivity in the sample is a measure of the sample's degree of hydration. This method is particularly suitable for measuring very small amounts of water uptake. Radioactive water has also been used to determine the transport of vapor water through polymer films [36]. The method is generally described as simple, fast and sensitive.

2.3 *L-tyrosine-derived polyarylate library*

The library of L-tyrosine-derived polyarylates consists of A-B-type copolymers having an alternating sequence of a diphenol and a diacid (Figure 2-2) [37]. This library was obtained by copolymerizing 14 tyrosine-derived diphenols with 8 aliphatic diacids in all possible combinations resulting in 112 distinct polymers. Changes in polymer backbone or pendent chain lengths affect polymer properties such as Tg and surface hydrophobicity [37].

2.4 *Hydration studies on the L-tyrosine-derived polyarylate library*

Suarez et al. [38, 39] studied the hydration of a series of polymers from this library by means of measuring thermally stimulated depolarization currents, showing that water is tightly bound to the amide carbonyl group and loosely bound to the ester carbonyl group in the pendent chain of the diphenol moiety. Also, they observed that polymer packing was affected by hydration, being more dense in more hydrated stages.

Water fills in polymer free volume and probably disrupts the interchain amide-hydrogen bond networks, enhancing polymer packing.

2.5 *Quantitative Structure-Property Relationships*

Quantitative Structure-Property Relationships (QSPR) are surrogate models that use multivalent statistical correlations that quantify the relationship between structural parameters (descriptors) and target properties, allowing the identification of the most important molecular descriptors that explain the variability of the experimental data, as well as build predictions over instances (polymers) that were not used in train the model. The predictions obtained from those methods are useful to find trends and relative order of the target property among the polymer set, and thus, QSPR models allow narrowing the search space for a desired value of the target property within the polymer family of study. Experimental measurements must be always generated to validate those predictions.

2.5.1 *Measurement of model accuracy*

Two typically used parameters to evaluate model accuracy are the correlation coefficient and the Pearson coefficient. The squared correlation coefficient (R^2) is defined by

$$R^2 = \frac{\left[n\sum_{i=1}^{n}(X_i Y_i) - \sum_{i=1}^{n}X_i \sum_{i=1}^{n}Y_i \right]^2}{\left[n\sum_{i=1}^{n}(X_i^2) - \left(\sum_{i=1}^{n}X_i\right)^2 \right]\left[n\sum_{i=1}^{n}(Y_i^2) - \left(\sum_{i=1}^{n}Y_i\right)^2 \right]}, \qquad (\,2\text{-}1\,)$$

where X_i is the experimental value of the parameter for each polymer ($i = 1,...,n$) and Y_i is the predicted value of the parameter for each polymer ($i = 1,...,n$). The Pearson coefficient (r) is defined by

$$r = \frac{1}{n-1}\sum_{i=1}^{n}\left(\frac{X_i - \overline{X}}{s_X}\right)\left(\frac{Y_i - \overline{Y}}{s_Y}\right)$$

(2-2)

where $\overline{X}$ and s_X are the average and standard deviation of the experiment values over all polymers, respectively, while $\overline{Y}$ and s_Y are the average and standard deviation of the predicted values over all polymers, respectively.

2.5.2   Linear regression

A linear regression is used to linearly correlate one or more independent variables (inputs) with one dependent variable (output) using a least square function. It is one of the simplest methods to build a surrogate model but it does not allow non-linear interaction of variables.

2.5.3   Artificial neural networks

An Artificial Neural Network (ANN) is an information processing system that is inspired by the way the brain processes information [40, 41]. One commonly used ANN is the Multi-Layer Perceptron that consists of a set of source nodes (neurons) as an input layer, a set of computational nodes combined into one (hidden) layer, and a set of nodes as an output layer (Figure 2-5). The input nodes pass values to the first hidden layer, its nodes to the second and so until producing outputs.

k hidden neurons

Descriptor 1 →

Descriptor 2 →

⋮

Descriptor j →

one output neuron

Output

neuron

input

j descriptors

w_{kj} adaptive weights

w_k adaptive weights
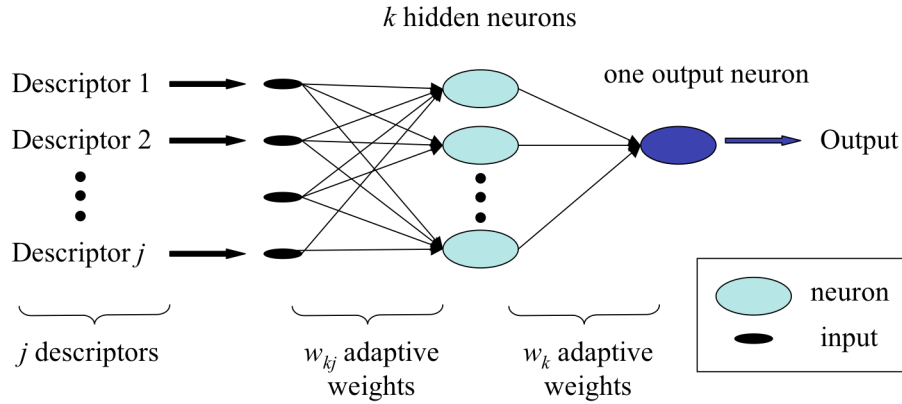
Figure 2-5: Scheme of an Artificial Neural Network (ANN).

The three basic elements of the neural network are: a set of synapses or connecting links, represented as a weight w_{kj} for each neuron (k) and each synapse (j); an adder that sums the input signals (x_j) weighted by the respective synapses linear combiner; and an activation function (φ), that limits the amplitude of the output (y_k):

$$y_k = \varphi \left(\sum_j w_{kj} x_j + b_k \right),$$ (2-3)

where b_k is the bias function of each neuron, used as a threshold to activate or not each node of the network. The activation function can be linear or non-linear, allowing nonlinear function mappings.

This ANN configuration is called feed-forward due to the evolving feature of the network, where the input signals propagate through the neural network in a forward direction on a layer-by-layer basis. Two types of signals pass through the network: function signals and error signals. Function signals are input signals that come in at the input end and propagate forward to the output. Error signals are originated at the output neuron and propagate backward.

2.5.4 Descriptors

Descriptors are required to build QSPR models. They can range from experimental to calculated measurements. Experimental measurements have the advantage that they relate directly to polymer properties, but they must be generated for all polymers for which predictions are expected. Calculated descriptors are often less representative of the actual polymer; for example, sometimes they only consider the monomer or a small oligomer structure, and not the complete polymer structure. However, calculated descriptors allow generating predictions for polymers that may not be synthesized yet.

Calculated descriptors can be as simple as the number of hydrogen atoms in the monomer and as complicated as 3D structures obtained from the trajectories during molecular dynamics simulations. Any descriptor must meet the following requirements: (i) independent of the number of atoms, (ii) unique regarding the 3D arrangement of atoms, and (iii) invariant against translation and rotation of the entire molecule [42].

For hydration studies, the following parameters have been commonly used: (1) radial distribution functions (RDFs), (2) self diffusion coefficients calculated from mean square displacements [43, 44], (3) coordination number calculated from the area under RDFs [44], (4) 3D atomic density maps known as spatial distribution functions [45], (5) angular distribution functions [46], (6) RDF over volume available for solvent [46], (7) dynamic water motions [44], and (8) chain flexibility parameters [46].

2.5.5 Decision tree analysis

Decision tree analysis [47, 48] is typically used to evaluate the significance of each descriptor with respect to the set of experimental data. Decision tree analysis is a

"divide and conquer approach" (Figure 2-6). An attribute (descriptor) is placed at the root

node and a branch is made for each possible value or class. If all instances (polymers) at a

node have the same classification, it stops developing that part of the tree.
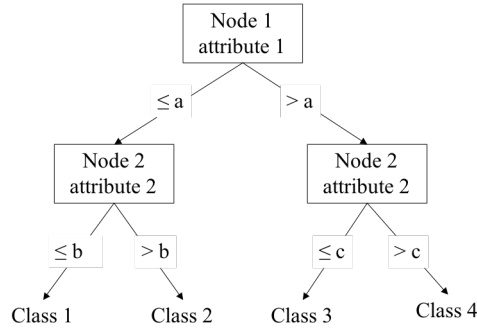
Figure 2-6: Scheme of a decision tree.

The algorithm of this decision tree is based on the information gain, defined as the

amount of information that would be needed to specify whether a new instance should be

classified in this node or not. The information is defined as

$$info(s) = -\sum_{j=1}^{k} \frac{freq(c_j s)}{|s|} \cdot \ln\left(\frac{freq(c_j s)}{|s|}\right), \qquad (2\text{-}4)$$

where *freq(c$_j$s)* is the proportion of instances of type *j* in the node at the attribute *s*. The

information gain of each attribute is calculated as

$$gain(attribute) = info(attribute) - \overline{info(attributes)}, \qquad (2\text{-}5)$$

where $\overline{info(attributes)}$ is the average information of all attributes.

The attribute that has the highest gain is selected at the root of the tree. Then, this

calculation is repeated recursively for each new node, until all instances have the same

classification or the data cannot be split any further. When the attributes are numerical,

numeric thresholds are placed halfway between the values that delimit the boundaries of each split.

2.5.6 Surrogate modeling for polymers

Several groups have used surrogate modeling on polymers. In general, those studies show that the larger the training set, the more accurate the model. The number of descriptors used in the model ranges from 2 to 11 descriptors from either experimental or calculated measurements. Gao et al. suggested that the number of descriptors should be less than 20% of the number of samples used in the training set [49]. In general, ANN models give more accurate predictions than linear models [50-55].

Models built with experimental descriptors have been developed for compressive strength [51], wear properties [56], and drug release [57]. Those models present very high accuracy (R^2 over 0.9) respect to a set of polymers that were not used in training the model (the "test set").

In general, models built with calculated descriptors present lower accuracy than those built with experimental descriptors. A large number of groups have studied Tg [50, 52, 53, 58-79], with correlation coefficients over 0.80 for training sets, and between 0.71 and 0.96 for test sets.

Other surrogate models for polymers include properties like density [52, 69], refraction indices [49, 52, 53, 55, 63, 80-83], lower critical solution temperature [84-86], intrinsic viscosity [54, 87, 88], gaseous diffusion [89, 90], imprinting factor [91, 92], contact angle [61], specific heat capacity [69], cohesive energy [69, 93], molar volume [53, 69], solubility [94, 95], dielectric constant [75], thermal decomposition [96], and molar stiffness [97]. They include linear and nonlinear models, with model accuracies

that depend on the polymer system, size of set, type and number of descriptors, and property. Reported correlation coefficient for test sets were over 0.7 with the exception of refraction index (R^2=0.38) [55] and imprinting factor (R^2=0.15) [91]. Biological response has been modeled by Kohn et al. for the libraries of L-tyrosine-derived polyarylates [98-103] and polymethacrylates [104], with Pearson correlation coefficient over 0.54 and R^2 over 0.78, respectively.

Ebube et al. [105] built an ANN model for water uptake by polymer blends of hydroxypropyl methylcellulose (HPMC), hydroxypropyl cellulose (HPC), polyvinylpyrrolidone (PVP), sodium alginate and carregeenan, using the composition of the blend as descriptor. Using 15 polymer blends as training set, they were able to predict within 8% of the value the water uptake of 9 polymer blends. They also were able to predict within less than 7% error, the wet Tg of the same polymer blends.

2.5.7 Surrogate modeling for the L-tyrosine-derived polyarylate library

Kohn et al. have built successful predictions of protein adsorption and cell response for the combinatorial library of L-tyrosine-derived polyarylates [98-103]. The authors developed surrogate models using two-dimensional molecular descriptors (i.e., independent on the polymer conformation) obtained from simple drawn polymer structures. With these models, they were able to correctly predict 38 of the 45 polymers for fibrinogen adsorption and and 41 of 48 polymers for rat lung fibroblast proliferation, with Pearson coefficient values of 0.54 ± 0.12 and 0.54 ± 0.09, respectively [100, 103]

Recently, Gubskaya et al. [106] calculated descriptors from relaxed three-dimensional polymeric structures obtained from MD simulations of tetramers in vacuum and implicit water. In this work, decision tree analysis and ANNs were used to predict

fibrinogen adsorption with a Pearson coefficient of 0.67 ± 0.13. The incorporation of three-dimensional descriptors leads to certain improvement in comparison with previous surrogate models.

Finally, Kholodovych et al. [107] predicted water uptake for the same polymer library using preliminary experimental data and QSPR modeling. They used water uptake measurements at room temperature after 20 days, for 13 polymers, with a correlation coefficient of 0.87 for the full training set.

3   Water Uptake studies

As fully discussed in Section 2.2, previous studies have shown high variability in the measurements of water uptake [18-21]. In this chapter, we evaluate the effects of film quenching or annealing after compression molding, and the effect of the initial molecular weight (Mw) of the test specimen on its water uptake behavior, for selected polymers from the L-tyrosine-derived polyarylate library. Water uptake was measured using ^{3}H-radiolabeled water (^{3}H$_2$O) for a subset of this library to explore the structure-property relationships of a combinatorial library of polymers respect to the water uptake behavior.

3.1   *Materials and methods*

3.1.1   *Materials*

L-tyrosine-derived polyarylates were synthesized as described previously by carbodiimide-mediated solution polycondensation of a diphenol and a diacid at room temperature [11]. Poly(D,L lactic acid) (PLA), 100 kDa, 0.84 dL/g, was obtained from Absorbable Polymer Technologies.

3.1.2   *General methods*

The following methods were used throughout:

3.1.2.1   Film processing

Polymer films of ~200 μm thickness were compression molded using a Carver Press (Fred S. Carver Inc.). Each sample was equilibrated for 5 minutes prior to pressing at 50-70 °C above the polymer's glass transition temperature (Tg). Pressure was then

ramped from 0 to 15 kpsi over 1.5 min, held at that pressure for 1 min, and ramped to ambient pressure in 1 min.

3.1.2.2   Molecular weight measurements

Mw was measured by a gel permeation chromatography (GPC) system consisting of two PL-gel columns (10^5 - 10^3 Å pore size and 30 cm in length, Polymer Laboratories LTD) connected to a Waters 717 autosampler and a Waters 2489 detector (Waters Corp., MA). The mobile phase was tetrahydroduran (THF) at a flow rate of 1 mL/min. The Mw was calculated relative to a set of commercially available monodispersed polystyrene standards (Waters Corp., MA). The degree of polymerization (DP) was calculated by dividing the number average molecular weight (Mn) by the molecular mass of one repeating unit of each polymer.

3.1.2.3   Glass transition temperature measurements

The Tg was determined by differential scanning calorimeter (DSC 910, TA Instruments, Inc). The temperature profile was: ramp from -55 ºC to 150 ºC at 10 ºC/min, isothermal for 2 min at 150 ºC, ramp from 150 ºC to -55 ºC at 10 ºC/min, isothermal for 1 min at -55 ºC, and -55 ºC to 150 ºC at 10 ºC/min. The wet and dry Tg's were determined from the first and second heating scan, respectively, by the half Cp extrapolated tangent method.

3.1.2.4   Water uptake by thermogravimetrical analysis

Samples of 1 cm in diameter were incubated in separated vials with 7 mL of water and stored at 37 ºC. After 1, 2, 3, and 4 weeks of incubation, the respective samples were removed from the vials, blotted dry, cut to squares of ~5 mm × 5mm, and placed into the

thermogravimetric analyzer (TGA 2950, TA Instruments). The samples were equilibrated at 30 degrees and then ramped to 200°C at a rate of 7 °C/min. Measurements were taken in triplicate (3 samples, each from a different film) at each time point.

Water content was measured using the following equation:

$$WU(\%) = 100 \cdot \frac{M_{loss}}{M_{dry}} - WU_0 ,$$

(3-1)

where M_{loss} is the mass loss of the sample between 30 and 180°C, M_{dry} is the (steady state) mass measured by the TGA at >180°C, and WU_0 is the water content at time zero, measured by TGA for a sample of each film before incubation in water.

3.1.2.5 Water uptake by ^{3}H-radiolabeled water (^{3}H$_2$O)

^{3}H-radiolabeled water (Sigma-Aldrich) with an activity of 1 mCi/mL was diluted with HPLC grade non-radiolabeled ("cold") water to a concentration of 0.2 µCi/mL. Samples 1 cm in diameter were incubated in separated vials with 7 mL of ^{3}H$_2$O (0.2 µCi/mL) and then stored at 37 ºC. After the same incubation times, the respective sample was removed from the vial, rinsed with distilled water, blotted dry and dissolved with 3 mL of THF (VWR) and 12 mL of liquid scintillation cocktail (LSC) (Ecolite). A control curve was constructed with 0, 0.5, 1, 2, 4, and 8 µL of 0.2 µCi/mL ^{3}H$_2$O (in triplicate), 3 mL of THF and 12 mL of LSC. Radioactive counts were measured using a scintillation counter (Beckmann 6500), and water content ($M_{^3H_2O}$) was calculated using the calibration curve. Water uptake (*WU*) was calculated as the water content relative to the original dry weight (M_{sample}):

$$WU(\%) = 100 \cdot \frac{M_{^3H_2O}}{M_{sample}}.$$

(3-2)

3.1.3   Experiments

3.1.3.1   Water uptake method validation

PLA (100 kDa) films were used as control samples to validate and compare the two methods for water uptake, TGA (n=4) and ^3H_2O (n=10). An ANOVA statistical test was used to compare the uptake values obtained from the two methods, while the relative standard deviation (rsd) was used to evaluate their reproducibility.

3.1.3.2   Effect of annealing and quenching on water uptake

Poly(DTB succinate) (145 ± 11 kDa), poly(DTE adipate) (127 ± 7 kDa), poly(DTE glutarate) (80 ± 1 kDa) and PLA (100 kDa) films were used for the study of sample preparation protocols. Films were pressed as described above and were then either quenched by fast cooling or annealed at 5 - 10 ºC above Tg for at least 20 h. Water uptake was measured using ^3H_2O, after 3 or 5 days of incubation in ^3H_2O at 37 ºC. A minimum of 5 samples were taken from different areas of the film. Plots of measured water uptake versus distance along the film were used to evaluate film heterogeneity (Figure 3-1), and the rsd of the average of all measurements on each film provided a further (quantitative) indication of the effect of sample preparation.
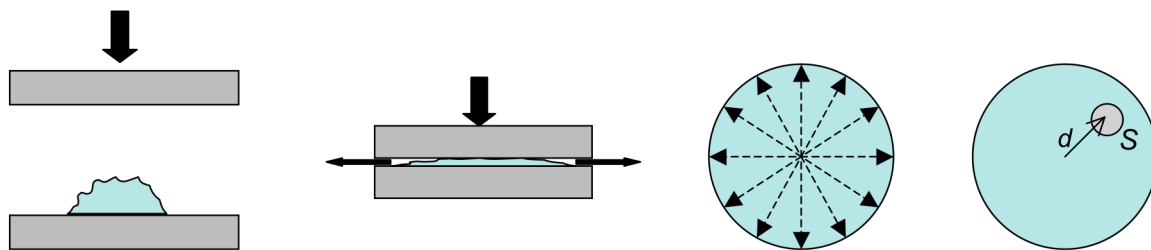
Figure 3-1: Scheme of the pressing and sampling procedure. *d* is the distance of sample *S* from the center of the film.

3.1.3.3   Effect of initial Mw on water uptake

The effect of initial Mw was studied by measuring the water uptake profiles of two poly(DTiP adipate) films, with Mw's of 144 ± 2 kDa (DP = 193 ± 5) and 40 ± 1 kDa (DP = 52 ±5), respectively.   Three films of each polymer were pressed and annealed above Tg for 20 h. Water uptake was measured using ^3H_2O, after 6 h, 12 h, and 1, 2, 3, 4, 7, 14, 21, and 28 days of incubation in ^3H_2O at 37 ºC.

3.1.3.4   Water uptake measurements

Water uptake was measured for a subset of 24 polymers of the library of L-tyrosine-derived polyarylates (Table 3-1). Three films of each polymer were pressed using the previously described protocol and annealed for at least 20 h at 5 to 10 ºC above their Tg. Following the ^3H_2O method described before, water uptake was measured for 6 h, 12 h, and 1, 2, 3, 4, 7, 14, 21, and 28 days after incubation. Wet Tg was measured for the same times by DSC, as described above.

Table 3-1: L-tyrosine-derived polyarylates used in this study.

Polymer	Tg (ºC)[1]	Mw (kDa)[2,3]	DP[4]
poly(DTO sebacate)	16	123 ± 1	87 ± 7
poly(HTH sebacate)	23	64 ± 5	65 ± 5
poly(DTH suberate)	24	106 ± 2	85 ± 1
poly(DTO adipate)	26	132 ± 2	111 ± 3
poly(DTH adipate)	34	98 ± 1	102 ± 1
poly(DTB (R)(+) methyladipate)	35	61 ± 1	59 ± 4
poly(DTsB sebacate)	36	116 ± 3	124 ± 6
poly(HTH adipate)	40	87 ± 2	93 ± 3
poly(DTB adipate)	42	111 ± 3	108 ± 3
poly(DTO succinate)	43	84 ± 6	105 ± 19
poly(DTM sebacate)	45	126 ± 4	152 ± 8
poly(DTsB (R)(+) methyladipate)	45	79 ± 3	86 ± 16
poly(DTsB glutarate)	46	86 ± 3	85 ± 2
poly(DTBn adipate)	48	69 ± 8	73 ± 8
poly(DTB glutarate)	50	105 ± 1	89 ± 2
poly(DTM (R)(+) methyladipate)	53	68 ± 1	75 ± 1
poly(DTiP adipate)	55	144 ± 2	193 ± 5
poly(DTBn methyladipate)	55	90 ± 1	56 ± 1
poly(DTE adipate)	59	126 ± 7	169 ± 11
poly(HTE adipate)	61	*	*
poly(DTE glutarate)	64	80 ± 1	115 ± 5
poly(DTB succinate)	67	145 ± 11	208 ± 20
poly(DTM adipate)	67	99 ± 3	127 ± 3
poly(HTE succinate)	78	*	*

[1]Glass transition temperatures are single measurements of polymer before pressing ± 1ºC.

[2]Molecular weight: mean value of three different films ± SD.

[3]The ´*´symbol indicates the polymers that did not dissolve in THF and thus, Mw could not be measured by THF-GPC.

[4]Degree of polymerization: mean value from Mw´s of three different films ± SD.

3.2   Results and discussion

3.2.1   Validation of water uptake methods

For water uptake of PLA films, the TGA and ^3H_2O methods were each internally reproducible, with rsd less than 11 and 6%, respectively. The ANOVA test showed no significant difference between the two methods (p-value 0.75) (Table 3-2). The advantages and disadvantages of the TGA and ^3H_2O methods are summarized on Table 3-3. The radioactive method was determined to be particularly suitable for high-throughput experimentation, since it was sensitive, simple, fast and allows for parallel measurements (in our set-up: 30 samples per hour), while the TGA method requires serial measurements at a rate of about 1 sample per hour (with our set-up). This advantage is very relevant when libraries of polymers are studied and many samples need to be evaluated at the same time, and thus, the ^3H_2O method was used for the rest of this study.

Table 3-2: Water uptake for poly(D,L lactic acid); comparison of TGA and ^3H_2O methods

Time (weeks)	Water uptake (%) by 3H2O[1,2]	Water uptake (%) by TGA[1,3]
1	67 ± 4	57 ± 6
2	60 ± 4	57 ± 6
3	53 ± 2	50 ± 1
4	48 ± 2	51 ± 2

[1]Each value is the mean value ± SD

[2]n=10

[3]n=4

Table 3-3: Advantages and disadvantages of water uptake methods: TGA and ^3H_2O

Thermogravimetric analysis (TGA)	Radiolabeled water (^3H_2O)
Advantages	Advantages
No need to pre-weigh	Samples can be measured in parallel
Little sample required (~ 10 mg)	Only water uptake (and not initial water content) is measured
	Very accurate for low water uptake
Disadvantages	
Water content of film before incubation must be measured	Disadvantages
Samples must be immediately measured after incubation	Administrative obstacles relating to the use of radioactive substances
Samples must be measured sequentially (time consuming)	Controls must be run each time
	Generally may require larger sample size than TGA
Polymer must be thermo-stable up to 120ºC	

3.2.2 *Processing study to achieve homogeneous films*

Results for the 4 polymers studied are summarized in Table 3-4, and representative data for poly(DTB succinate) are shown in Figure 3-2. Quenched films presented high variability (rsd of 38%) and spatial dependence along the film. Annealing for 24 h significantly reduced the rsd to 16 % of the water uptake (p-value < 0.0001), without changing the average water uptake value.

In separate experiments, quenched and annealed films of poly(DTE glutarate) presented similar water uptake profiles and no spatial variability, while for poly(DTE adipate), quenched films presented significantly higher water uptake values than annealed films (p-value < 0.0001) and no significant spatial variability (Table 3-4).

Table 3-4: Water uptake after incubation in radioactive water and 37ºC.

Polymer	Days of incubation	n	Water uptake (%)[1]			
			Quenched film	rsd[2]	Annealed film	rsd[2]
poly(D,L lactic acid)	3	15	$30.4 \pm 5.2\%$	17%	$35.0 \pm 5.3\%$	15%
poly(DTB succinate)	3	15	$5.8 \pm 2.2\%$	38%	$5.0 \pm 0.8\%$	16%[3]
poly(DTE adipate)	5	5	$17.9 \pm 1.1\%$	6%	$14.3 \pm 1.3\%$[4]	9%
poly(DTE glutarate)	5	5	$15.4 \pm 1.0\%$	6%	$15.1 \pm 0.6\%$	4%

[1]Samples were taken along a film that was quenched or annealed. Each value is the mean value of n samples from the same film ± SD

[2]Relative standard deviation is the SD divided by the mean value

[3]Annealing significantly reduces variability on water uptake of poly(DTB succinate) at $p < 0.0001$

[4]Quenched and annealed for poly(DTE adipate) are different at $p < 0.0001$
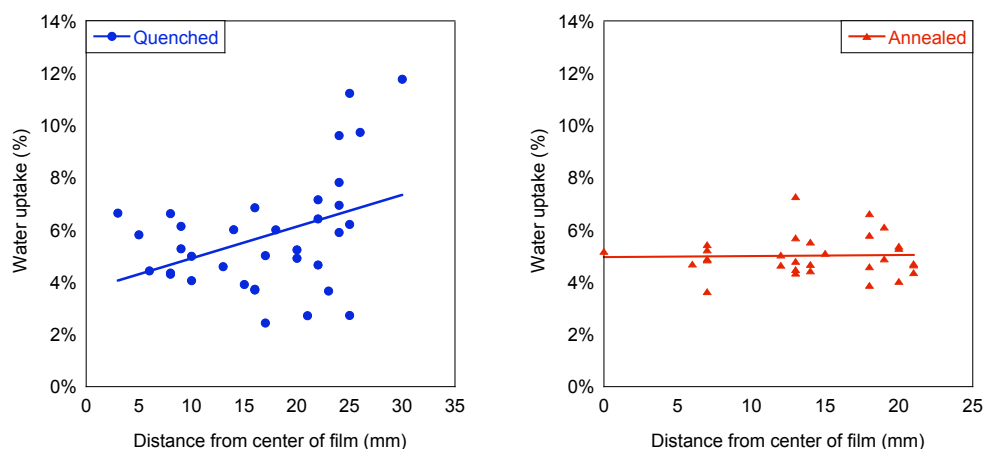
Figure 3-2: Water uptake after 3 days of incubation in radioactive water and 37 ºC of poly(DTB succinate). Samples were taken along a film that was quenched or annealed, showing reduction in water uptake variability after annealing. See also Table 3-4.

In a control experiment with PLA, which is an amorphous polymer, quenched and annealed films presented similar water uptake profiles, and no difference in the water uptake spatial variability (Table 3-4).

One possible explanation for this result is that for some polymers, residual stresses and radial orientation are induced during pressing (Figure 3-1) and are not

released during quenching but can be released during annealing. In contrast, other polymers do not have significant residual stresses after processing and therefore, for these polymers, the results of water uptake measurements are independent of the specific processing method used. Unless it has been established that the morphology of a particular polymer is fully relaxed after processing, these results indicate that for comparative water uptake studies, all test specimens should be annealed to reach equilibrium.

3.2.3   *Effect of initial Mw on water uptake*

In an experiment performed using films of poly(DTiP adipate) having different Mw, the films with lower initial Mw had a higher equilibrium water content (Figure 3-3) and a faster initial degradation constant ($k = 0.437$ and 0.207, respectively, in a first order kinetics. See Chapter 7). We believe that the higher content of hydrophilic end groups in the lower Mw polymers provokes a higher driving force for water uptake, and a subsequently faster hydrolytic degradation, which will increase the hydrophilic end groups even more, in a positive feedback loop.
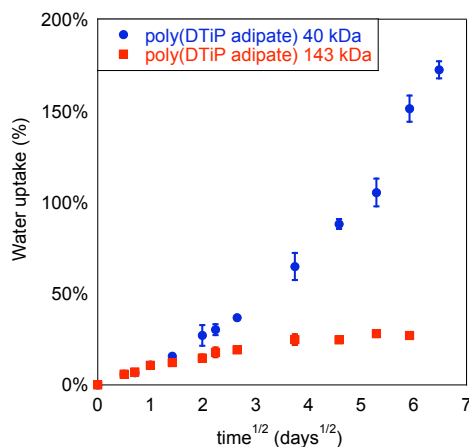
Figure 3-3: Water uptake profiles for poly(DTiP adipate) polymers with initial Mw of 40 kDa and 144 kDa. Each value is the mean value of three samples from three different films ± SD.

3.2.4 Effect of water on glass transition temperature

As expected, the Tg of all polymers decreases initially upon hydration. This behavior can be explained by the plasticization effect of water [5]. In some polymers the initial decrease in Tg was followed by a slight increase in Tg, showing an antiplasticization effect, probably due to hydrogen bonding formation [108] (Figure 3-4 and Table 3-5).
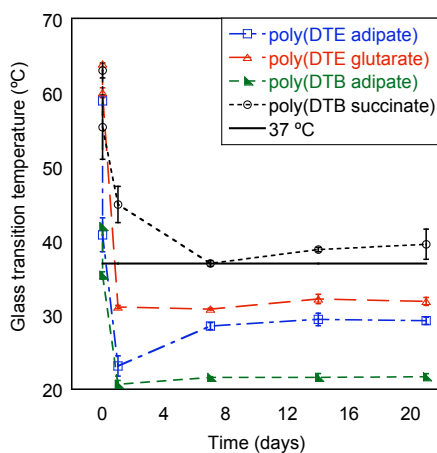
Figure 3-4: Glass transition temperature (Tg) for a subset of the library of tyrosine-derived polyarylates. Each value is the mean value of three samples from three different films ± SD.

Table 3-5: Glass transition temperature (Tg) (ºC) for the subset of tyrosine-derived polyarylates.

Polymer	Mw (kDa)[3,4]	Dry Tg[1]	Initial Tg[1,2]	1d[1,2]	7d[1,2]	14d[1,2]	21d[1,2]	28d[1,2]
poly(DTO sebacate)	123 ± 1	16	**	**	**	**	**	**
poly(HTH sebacate)	64 ± 5	23	9 ± 1	**	9 ± 2	9 ± 4	**	16 ± 4
poly(DTH suberate)	106 ± 2	24	13 ± 2	12 ± 2	12 ± 1	12 ± 1	13 ± 1	13 ± 1
poly(DTO adipate)	132 ± 2	26	22 ± 1	13 ± 1	15 ± 1	16 ± 1	16 ± 1	15 ± 1
poly(DTH adipate)	98 ± 1	34	29 ± 1	18 ± 1	18 ± 1	18 ± 1	20 ± 1	19 ± 1
poly(DTB (R)(+) methyladipate)	61 ± 1	35	24 ± 1	21 ± 1	24 ± 1	25 ± 1	26	31 ± 4
poly(DTsB sebacate)	116 ± 3	36	28 ± 1	19 ± 1	20 ± 1	20 ± 1	21 ± 1	21 ± 2
poly(HTH adipate)	87 ± 2	40	24 ± 1	20 ± 1	22 ± 1	22 ± 1	22 ± 1	23 ± 1
poly(DTB adipate)	111 ± 3	42	35 ± 1	21 ± 1	22 ± 1	22 ± 1	22	22
poly(DTO succinate)	84 ± 6	43	37 ± 1	28 ± 1	**	30 ± 1	32 ± 2	30 ± 1
poly(DTM sebacate)	126 ± 4	45	28 ± 3	21 ± 1	24 ± 1	24 ± 1	24 ± 1	24 ± 1
poly(DTsB (R)(+) methyladipate)	79 ± 3	45	41 ± 1	29 ± 1	32 ± 1	33 ± 1	33 ± 1	33 ± 1
poly(DTsB glutarate)	86 ± 3	46	41 ± 1	30 ± 1	32 ± 1	33 ± 1	34 ± 3	34 ± 1
poly(DTB glutarate)	105 ± 1	50	41 ± 1	26 ± 1	28 ± 1	28 ± 1	28 ± 1	28 ± 1
poly(DTM (R)(+) methyladipate)	68 ± 1	53	47 ± 2	28 ± 1	34 ± 1	35 ± 1	35 ± 1	36 ± 1
poly(DTBn methyladipate)	90 ± 1	55	42 ± 1	30 ± 1	33 ± 1	34 ± 1	34 ± 1	35 ± 1
poly(DTiP adipate)	144 ± 2	55	35 ± 1	27 ± 1	32 ± 1	34 ± 1	33 ± 1	33 ± 1
poly(DTE adipate)	126 ± 7	59	41 ± 2	23 ± 1	29 ± 1	29 ± 1	29 ± 1	**
poly(HTE adipate)	*	61	54 ± 1	54 ± 1	56 ± 1	57 ± 1	58 ± 1	58 ± 1
poly(DTE glutarate)	80 ± 1	64	61 ± 1	31 ± 1	31 ± 1	32 ± 1	32 ± 1	32 ± 1
poly(DTB succinate)	145 ± 11	67	55 ± 4	45 ± 2	37 ± 1	39 ± 1	40 ± 2	39 ± 1
poly(DTM adipate)	99 ± 3	67	54 ± 1	28 ± 1	28 ± 4	31 ± 1	33 ± 1	33 ± 1
poly(HTE succinate)	*	78	49 ± 6	32 ± 1	44 ± 1	45 ± 2	45 ± 3	45 ± 4

[1]Each value is the mean value of three samples from three different films ± SD.

[2]The ´**´symbol indicates that the Tg was not measured for that time and polymer.

[3]Each value of Mw is the mean value of three different films ± SD, measured by THF-GPC.

[4]The ´*´symbol indicates the polymers that did not dissolve in THF and thus, Mw could not be measured by THF-GPC.

3.2.5   Water uptake measurements

After elucidating the effect of initial Mw and polymer processing, water uptake measurements were obtained for a subset of 23 polymers from this library. In most of the cases, rsd values were below 10% of the water uptake value, showing the importance of having high Mw polymers and an annealing step after polymer pressing. The water uptake after 28 days of incubation ranges from 2% to 250% and equilibration time ranges from less than 6 h to more than 42 days (Table 3-6).

3.2.6   Structure-property relationships for water uptake

Previous studies performed for this polymer library, showed a strong correlation between Tg and the hydrophobic nature of the polymer, where Tg increases as the number of carbon or oxygen atoms in the polymer backbone and pendent chain decreases [37]. Contrary to our initial expectations, we observed that water uptake (Table 3-6) does not yield a simple correlation with the hydrophilic factor (as calculated by Smith et al. [100]) (Figure 3-5) or the Tg of the polymers (Figure 3-6).

Two polymers that do not follow this trend are poly(DTB succinate) and poly(HTE adipate). Their hydrophilic factors suggest higher water uptake levels than were observed. However, those polymers are in glassy state during incubation (i.e., their wet Tg remains above the incubation temperature of 37 ºC) (Figure 3-4 and Table 3-5) and thus, their physical state prevented more water from penetrating into the polymer matrix.

Table 3-6: Water uptake for a subset of the library of tyrosine-derived polyarylates.

Polymer	Mw (kDa)[1,2]	1d[3]	7d[3]	14d[3]	21d[3]	28d[3]
poly(HTH sebacate)	64 ± 5	2.2 ± 0.3%	2.1 ± 0.1%	2.0 ± 0.4%	2.4 ± 0.3%	2.3 ± 0.2%
poly(DTO sebacate)	123 ± 1	2.4 ± 0.4%	2.4 ± 0.4%	2.5 ± 0.3%	2.7 ± 0.5%	2.8 ± 0.2%
poly(DTO succinate)	84 ± 6	4.0 ± 0.3%	3.0 ± 0.2%	3.3 ± 0.5%	4.1 ± 1.1%	3.1 ± 0.6%
poly(DTB succinate)	145 ± 11	3.4 ± 0.3%	4.0 ± 0.7%	3.9 ± 0.3%	4.3 ± 0.2%	4.0 ± 0.4%
poly(DTO adipate)	132 ± 2	3.1 ± 0.5%	3.9 ± 0.5%	4.7 ± 0.3%	4.5 ± 0.5%	5.8 ± 0.1%
poly(HTE adipate)	*	5.4 ± 0.3%	7.5 ± 0.7%	7.9 ± 0.6%	7.3 ± 0.2%	8.2 ± 0.5%
poly(DTH suberate)	106 ± 2	5.5 ± 0.1%	8.3 ± 1.0%	9.6 ± 1.3%	11.1 ± 0.5%	13.0 ± 0.1%
poly(DTM sebacate)	126 ± 4	7.5 ± 0.9%	12.1 ± 3.1%	13.6 ± 1.9%	11.7 ± 2.7%	13.6 ± 3.0%
poly(DTM adipate)	99 ± 3	7.3 ± 0.7%	12.7 ± 2.9%	13.6 ± 2.0%	15.4 ± 5.6%	14.7 ± 3.5%
poly(DTB glutarate)	105 ± 1	6.2 ± 0.2%	9.4 ± 0.5%	12.4 ± 1.3%	14.3 ± 0.9%	15.8 ± 1.9%
poly(HTH adipate)	87 ± 2	7.6 ± 0.6%	13.3 ± 1.6%	15.6 ± 1.2%	17.2 ± 1.9%	16.8 ± 1.8%
poly(DTH adipate)	97.7 ± 0.2	5.0 ± 0.5%	10.2 ± 0.9%	13.7 ± 0.4%	14.9 ± 0.8%	17.9 ± 1.1%
poly(DTB adipate)	111 ± 3	5.3 ± 0.6%	10.0 ± 0.7%	12.2 ± 1.4%	17.4 ± 0.1%	18.9 ± 1.3%
poly(DTsB sebacate)	116 ± 3	5.1 ± 0.2%	13.2 ± 0.8%	17.8 ± 0.7%	21.1 ± 0.9%	21.8 ± 1.4%
poly(DTE glutarate)	80 ± 1	7.4 ± 0.1%	14.8 ± 1.9%	17.9 ± 1.3%	21.4 ± 1.3%	24.0 ± 1.7%
poly(DTBn methyladipate)	90 ± 1	7.4 ± 0.8%	19.2 ± 3.3%	27.1 ± 3.4%	29.7 ± 3.7%	34.5 ± 4.7%
poly(DTiP adipate)	144 ± 2	10.4 ± 0.4%	19.8 ± 1.1%	24.6 ± 2.5%	24.8 ± 1.7%	28.1 ± 0.8%
poly(DTE adipate)	126 ± 7	11.3 ± 0.3%	22.7 ± 1.4%	25.7 ± 2.3%	30.7 ± 6.9%	36.1 ± 3.5%
poly(HTE succinate)	*	26.3 ± 7.8%	36.1 ± 13.1%	42.9 ± 11.9%	44.5 ± 5.1%	50.0 ± 20.7%
poly(DTsB glutarate)	86 ± 3	14.8 ± 1.3%	53.7 ± 2.1%	89.3 ± 2.6%	103.4 ± 5.2%	108.5 ± 0.8%
poly(DTM (R)(+) methyladipate)	68 ± 1	25.4 ± 1.2%	88.7 ± 2.2%	89.0 ± 3.1%	84.9 ± 6.5%	88.4 ± 1.2%
poly(DTsB (R)(+) methyladipate)	79 ± 3	24.4 ± 0.5%	91.1 ± 8.9%	110.4 ± 5.6%	119.9 ± 5.7%	126.7 ± 7.1%
poly(DTB (R)(+) methyladipate)	61 ± 1	32.9 ± 0.5%	80.1 ± 6.4%	135.1 ± 7.3%	196.6 ± 14.1%	252.9 ± 21.4%

[1]Each value of Mw is the mean value of three different films ± SD, measured by THF-GPC.

[2]The '*' symbol indicates the polymers that did not dissolve in THF and thus, Mw could not be measured by THF-GPC.

[3]Each value of water uptake is the mean value of three samples from three different films ± SD.
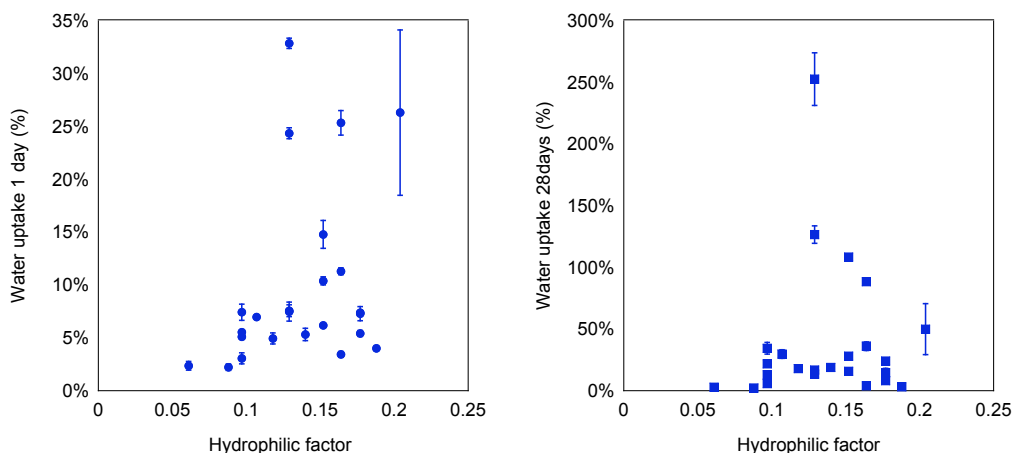
Figure 3-5: Water uptake after 1 day (●) and 28 days (■) of incubation, respectively, versus the hydrophilic factor as calculated by Smith et al. [55]. Each value is the mean value of three samples from three different films ± SD.
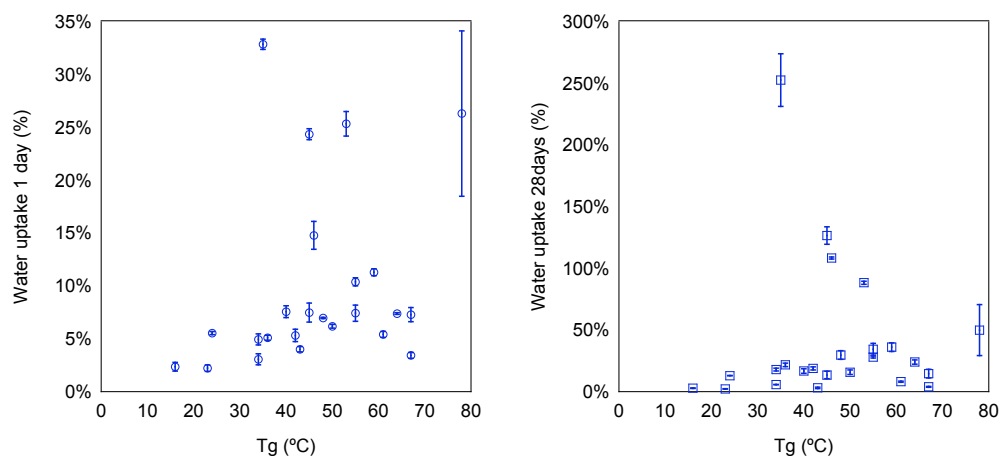
Figure 3-6: Water uptake after 1 day (○) and 28 days (□) of incubation, versus Tg. Each value is the mean value of three samples from three different films ± SD.

Comparing five of the adipates of the study that have different number of carbons in the pendant chain (DTM:1, DTE:2, DTB:4, DTH:6, and DTO:8) (Figure 3-7), one would expect that the longer the pendant chain, the more hydrophobic the polymer, and thus the lower the water uptake. This is true for poly(DTE adipate), poly(DTB adipate)

and poly(DTO adipate). However, poly(DTM adipate) has lower water uptake levels than poly(DTE adipate), even though they have one and two carbons in the pendant chain, respectively. Also, poly(DTM adipate), poly(DTB adipate) and poly(DTH adipate) have no significantly different levels of water uptake, while they have different number of carbons in their pendant chains (1, 4 and 6, respectively).
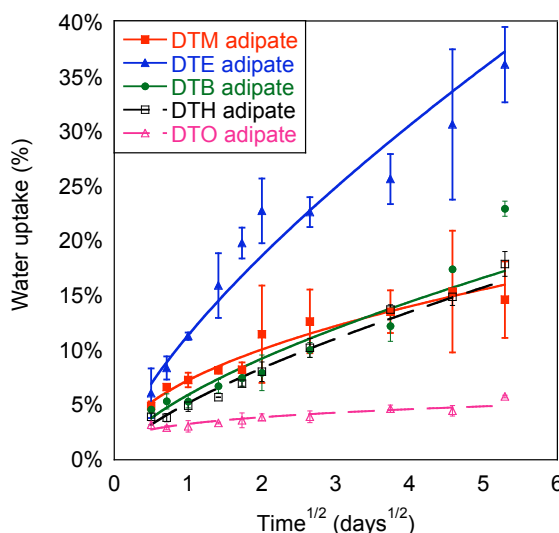
Figure 3-7: Water uptake of five adipates. Each value is the mean value of three samples from three different films ± SD.

3.3   Conclusions

The study of water uptake for a subset of L-tyrosine-derived polyarylates gave us interesting insights. Polymer processing and Mw, two commonly overlooked polymer parameters when comparing different polymers, were found to be highly relevant to obtaining reproducible water uptake measurements for certain polymers. We believe that this is responsible for part of the high variability observed in our previous results and other published studies. Initial polymer film characteristics affect water uptake at later stages in the process and not only the initial water uptake values. Thus, the polymer

processing techniques and the initial Mw must be controlled. In particular, an annealing step is recommended after thermal processing and prior to analyses to enable comparable measurements across sets of diverse polymers that may have different relaxation properties.

With proper attention to sample preparation, both TGA and ^3H_2O methods for measuring water update can produce satisfactory results. For investigations of large polymer sets, as in the study of combinatorial polymer libraries, the ^3H_2O method affords the important advantage of parallel processing, which becomes more and more significant as the number of water-update determinations increases.

From the measurements of water uptake for several polymers in the polyarlyate library, it became evident neither initial water uptake nor equilibration kinetics could be predicted by merely looking at the hydrophobic character and/or Tg of each polymer, which is further explored in Chapter 6.

4   Kinetic analysis of water uptake

Different equations can be used to model water uptake. Some examples include the Fick diffusion, power law and the Weibull equation. This chapter presents the results of applying several kinetic models to the previously obtained water uptake data for 24 polymers of the L-tyrosine-derived polyarylate library.

4.1   Kinetic equations for water uptake

4.1.1   Fick diffusion

Fick's diffusion is often used to model the diffusion of a solvent into a polymeric matrix [7, 21, 30, 109-142]. Fick's second law is defined by:

$$\frac{\partial C}{\partial t} = \frac{\partial}{\partial x}\left(D\frac{\partial C}{\partial x}\right), \tag{4-1}$$

where C is the concentration of the water at time t along the axis x, and D is the diffusion coefficient or diffusivity. It can be constant or dependent on concentration, position, history [119, 143], and the microporous structure [118] of the system.

If the initial concentration of the solvent is zero and the polymer matrix is placed in an infinite bath of the solvent, Fick's second law can be rearranged as:

$$\frac{WU(t)}{WU_{eq}} = 1 - \frac{8}{\pi^2}\sum_{m=0}^{\infty}\frac{1}{(2m+1)^2}\exp\left[-\frac{\pi^2(2m+1)^2}{L^2}Dt\right], \tag{4-2}$$

where $WU(t)$ is the water uptake at time t, WU_{eq} is the water uptake at $t = \infty$, and L is the thickness of the sample. At short times, when $WU(t)/WU_{eq} < 0.50$, it can be approximated by:

$$\frac{WU(t)}{WU_{eq}} = \frac{4}{L}\sqrt{\frac{Dt}{\pi}}. \tag{4-3}$$

For longer times, when $WU(t)/WU_{eq} > 0.60$, the diffusion-relaxation model (first order equation) by Berens -Hopfengerg [144-146] [33, 147, 148] has been used. Relaxation increases the overall sorption due to a rearrangement of the polymer chains that tends to increase the available free volume, while diffusion tends to distribute the solvent homogeneously over the available free volume. This equation is defined as:

$$\frac{WU(t)}{WU_{eq}} = 1 - A \cdot \exp(-k_{BH}t),$$

(4-4)

where A and k_{BH} are constants of the model.

4.1.2 Power law equation

A power law equation has been used by several groups to explain water uptake and drug release behavior [125, 138, 143, 145, 149-164], in particular in hydrogel systems:

$$\frac{WU(t)}{WU_{eq}} = kt^n,$$

(4-5)

where k and n are constants. An exponent of $n = 0.5$ (Case I) indicates Fickian diffusion. When $n = 1$ (Case II), the equation corresponds to zero order [147]. When $1 > n > 0.5$ (also called anomalous diffusion), the water uptake is controlled by either swelling or erosion of the polymer matrix [154, 157]. No current explanation was found in the literature for the case of $n < 0.5$.

The Deborah number (De) has been used to explain the effect of diffusion and relaxation in the previous classification [112, 151, 165, 166]. The Deborah number is defined by:

$$De = \frac{\lambda}{\theta},$$

(4-6)

where λ is the characteristic stress-relaxation time of polymer/solvent system, and θ is the characteristic diffusion time of solvent. The zero order release (equivalent to $1 > n > 0.5$) occurs when $De \sim 1$, and the rate of diffusion is similar to the rate of relaxation. When $De \gg 1$, the diffusion is much faster than relaxation and elastic Fickian diffusion is observed. When $De \ll 1$, the relaxation is faster than the diffusion and viscous Fickian diffusion is observed.

Another equation used to decouple the effect of diffusion and relaxation is:

$$\frac{WU(t)}{WU_{eq}} = k_D t^m + k_R t^{2m}, \qquad (4\text{-}7)$$

where k_D is the contribution of Fickian diffusion and k_R is the contribution from polymer relaxation [144, 145, 162, 167, 168].

4.1.3   Weibull equation

Some authors have previously used the Weibull equation [169, 170], to study water or moisture uptake, especially in food science [122, 131, 171-179] and drug delivery systems [180-182]. The Weibull equation is defined by:

$$\frac{WU(t)}{WU_{eq}} = \left\{ 1 - \exp^{-\left(\frac{t}{t_{scale}}\right)^b} \right\}, \qquad (4\text{-}8)$$

where t_{scale} is the time scale of the release or uptake process (rate parameter), and b is the shape parameter, which depends on the process mechanisms, the lower the value of b, the faster is the process at short times.

As explained by Machado et al. for the water uptake by cereals in water [171], this model represents the process as a sequence of probabilistic events eventually controlled by the failure of the matrix structure as a barrier to mass transfer. They show

that $1/t_{scale}$ follows an Arrhenius type of relationship respect to the temperature of incubation.

4.1.4 Other models

Other models used for water uptake included a series of first order reactions due to different interactions [35, 183]:

$$WU(t) = \sum_i WU_i \cdot \left\{1 - \exp(-k_i \cdot t)\right\} + WU_{eq} \cdot \left\{1 - \exp(-k_{eq} \cdot t)\right\}, \tag{4-9}$$

where WU_i and k_i are the water uptake and the kinetic coefficient due to each specific interaction, respectively.

Two stage sorption has also been used to model water uptake, where the first part is modeled as Fickian and the second part is associated with an increase of surface concentration or polymer relaxation [146, 184-188].

The Langmuir model has been applied for diffusion. In this model, water is separated in two types: free water and trapped water that cannot freely diffuse in the polymer matrix [139]:

$$\frac{WU(t)}{WU_{eq}} = 1 - \frac{\gamma}{\gamma + \alpha} \exp(-\alpha \cdot t) - \frac{8}{\pi^2} \frac{\alpha}{\alpha + \gamma} \sum_{n=0}^{\infty} \frac{1}{(2n+1)^2} \exp\left\{-\left[\frac{\pi(2n+1)^2}{2L} Dt\right]\right\}, \tag{4-10}$$

where γ is the probability that a water molecule become linked or trapped in the polymer at a given time and place, while α represents the probability that a water molecule becomes mobile at a given time and place.

Also, empirical models have been used to explain water uptake behavior. Riggs et al. (1999) used an error function to explain the water uptake behavior of a polymer system [189]:

$$WU(t) = WU_{eq} \cdot erfc\left(\frac{x}{2\sqrt{Dt}}\right), \qquad\qquad (4\text{-}11)$$

while the Peleg equation has been extensively used to explain the water uptake of food systems [131, 177, 178, 190-194]:

$$WU(t) = \frac{t}{k_{P1} + k_{P2}t}, \qquad\qquad (4\text{-}12)$$

where k_{P1} and k_{P2} are constant of the model, fitted from the experimental values of water uptake.

4.2   Models for the water uptake of L-tyrosine-derived polyarylate library

4.2.1   Equilibration water uptake

Water uptake measurements for 24 polymers from the L-tyrosine-derived polyarylate library (Chapter 3) showed that equilibrium water uptake was achieved for 19 of the polymers. Equilibration times varied from less than 6 hours to more than 42 days (Table 4-1). These results were used in the analysis of different kinetic models as follows:

4.2.2   Fick diffusion

Fick's diffusion (eq. 4-3) was used to model the previous obtained water uptake data for the beginning of the water uptake profiles ($WU/WU_{eq} < 0.5$). For values closer to equilibrium, a first order equation was used (eq. 4-4). Models were obtained by minimizing the root mean squared error of the calculated value respect to the experimental value for each time point. Nine of the 24 polymers equilibrate before 1 day, and thus, Fick's diffusion equation could not be used. Five of the 24 polymers do not equilibrate by

42 days, and thus, the Fick's diffusion model was used for their complete water uptake profiles. This combined model produces relative absolute error of calculated values respect to experimental values that ranges from 2 to 28%, depending of the polymer, with an average of 10% (Table 4-2).

Table 4-1: Equilibrated water uptake for the 24 polymers of the L-tyrosine-derived polyarylates.

Polymer[1]	Water uptake equilibrium (%)[2]	Time of water equilibration
poly(HTH sebacate)	2.3 ± 0.4%	1d
poly(DTO sebacate)	2.7 ± 0.4%	3d
poly(DTO succinate)	3.5 ± 0.6%	< 6h
poly(DTB succinate)	4.0 ± 0.3%	4d
poly(DTO adipate)	6.1 ± 0.3%	28d
poly(HTE adipate)	7.8 ± 1.1%	7d
poly(DTH suberate)	not equilibrated	> 42d
poly(DTM sebacate)	12.3 ± 2.7%	7d
poly(DTM adipate)	14.5 ± 3.5%	14d
poly(DTB glutarate)	not equilibrated	> 42d
poly(HTH adipate)	18.0 ± 2.1%	21d
poly(DTH adipate)	not equilibrated	> 42d
poly(DTB adipate)	18.2 ± 1.2%	21d
poly(DTsB sebacate)	21.0 ± 1.2%	21d
poly(DTE glutarate)	29.6 ± 3.4%	35d
poly(DTiP adipate)	27.6 ± 1.0%	28d
poly(DTBn adipate)	32.2 ± 7.2%	21d
poly(DTBn methyladipate)	not equilibrated	> 42d
poly(DTE adipate)	36.2 ± 3.2%	28d
poly(HTE succinate)	43.1 ± 10.6%	14d
poly(DTM (R)(+) methyladipate)	90.1 ± 8.8%	7d
poly(DTsB glutarate)	97.4 ± 4.1%	21d
poly(DTsB (R)(+) methyladipate)	136.5 ± 10.0%	28d
poly(DTB (R)(+) methyladipate)	not equilibrated	> 42d

[1]Polymers are ordered by water uptake after 28 days.

[2]Each value is the mean value of all samples after equilibration ± SD.

4.2.3   Power law

A power law equation (eq. 4-5) was used to model the water uptake data. As in the previous model, it could be applied only for the beginning of the water uptake profiles ($WU/WU_{eq} < 0.5$). For values closer to equilibration, a first order equation was used (eq. 4-4). As in Fick's diffusion, the power law could not be used on polymers that equilibrate before 1 day of incubation and the linear model was not needed for polymers that do not equilibrate by 42 days. This combined model produces relative absolute error of calculated values respect to experimental values that ranges from 2 to 15%, depending of the polymer, with an average of 6%. The exponent of the power law (n) varies from 0.2 to 0.7. This result shows that there are different mechanisms present in the water uptake for this polymer library, ranging from Fickian diffusion ($n \sim 0.5$), anomalous diffusion ($0.5 < n < 1$), and a third case that has not been explained in the literature ($n < 0.5$) (Table 4-3). Future studies should focus on explaining this behavior.

4.2.4   Weibull equation

The Weibull equation (eq. 4-8) was used to model the water uptake data. It can be used for the complete water uptake profile, with the exception of polymers where the water uptake does not reach equilibrium. The model produces relative absolute errors of calculated values with respect to experimental values that range from 3 to 16%, depending of the polymer, with an average of 9% (Table 4-4).

Table 4-2: Parameters for Fick diffusion model, calculated to fit the experimental water uptake of L-tyrosine-derived polyarylates.

Polymer[1]	Transition between Fick diffusion and 1st order model $(WU/WU_{eq}\sim0.5)$[2]	k (Fick diffusion model)[3]	A (1st order model)[2]	k_{BH} (1st order model)[2]	Relative absolute error (%)[4]
poly(HTH sebacate)	<6h	**	0.28	2.2941	7%
poly(DTO sebacate)	<6h	**	0.12	0.1057	5%
poly(DTO succinate)	<6h	**	0.00	0.7992	9%
poly(DTB succinate)	<6h	**	0.27	0.5909	2%
poly(DTO adipate)	1d	**	0.50	0.0568	5%
poly(HTE adipate)	<6h	**	0.34	0.1932	4%
poly(DTH suberate)	*	0.03	*	*	28%
poly(DTM sebacate)	12h	0.00	0.62	0.4996	5%
poly(DTM adipate)	1d	**	0.63	0.1879	6%
poly(DTB glutarate)	*	0.04	*	*	24%
poly(HTH adipate)	2d	0.09	0.52	0.1040	5%
poly(DTH adipate)	*	0.04	*	*	15%
poly(DTB adipate)	7d	0.05	0.99	0.1066	17%
poly(DTsB sebacate)	7d	0.05	1.12	0.1566	9%
poly(DTE glutarate)	14d	0.07	1.12	0.0724	9%
poly(DTiP adipate)	3d	0.10	0.69	0.1295	7%
poly(DTBn adipate)	7d	0.07	2.40	0.2313	7%
poly(DTBn methyladipate)	*	0.07	*	*	8%
poly(DTE adipate)	3d	0.12	0.55	0.0642	4%
poly(HTE succinate)	1d	0.00	0.66	0.1838	15%
poly(DTM (R)(+) methyladipate)	3d	0.22	8.80	0.8078	14%
poly(DTsB glutarate)	7d	0.14	2.08	0.2055	5%
poly(DTsB (R)(+) methyladipate)	4d	0.24	0.72	0.0979	8%
poly(DTB (R)(+) methyladipate)	*	0.35	*	*	17%

[1]Polymers are ordered by water uptake after 28 days.

[2]The '*' symbol represents polymers that did not equilibrate, and thus, no transition is observed (no need for 1st order model).

[3]The '**' symbol represents polymers that equilibrate before 1 day, and thus, no Fickian diffusion model can be applied.

[4]The relative absolute error was calculated as the sum of the contribution from the Fickian model and the 1st order model.

Table 4-3: Parameters for power law model, calculated to fit the experimental water uptake of L-tyrosine-derived polyarylates.

Polymer[1]	Transition between power law and 1st order model (WU/WU_{eq}~0.5)[2]	k (power law model)[3]	n (power law model)[3]	Relative absolute error (%)[4]
poly(HTH sebacate)	<6h	**	**	5%
poly(DTO sebacate)	<6h	**	**	9%
poly(DTO succinate)	<6h	**	**	2%
poly(DTB succinate)	<6h	**	**	5%
poly(DTO adipate)	1d	**	**	4%
poly(HTE adipate)	<6h	**	**	5%
poly(DTH suberate)	*	0.05	0.23	5%
poly(DTM sebacate)	12h	0.00	0.00	6%
poly(DTM adipate)	1d	**	**	9%
poly(DTB glutarate)	*	0.06	0.29	3%
poly(HTH adipate)	2d	0.07	0.23	8%
poly(DTH adipate)	*	0.05	0.37	7%
poly(DTB adipate)	7d	0.06	0.20	5%
poly(DTsB sebacate)	7d	0.06	0.33	4%
poly(DTE glutarate)	14d	0.07	0.36	3%
poly(DTiP adipate)	3d	0.10	0.33	7%
poly(DTBn adipate)	7d	0.06	0.52	8%
poly(DTBn methyladipate)	*	0.07	0.50	3%
poly(DTE adipate)	3d	0.11	0.46	15%
poly(HTE succinate)	1d	0.00	0.00	10%
poly(DTM (R)(+) methyladipate)	3d	0.22	0.74	3%
poly(DTsB glutarate)	7d	0.14	0.58	2%
poly(DTsB (R)(+) methyladipate)	4d	0.25	0.67	12%
poly(DTB (R)(+) methyladipate)	*	0.31	0.60	5%

[1]Polymers are ordered by water uptake after 28 days.

[2]The '*' symbol represents polymers that did not equilibrate, and thus, no transition is observed (no need for 1st order model).

[3]The '**' symbol represents polymers that equilibrate before 1 day, and thus, no power law model can be applied.

[4]The relative absolute error was calculated as the sum of the contribution from the power law model and the 1st order model.

Table 4-4: Parameters for Weibull model, calculated to fit the experimental water uptake of L-tyrosine-derived polyarylates.

Polymer[1]	WU_{eq} (Weibull model)[2]	b (Weibull model)[2]	t_{scale} (days) (Weibull model)[2]	Relative absolute error (%)[2]
poly(HTH sebacate)	2.3 ± 0.4%	0.53	0.08	7%
poly(DTO sebacate)	2.7 ± 0.4%	0.25	0.05	5%
poly(DTO succinate)	3.5 ± 0.6%	1.00	0.01	9%
poly(DTB succinate)	4.0 ± 0.3%	0.45	0.24	3%
poly(DTO adipate)	6.1 ± 0.3%	0.24	2.79	9%
poly(HTE adipate)	7.8 ± 1.1%	0.25	0.26	0.06
poly(DTH suberate)	*	*	*	*
poly(DTM sebacate)	12.3 ± 2.7%	0.47	0.82	7%
poly(DTM adipate)	14.5 ± 3.5%	0.42	2.21	8%
poly(DTB glutarate)	*	*	*	*
poly(HTH adipate)	18.0 ± 2.1%	0.45	3.06	5%
poly(DTH adipate)	*	*	*	*
poly(DTB adipate)	18.2 ± 1.2%	0.42	9.18	16%
poly(DTsB sebacate)	21.0 ± 1.2%	0.54	7.57	12%
poly(DTE glutarate)	29.6 ± 3.4%	0.49	12.66	7%
poly(DTiP adipate)	27.6 ± 1.0%	0.51	4.60	5%
poly(DTBn adipate)	32.2 ± 7.2%	0.67	8.76	12%
poly(DTBn methyladipate)	*	*	*	*
poly(DTE adipate)	36.2 ± 3.2%	0.54	5.79	5%
poly(HTE succinate)	43.1 ± 10.6%	0.40	3.42	16%
poly(DTM (R)(+) methyladipate)	90.1 ± 8.8%	0.91	3.74	12%
poly(DTsB glutarate)	97.4 ± 4.1%	0.78	10.72	11%
poly(DTsB (R)(+) methyladipate)	136.5 ± 10.0%	0.79	7.22	4%
poly(DTB (R)(+) methyladipate)	*	*	*	*

[1]Polymers are ordered by water uptake after 28 days.

[2]The '*' symbol represents polymers that did not equilibrate, and thus, the Weibull model cannot be applied.

Table 4-5: Parameters for Peleg model, calculated to fit the experimental water uptake of L-tyrosine-derived polyarylates.

Polymer[1]	k_{P1} (Peleg model)	k_{P2} (Peleg model)	Relative absolute error (%)
poly(HTH sebacate)	1.57	43.56	7%
poly(DTO sebacate)	5.91	36.74	5%
poly(DTO succinate)	0.00	29.16	8%
poly(DTB succinate)	4.68	24.38	3%
poly(DTO adipate)	5.09	22.44	16%
poly(HTE adipate)	1.94	13.81	9%
poly(DTH suberate)	4.99	11.38	16%
poly(DTM sebacate)	3.08	8.34	9%
poly(DTM adipate)	4.10	8.09	15%
poly(DTB glutarate)	8.39	7.58	22%
poly(HTH adipate)	5.03	6.24	12%
poly(DTH adipate)	14.49	6.38	24%
poly(DTB adipate)	7.82	8.13	26%
poly(DTsB sebacate)	12.65	5.22	20%
poly(DTE glutarate)	8.23	4.70	19%
poly(DTiP adipate)	4.88	4.22	14%
poly(DTBn adipate)	13.24	2.91	19%
poly(DTBn methyladipate)	13.07	2.60	15%
poly(DTE adipate)	4.71	3.19	12%
poly(HTE succinate)	1.70	2.83	18%
poly(DTM (R)(+) methyladipate)	3.37	0.89	12%
poly(DTsB glutarate)	7.01	0.84	13%
poly(DTsB (R)(+) methyladipate)	3.14	0.67	7%
poly(DTB (R)(+) methyladipate)	3.78	0.34	27%

[1]Polymers are ordered by water uptake after 28 days.

4.2.5 Peleg equation

The Peleg equation (eq. 4-12) was also used to model the water uptake data. In this case, it can be used for the complete water uptake profile, even for polymers that did not reach equilibrium water uptake. However, in this case, the parameters do not have any practical meaning. This equation produces relative absolute error of calculated values respect to experimental values that range from 3 to 27%, depending of the polymer, with an average of 15% (Table 4-5).

4.3 Summary

Figure 4-1, Figure 4-2, Figure 4-3, and Figure 4-4 show the water uptake profiles and the models described in this chapter. For polymers that equilibrate fast and have low values of water uptake, all models present very similar profiles. For other polymers, each model gives a different profile. Fick's diffusion and the power law models give a mechanistic explanation of the diffusion behavior. However, there is no explanation available for the case when $n < 0.5$ in the power law equation. Both of these models require more data than the available for the beginning of the water uptake profiles, since they are only applicable when the water uptake is less than 50% of the equilibration value. The use of the first order equation for late stages of water uptake is useful in those cases.

In contrast, both Weibull and Peleg equations were derived empirically, so they do not give a clear mechanistic explanation of the process. However, they can be used in almost all the cases with very good fitting accuracy. Since the Weibull equation presented

higher accuracy than the Peleg equation, the Weibull equation was selected to be used in

building a surrogate model for the water uptake data (Chapter 6).
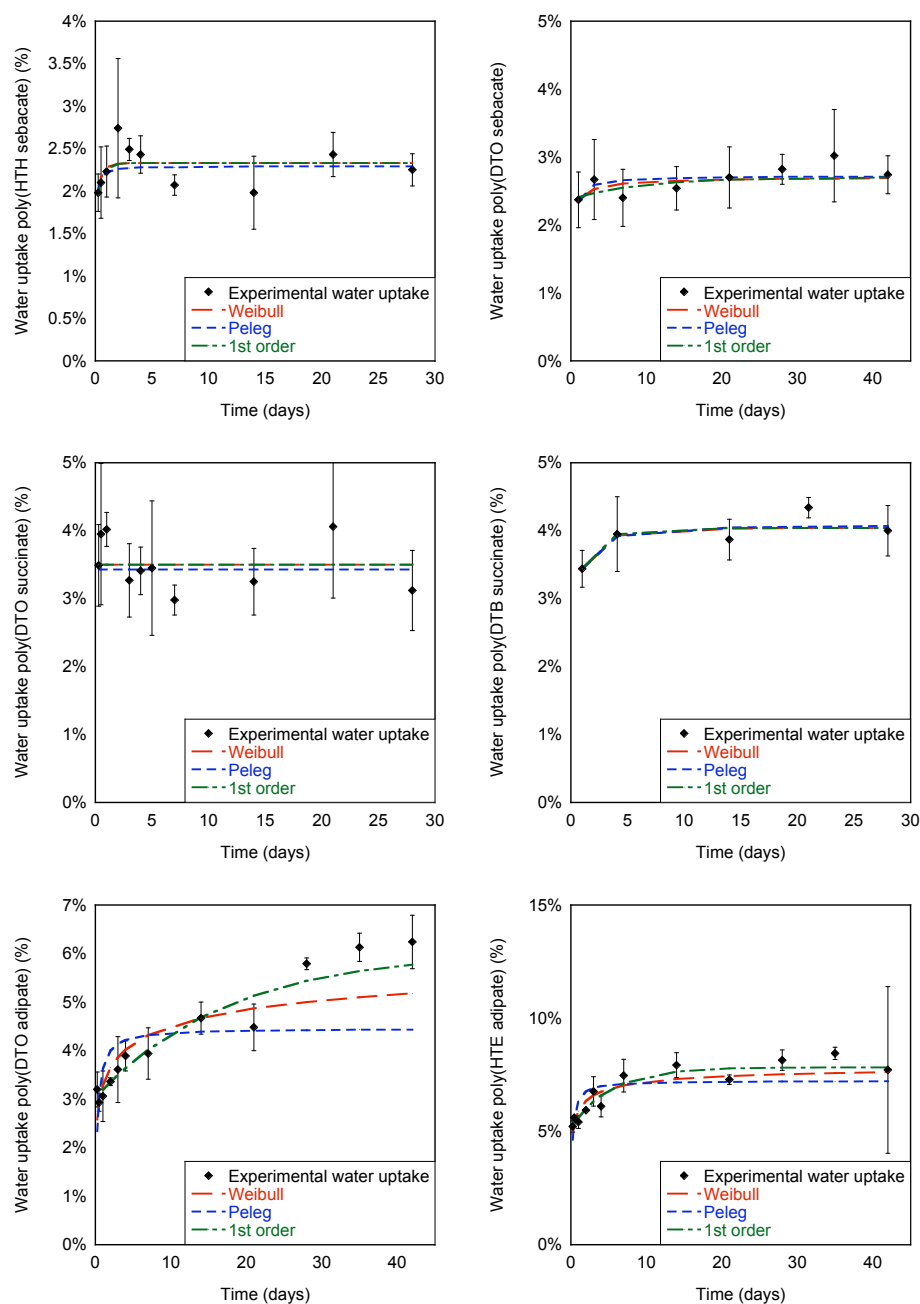
Figure 4-1: Profiles of water uptake for L-tyrosine-derived polyarylates with the kinetic models (part 1).
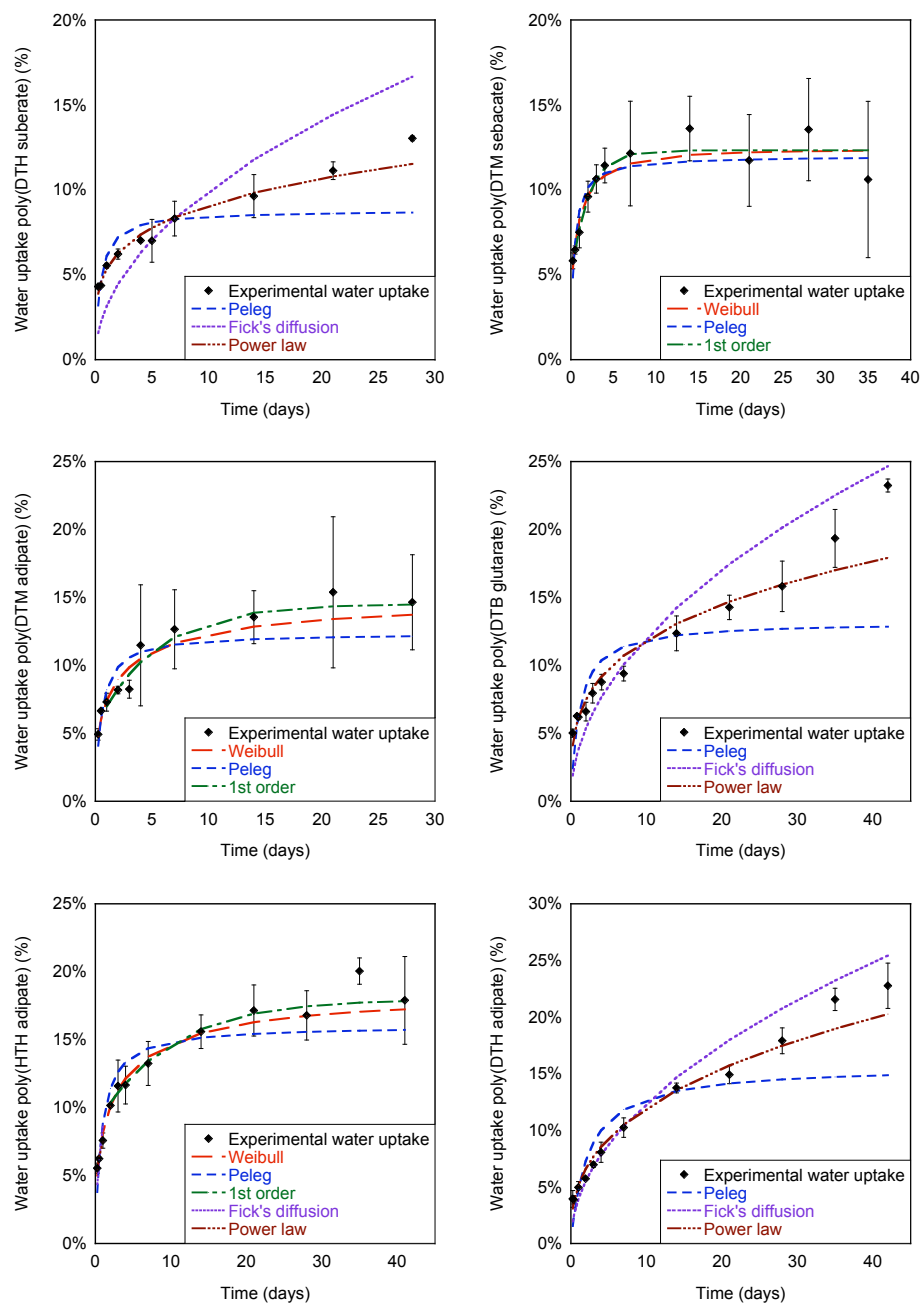
Figure 4-2: Profiles of water uptake for L-tyrosine-derived polyarylates with the kinetic models (part 2).
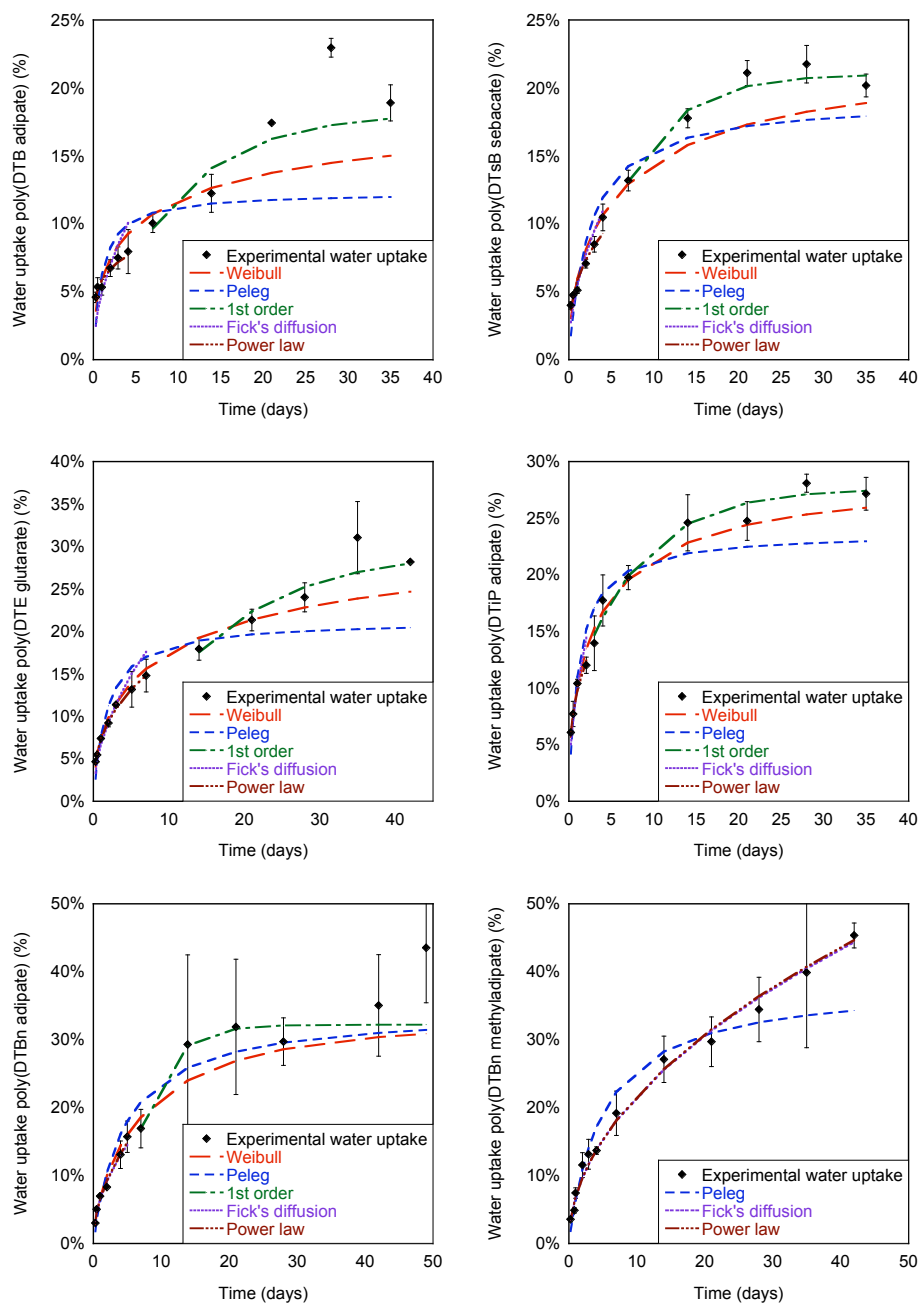
Figure 4-3: Profiles of water uptake for L-tyrosine-derived polyarylates with the kinetic models (part 3).
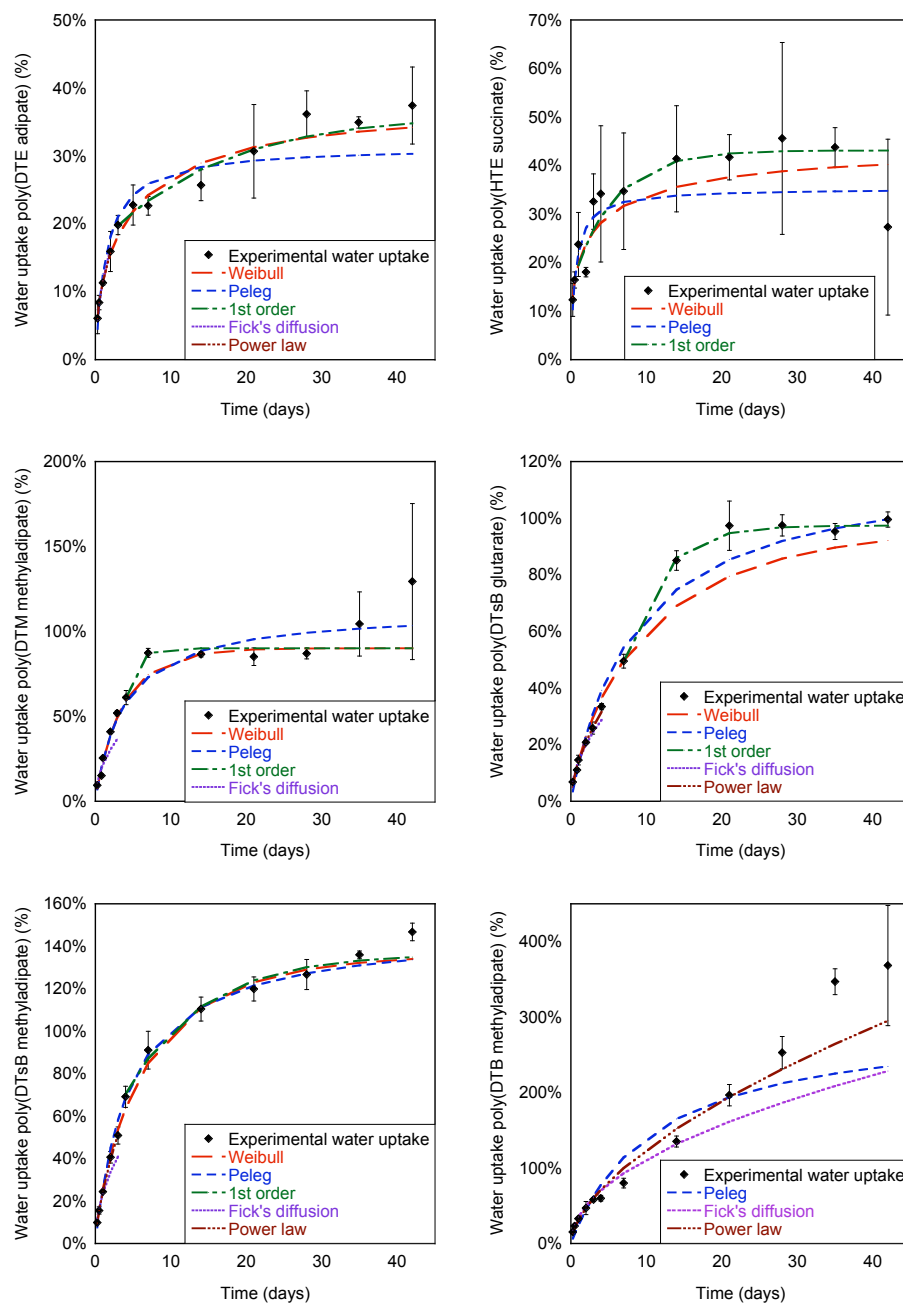
Figure 4-4: Profiles of water uptake for L-tyrosine-derived polyarylates with the kinetic models (part 4).

4.4 *Conclusions*

Different models can be used to fit the water uptake profiles obtained for a subset of the L-tyrosine-derived polyarylate library. Fick's diffusion and power law are only applicable to certain of those polymers because the equations were derived for short periods of time, related to equilibration time. Following the power law model, water uptake for the polymers from this library can behave very differently, ranging from Fickian to anomalous diffusion. The results for some polymers indicate slower water uptake profiles, with parameters not explained by the available literature.

Using empirical equations, both Weibull and Peleg can successfully fit the water uptake profiles for almost all polymers that equilibrate within the time of study. However, they do not explain the mechanism of water uptake. The Weibull equation was selected to build a surrogate model for water uptake, as described in Chapter 6.

Future studies should be designed to further elucidate the water uptake kinetics for this polymer library. They should include early measurements of water uptake to capture enough data points before equilibration, and longer studies are needed to capture the equilibration times and levels, for slowly equilibrating polymers.

5   Polymer selection for water uptake modeling

The Combinatorial-Computational Method (CCM) [1], developed in The New Jersey Center for Biomaterials, was used to select a representative subset of polymers from the L-tyrosine-derived polyarylate library to build a semi-empirical model for water uptake. The first six polymers were selected randomly from the available polymer group. The remaining 17 polymers were selected in two iterations of the CCM. All 23 polymers were used in training, test and validation of a semi-empirical model for water uptake, as detailed in Chapter 6.

5.1   *Materials and methods*

5.1.1   *Combinatorial-Computational Method*

The CCM is an iterative process that integrates fabrication, experiments and modeling to predict biomaterial properties and accelerate the discovery, design and optimization of materials for biomedical applications, as illustrated in Figure 5-1.

The CCM usually begins with a materials need and a virtual library of many polymers that are potential candidates to meet the materials need. A small subset of polymers is synthesized and characterized. Calculated and experimental descriptors are generated from the chemical structure of each polymer and from physico-chemical and biological data. The polymer properties and the descriptors are fed into a computational model, leading to predictions of polymer properties for all members of the original polymer library. Based on these predictions, a small number of "lead polymers" can be selected for synthesis and detailed characterization. The last step can have three possible outcomes: (a) the predictions are validated and the "lead polymers" fulfill the materials need; (b) the predictions are not sufficiently accurate, requiring a second iteration of the

CCM; and (c) the predicted lead polymers show that no appropriate materials are contained within the particular library to fulfill the materials need, and a new library must be developed [1].
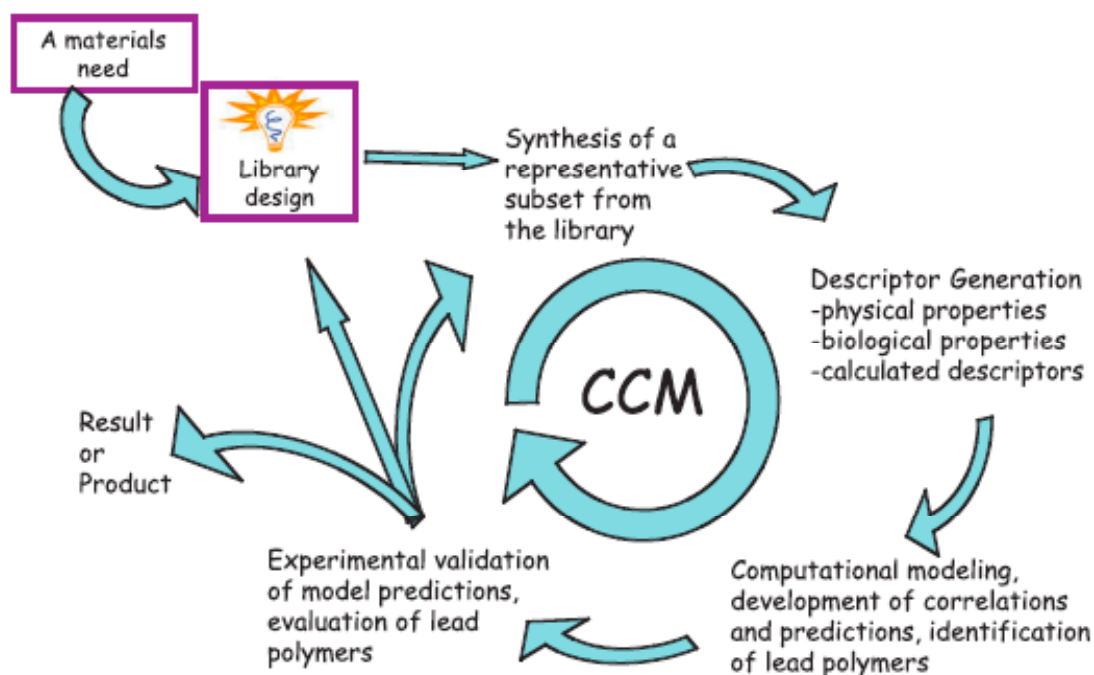
Figure 5-1: Scheme of the Combinatorial-Computational Method (CCM). Copyright ©2007 New Jersey Center for Biomaterials [1].

5.1.2 Experimental methods

Water uptake measurements after 1, 7, 14, 21, and 28 days of incubation at 37ºC in radiolabeled water, were performed for a subset of polymers of the L-tyrosine-derived polyarylate library (Table 5-1), as described in Chapter 3.

Table 5-1: Subset of the library of L-tyrosine-derived polyarylates used in this study.

Polymer[1]	Mw (kDa)[2,3]	Tg (°C)[4]	Set N°1	Set N°2	Set N°3	Final Set	Predictions
poly(DTO sebacate)	123 ± 1	16	●	●	●	●	●
poly(DTB adipate)	111 ± 3	42	●	●	●	●	●
poly(DTO succinate)	84 ± 6	43	●	●	●	●	●
poly(DTE adipate)	126 ± 7	59	●	●	●	●	●
poly(DTE glutarate)	80 ± 1	64	●	●	●	●	●
poly(DTB succinate)	145 ± 11	67	●	●	●	●	●
poly(HTH sebacate)	64 ± 5	23		●	●	●	●
poly(DTH suberate)	106 ± 2	24		●	●	●	●
poly(HTH adipate)	87 ± 2	40	●	●	●	●	●
poly(DTM sebacate)	126 ± 4	45	●	●	●	●	●
poly(DTiP adipate)	144 ± 2	55	●	●	●	●	●
poly(DTM adipate)	99 ± 3	67		●	●	●	●
poly(DTB (R)(+) methyladipate*)	61 ± 1	35			●	●	●
poly(HTE succinate)	★	78			●	●	●
poly(DTO adipate)	132 ± 2	26				●	●
poly(DTH adipate)	97.7 ± 0.2	34				●	●
poly(DTsB* (R)(+) methyladipate*)	79 ± 3	45				●	●
poly(DTsB* glutarate)	86 ± 3	46				●	●
poly(DTB glutarate)	105 ± 1	50				●	●
poly(DTM (R)(+) methyladipate*)	68 ± 1	53				●	●
poly(DTBn methyladipate*)	90 ± 1	55				●	●
poly(DTBn adipate)	69 ± 8	61				●	●
poly(HTE adipate)	★	61				●	●
poly(DTO suberate)		21					●
poly(HTH suberate)		27					●
poly(DTO glutarate)		32					●
poly(DTiB sebacate)		33					●
poly(DTH methyladipate*)		33					●
poly(DTB suberate)		37					●
poly(DTO diglycolate)		40					●
poly(DTBn sebacate)		42					●
poly(DTH glutarate)		43					●
poly(DTH diglycolate)		45					●
poly(DTsB* suberate)		46					●
poly(DTBn suberate)		47					●
poly(DTsB* adipate)		50					●
poly(DTH succinate)		53					●
poly(HTE suberate)		54					●
poly(DTiP methyladipate*)		54					●
poly(DTM suberate)		55					●
poly(DTiB adipate)		56					●
poly(DTE methyladipate*)		63					●
poly(HTE methyladipate*)		63					●
poly(DTB diglycolate)		64					●
poly(DTiB succinate)		75					●

[1]The '*' symbol indicates the presence of more than one chiral center in the polymer repeat unit.

[2]Molecular weight (Mw) was measured by THF-GPC (mean value of three different films ± SD).

[3]The '★' symbol indicates the polymers that did not dissolve in THF and thus, Mw could not be measured.

[4]Glass transition temperature (Tg) was measured by DSC for the dry polymer before pressing.

5.1.3 Computational methods

The data-mining package WEKA (Waikato Environment for Knowledge Analysis) [48] was used for the computational procedure that includes cluster analysis, decision tree analysis, and Artificial Neural Networks (ANNs). A schematic representation of this procedure is shown in Figure 5-2. A model was built for the water uptake after 1, 7, 14, 21 and 28 days of incubation.
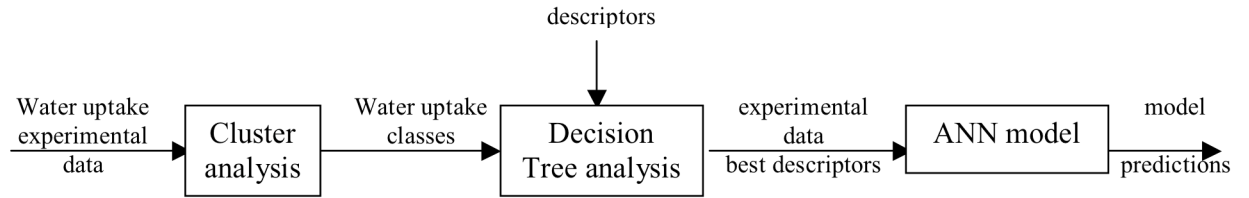
Figure 5-2: Schematic representation of the computational procedure.

5.1.3.1 Cluster analysis

Expectation-maximization (EM) [48] cluster analysis was employed to categorize the water uptake data for the polymers in the training set into three clusters or groups (i.e., low, medium, and high). EM is an iterative process consisting of an expectation (E) and a maximization (M) step. During the E step, cluster probabilities are calculated, given the current estimate of the parameters. During the M step, parameters are re-estimated to achieve maximum likelihood, using the distribution information determined in the E step. The overall likelihood is defined as

$$\prod_i \left(p_1 \cdot P_R\left[x_i|C_1\right] + p_2 \cdot P_R\left[x_i|C_2\right] + p_3 \cdot P_R\left[x_i|C_3\right] \right), \qquad (5\text{-}1)$$

where p_1, p_2, and p_3 represent the proportion of the instances i in the cluster C_1, C_2 or C_3, respectively. $P_R\left[x_i|C_1\right]$, $P_R\left[x_i|C_2\right]$, and $P_R\left[x_i|C_3\right]$ represent the probability of each cluster.

5.1.3.2 <u>Descriptors</u>

The descriptors in this study include (i) "2D" descriptors based on the chemical structure of the polymers [195], and (ii) "3D" descriptors based on the chemical structure of the polymers in implicit water or vacuum incorporating polymer conformation [106].

Two-dimensional descriptors for the entire library of 112 polymers were obtained by Smith et al. [195], using the basic molecular structure derived from the chemical formulae, and either Molecular Operating Environment (MOE, Chemical Computing Group Inc.) [196] or Dragon (Milano Chemometrics and QSAR Research Group [197]) commercial software packages. The 735 Dragon descriptors were calculated for each polymer by its monomeric unit, while the 127 MOE descriptors were calculated using chains of 32 repeat units in length. Descriptors vary from atomic and bond counting schemes to those representing the projection of a particular property onto the van der Waals surface of the molecule.

Three-dimensional descriptors were obtained by Gubskaya et al. [106] for the 45 polymers from the polyarylate library for which data on fibrinogen adsorption was available. Eleven of these 45 polymers exhibit a chiral center located in a pendent chain (DTsB) or/and in a diacid component (methyl adipate), and descriptors were calculated for both L and R isomers. Descriptors were obtained by Dragon commercial package using the 3D structures of the tetramers after structure minimization and 1 ns of molecular dynamics simulations using MacroModel v. 8.5 (Schrödinger) [198] commercial package with the generalized Born/surface area implicit solvent model [199] and the OPLS-all atom force field [200]. 721 descriptors were obtained for each implicit solvent (i.e., vacuum or water). The 3D geometrical representation was encoded in radial

distribution function descriptors, 3D-MoRSE (3D-MOlecule Representation of Structures based on Electron diffraction) descriptors, and WHIM (Weighted Holistic Invariant Molecular) descriptors [42]. Topological molecular indices were derived from the structural graph of a molecule by using the geometric distances between atoms instead of the topological distances, while GETAWAY (GEometry, Topology and Atom-Weights AssemblY) descriptors account for both geometrical and topological information [201].

5.1.3.3 <u>Decision Tree Analysis</u>

J48 (an algorithm of C4.5 decision tree family) [47, 48] was used to evaluate the significance of each descriptor with respect to the set of experimental water uptake data according to the classes identified by the cluster analysis, as explained in the introduction.

5.1.3.4 <u>Artificial Neural Networks</u>

An ANN [40, 41] is an information processing system that is inspired by the way the brain processes information. As explained in Section 2.5.3, in the WEKA data-mining package, ANN is represented by Multi-Layer Perceptron module.

For this study, all input variables were scaled to the unit interval while the learning rate and the momentum applied for updating the weights were 0.3 and 0.2, respectively. Randomization of the initial weights and shuffling of the training data were performed by varying (up to 10 times) the seed for the random number generator to achieve full convergence of predicted values.

ANN model for water uptake was built using the most significant descriptors identified by J48 decision tree analysis, and full training set. The relative absolute error

was used in comparison with the experimental error to evaluate the efficacy of each model. ANN predictions were obtained for the 56 polymers of the library (Table 5-1), whose 3D descriptors were available [106].

5.2 *Results and discussion*

5.2.1 *Iteration 1*

The first iteration of the CCM was performed using six polymers that were selected from the L-tyrosine-derived polyarylate library, upon availability and quality (i.e., high molecular weight (Mw)) (Table 5-1).

5.2.1.1 Cluster analysis

From the experimental results, a cluster analysis was performed for each time of water uptake independently (i.e., 1, 7, 14, 21 and 28 days) using the EM algorithm in WEKA. Three classes of polymers in terms of water uptake levels (i.e., low, medium and high) were selected for all time points (Table 5-2).

Table 5-2: Water uptake classes of polymers of Iteration 1 of the CCM.

Polymer[1]	Water uptake (1-28d)
poly(DTO sebacate)	LOW
poly(DTO succinate)	LOW
poly(DTB succinate)	LOW
poly(DTB adipate)	MEDIUM
poly(DTE glutarate)	MEDIUM
poly(DTE adipate)	HIGH

[1] Polymers are ordered by water uptake level.

5.2.1.2   Decision tree analysis

A J48 decision tree with full training set was applied to the six polymers classes. Two descriptors (PJI2 and LP1) were selected to fully classify the 6 polymers (Figure 5-3). Both descriptors were part of the 2D set. Further analysis of the descriptors is included at the end of this chapter.
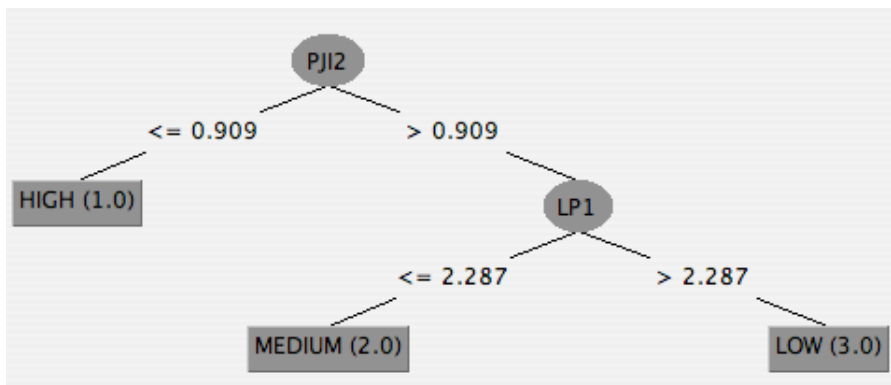
Figure 5-3: Decision tree for water uptake (1 to 28d) for Iteration 1 of the CCM.
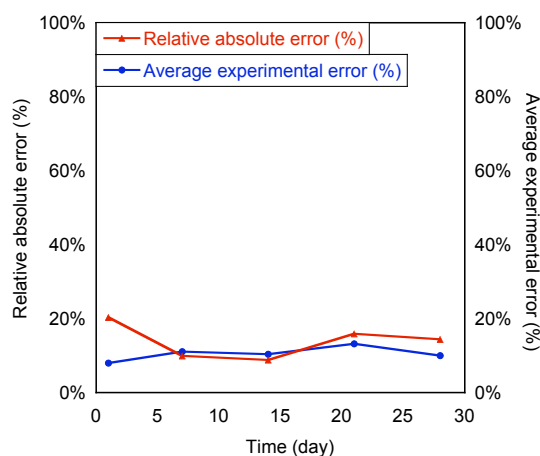
Figure 5-4: Comparison of relative absolute error of ANN and experimental error for water uptake of the 6 polymer set when using PJI2 and LP1 descriptors

5.2.1.3 Artificial neural networks

Using the previous selected two descriptors, an ANN model was built for the subset of six polymers. The average relative absolute error of the model was 13.9%, and it compares favorably with the average experimental error of 10.5% (Figure 5-4).

5.2.1.4 Predictions over rest of the library

The descriptors selected by the decision tree analysis were only 2D, which are available for the entire library [195], and thus predictions could be obtained for the complete library of 112 polymers. Using these ANN models, feasible predictions of water uptake were obtained for 50 polymers from the rest of the library of L-tyrosine-derived polyarylates, while "unfeasible predictions" (i.e., negative water uptake) were obtained for 56 polymers. Those unfeasible predictions include all the DTBn, DTiP, DTsB, HTE, HTH and HTO polymers. Also, almost all methyl adipates, poly (DTiB diglycolate) and poly(DTiB glutarate) gave unfeasible predictions, showing that the model is not applicable for many nonlinear pendant chains and all HTR polymers.

5.2.2 Iteration 2

A second iteration of the CCM was performed with 12 polymers, including the six polymers from the first iteration, three new polymers that presented unfeasible predictions in the first iteration of the CCM (poly(HTH sebacate), poly(HTH adipate) and poly(DTiP adipate)), and three that presented feasible predictions of water uptake (Table 5-1).

5.2.2.1   Cluster analysis

A cluster analysis was performed for the experimental results of the 12 polymers. Three classes of polymers in terms of water uptake levels (i.e., low, medium and high) were selected for each time point. The classification was different for 1 to 14 days as compared with the water uptake at 21 and 28 days (Table 5-3). The new polymers appeared in all three classes, and the classification for poly(DTE glutarate) changes from medium to high water uptake after 21 days (as compared with the first iteration of the CCM). This situation is possible because clusters are generated comparing individual values with the complete set, and so, if the set changes, this comparison may be affected.

Table 5-3: Water uptake classes of polymers of Iteration 2 of the CCM.

Polymer[1]	Water uptake (1-14d)	Water uptake (21-28d)
poly(HTH sebacate)	LOW	LOW
poly(DTO sebacate)	LOW	LOW
poly(DTO succinate)	LOW	LOW
poly(DTB succinate)	LOW	LOW
poly(DTH suberate)	MEDIUM	MEDIUM
poly(DTM sebacate)	MEDIUM	MEDIUM
poly(DTM adipate)	MEDIUM	MEDIUM
poly(HTH adipate)	MEDIUM	MEDIUM
poly(DTB adipate)	MEDIUM	MEDIUM
poly(DTE glutarate)	MEDIUM	HIGH
poly(DTiP adipate)	HIGH	HIGH
poly(DTE adipate)	HIGH	HIGH

[1] Polymers are ordered by water uptake level.

5.2.2.2   Decision tree analysis

Using the experimental data for the second set of 12 polymers, the principal descriptors were selected by decision tree analysis using descriptors from 2D, 3D in water and 3D in vacuum. Two descriptors were enough to fully classify the experimental

data of water uptake. Removing those two descriptors, a second decision tree was obtained with two new descriptors (Table 5-4). Descriptors selected belong to the three possible sets of descriptors (2D, 3D in vacuum and 3D in water). Further analysis of the descriptors is included at the end of this chapter.

Table 5-4: Most relevant descriptors that appear in decision tree analysis for water uptake in Iteration 2.

Time point	Descriptors[1]	Type
1-14d	PEOE_VSA-0 (2D)	Partial charge
	P1m (3Dvacuum)	WHIM
	H0e (3D water)	GETAWAY
	petitjean (2D)	Shape
21-28d	H-052 (2D)	Atom-centered fragment
	P1m (3Dvacuum)	WHIM
	PEOE_VSA-0 (2D)	Partial charge
	P1s (3Dvacuum)	WHIM

[1]Descriptors are shown in order of relevance.

5.2.2.3 Artificial neural networks

ANN models were built using the descriptors selected by decision tree analysis (two, three or four) and all the polymers as training set. Models built with more descriptors were more accurate (i.e., lower relative absolute errors respect to experimental error). The models obtained with four descriptors compare favorably with the experimental error (Figure 5-5).

5.2.2.4 Predictions over rest of the library

Using the models with four descriptors, unfeasible predictions were obtained for two polymers from the 44 remaining polymers of the library (poly(HTE succinate) and poly(DTB (R) methyl adipate)).
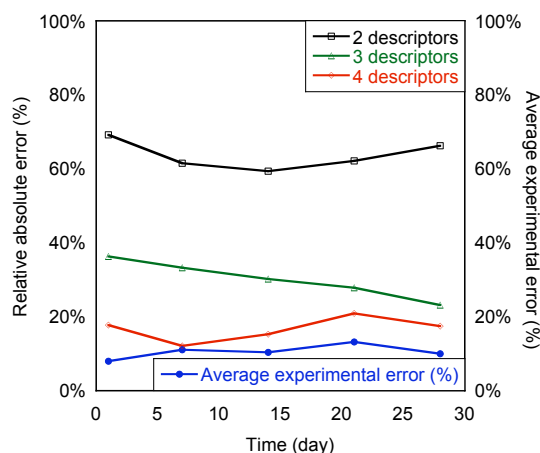
Figure 5-5: Comparison of relative absolute error of ANN and experimental error for water uptake of the second set of 12 polymers.

5.2.3 Iteration 3

A third set of polymers was used to run a third iteration of the CCM. It includes the previous 12 polymers used on the second set and the two polymers that presented unfeasible predictions (Table 5-1).

5.2.3.1 Cluster analysis

A cluster analysis was performed for the experimental results of the 14 polymers. Three classes of polymers in terms of water uptake levels (i.e., low, medium and high) were selected for each time point. The classification was different for each time of measured water uptake (Table 5-5). Both new polymers presented high levels of water uptake. In particular poly(DTB (R) methyladipate) presented water uptake higher than some other polymers in the set for more than one order of magnitude. This situation produced a change in the previous classification, in particular for the polymers that belong to the medium and high classes on previous iterations.

Table 5-5: Water uptake classes of polymers of Iteration 3 of the CCM.

Polymer[1]	Water uptake 1d	Water uptake 7d	Water uptake 14d	Water uptake 21d	Water uptake 28d
poly(HTH sebacate)	LOW	LOW	LOW	LOW	LOW
poly(DTO sebacate)	LOW	LOW	LOW	LOW	LOW
poly(DTO succinate)	MEDIUM	LOW	LOW	LOW	LOW
poly(DTB succinate)	LOW	LOW	LOW	LOW	LOW
poly(DTH suberate)	MEDIUM	MEDIUM	LOW	LOW	LOW
poly(DTM sebacate)	MEDIUM	MEDIUM	LOW	LOW	LOW
poly(DTM adipate)	MEDIUM	MEDIUM	LOW	MEDIUM	LOW
poly(HTH adipate)	MEDIUM	MEDIUM	LOW	MEDIUM	LOW
poly(DTB adipate)	MEDIUM	MEDIUM	LOW	MEDIUM	LOW
poly(DTE glutarate)	MEDIUM	MEDIUM	LOW	MEDIUM	MEDIUM
poly(DTiP adipate)	MEDIUM	MEDIUM	MEDIUM	MEDIUM	MEDIUM
poly(DTE adipate)	MEDIUM	MEDIUM	MEDIUM	MEDIUM	MEDIUM
poly(HTE succinate)	HIGH	MEDIUM	MEDIUM	MEDIUM	MEDIUM
poly(DTB (R) methyladipate)	HIGH	HIGH	HIGH	HIGH	HIGH

[1] Polymers are ordered by water uptake level.

5.2.3.2 <u>Decision tree analysis</u>

Following the same methodology than for the second iteration, four descriptors were selected to classify the water uptake for each time point, as classified as low, medium or high (Table 5-6). Descriptors selected belong to the three possible sets of descriptors (2D, 3D in vacuum and 3D in water). Further analysis of the descriptors is included at the end of this chapter.

Table 5-6: Most relevant descriptors that appear in decision tree analysis for water uptake in Iteration 3.

Time point	Descriptors[1]	Type
1d	R7e+ (3D water)	GETAWAY
	R7e+ (3D vacuum)	GETAWAY
	Gu (3D water)	WHIM
	PW5 (2D)	Shape
7d	SlogP_VSA4 (2D)	Subdivided Surface Areas
	P1s (3D vacuum)	WHIM
	SEigZ (2D)	Eigenvalue-based indices
	JGI5 (2D)	Topological (charge)
14d	SlogP_VSA4 (2D)	Subdivided Surface Areas
	HATS8v (3D vacuum)	GETAWAY
	SEigZ (2D)	Eigenvalue-based indices
	HATS8p (3D vacuum)	GETAWAY
21d	SlogP_VSA4 (2D)	Subdivided Surface Areas
	VRA1 (2D)	Eigenvalue-based indices
	SEigZ (2D)	Eigenvalue-based indices
	VRA2 (2D)	Eigenvalue-based indices
28d	SlogP_VSA4 (2D)	Subdivided Surface Areas
	H-052 (2D)	Atom-centered fragment
	SEigZ (2D)	Eigenvalue-based indices
	MATS7m (2D)	2D autocorrelation descriptor

[1]Descriptors are shown in order of relevance.

5.2.3.3 Artificial neural networks

ANN models were built using the descriptors selected by decision tree analysis (two, three or four). For the water uptake at 1 day, the models built with three or four descriptors were more accurate in terms of relative absolute errors than the model with two descriptors. For all other time points, no further improvement was obtained by the inclusion of more than two descriptors. In this iteration, models obtained did not compare favorably with the experimental error (Figure 5-6).
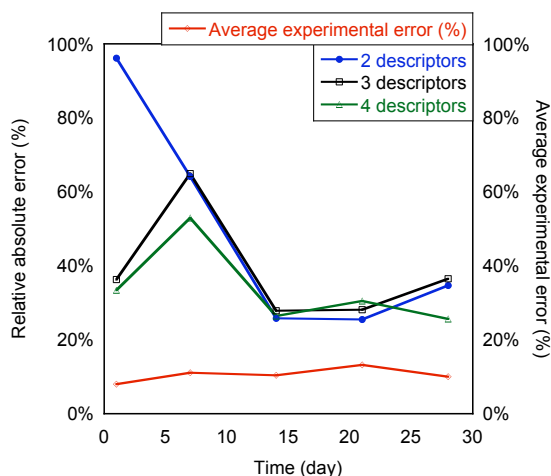
Figure 5-6: Comparison of relative absolute error of ANN and experimental error for water uptake of the third set of 14 polymers.

5.2.3.4 Predictions over rest of the library

The model was used to predict water uptake for the remaining 31 polymers of the library and feasible predictions (i.e., positive values) were obtained for all polymers. A new set of nine polymers was selected from the predictions of this iteration for validation.

Table 5-7 shows the accuracy of those predictions on the nine polymers selected as test set. Four descriptors did not significantly improve water uptake predictions. The model built with three descriptors predicted with more than 35% error the water uptake for all the tested polymers, from which predictions for poly(DTO adipate), poly(DTBn methyladipate) and poly(HTE adipate) were extremely inaccurate (relative absolute error of more than 150%).

Since these predictions were inaccurate, a separate semi-empirical model was used to model the water uptake of this polymer library, as further discussed in Chapter 6.

Table 5-7: Relative absolute error of model respect to experimental value for predictions made

with model obtained in Iteration 3.

Polymer	2 descriptors[1]	3 descriptors[1]	4 descriptors[1]
poly(DTO adipate)	152%	176%	150%
poly(DTH adipate)	38%	36%	57%
poly(DTsB (R)(+) methyladipate)	57%	38%	34%
poly(DTsB glutarate)	77%	71%	70%
poly(DTB glutarate)	32%	38%	54%
poly(DTM (R)(+) methyladipate)	85%	55%	52%
poly(DTBn methyl adipate)	409%	352%	351%
poly(HTE adipate)	193%	196%	222%
poly(DTBn adipate)	323%	119%	108%

[1] Average over all time points.

5.2.4   Analysis of descriptors

Table 5-8 summarizes all the calculated descriptors that were selected in the three iterations of the CCM. Only a few descriptors were selected in more than one iteration. Nevertheless, they represent only a few types of descriptors (i.e., topological, partial charge, atom-centered, subdivided surface area, WHIM and GETAWAY).

Several topological descriptors were selected in the different instances. SEigZ, LP1, VRA1 and VRA2 are eigenvalue-based indices. They are computed from Weighted Distance Matrices of a Hydrogen-depleted Molecular Graph. SEigZ is the eigenvalue sum from Z weighted distance matrix [202]. LP1 (Lovasz-Pelikan index) is a topological descriptor that captures information about the molecular branching. LP1 is calculated by the eigenvalues of the adjacency matrix representing the molecular graph [203]. VRA1 and VRA2 are defined by applying the Randic operator to the coefficients of the eigenvector-based index from the adjacency matrix [204]. PW5 is a Randic shape index obtained from an H-depleted molecular graph [205].

Table 5-8: Summary of descriptors on Iterations 1, 2 and 3 of the CCM.

Descriptor	Type	Set Nº1	Set Nº2	Set Nº3
SEigZ (2D)				●
LP1 (2D)	Eigenvalue-based index	●		
VRA1 (2D)	(topological)			●
VRA2 (2D)				●
PJI2 (2D)		●		
petitjean (2D)	Shape (topological)		●	
PW5 (2D)				●
JGI5 (2D)				●
PEOE_VSA-0 (2D)	Partial charge		●	
H-052 (2D)	Atom-centered fragment		●	●
SlogP_VSA4 (2D)	Subdivided surface area			●
MATS7m (2D)	2D autocorrelation descriptor			●
Gu (3D water)				●
P1m (3D vacuum)	WHIM		●	
P1s (3D vacuum)			●	●
R7e+ (3D water)				●
R7e+ (3D vacuum)	R-GETAWAY			●
H0e (3D water)			●	
HATS8v (3D vacuum)	H-GETAWAY			●
HATS8p (3D vacuum)				●

PJI2 and petitjean represent the petitjean shape index that captures the topological anisometry of the molecule (in 2D). They are obtained from the distance matrix that is derived from the molecular graph [206]. JGI5 is a mean topological charge index, used to evaluate the charge transfer between pairs of atoms and therefore, the global charge transfer in the molecule. The topological charge indices are computed using the topological level matrix, reciprocal square distance matrix and the adjacency matrix [207].

Among other 2D descriptors, PEOE_VSA-0 is a charge descriptor that is calculated using the Partial Equalization of Orbital Electronegativities (PEOE) method. The PEOE charges depend only on the connectivity of the input structures: elements, formal charges and bond orders [208]. H-052 is an atom-centered fragment, a type of descriptor that gives information about the different functional groups describing each atom by its own atom type and bonds and atom types of its first neighbors [209]. SlogP_VSA4 is a subdivided surface area descriptor. SlogP descriptors are based on an approximate accessible van der Waals surface area calculation for each atom, along with the contribution to logP(o/w) for each atom [210]. MATS7m is a Moran autocorrelation coefficient, a general index of spatial autocorrelation obtained from the molecular graph [42].

Three-dimensional descriptors include WHIM (Weighted Holistic Invariant Molecular descriptors) and GETAWAY (GEometry, Topology, and Atom-Weights AssemblY) obtained in MD simulations performed in either water or vacuum.

WHIM descriptors are based on the projections of the atoms along principal axes. They capture relevant 3D information regarding molecular size, shape, symmetry, and atom distribution with respect to invariant reference frames. Depending on the weighting scheme, different covariance matrices and different principal axes are obtained [211].

Finally, GETAWAY descriptors can be of two types, H-GETAWAY and R-GETAWAY. H-GETAWAY descriptors are calculated from the molecular influence matrix H. The diagonal elements (leverages) of H encode atomic information and represent the influence of each atom in determining the whole shape of the molecule. They account only implicitly for chemical properties of molecular atoms. They allow

consideration of chemical information provided by leverages with atomic weightings that account for specific physicochemical properties on the atomistic level [201]. R-GETAWAY descriptors are calculated from the molecular influence matrix H in combination with geometric interatomic distances in the molecule. They account for the local aspects of the molecule such as branching, cyclicity and conformational changes [201].

5.3   Conclusions

Although the model obtained in this third iteration of the CCM was not highly accurate, the CCM was shown to be very valuable in the selection of the final polymer set for which water uptake was measured. The inclusion of polymers such as poly(DTB (R) methyladipate) in the model was essential since its water uptake differs dramatically from most other polymers. With this, the final set of 23 polymers is more likely to represent the complete range of water uptake values for the entire library of polymers. In the next chapter, this result is used as starting point to build a semi-empirical model for water uptake for this polymer library.

6   Surrogate modeling of water uptake

As presented in Chapter 3, water uptake from polymers of the L-tyrosine-derived polyarylate library could not be predicted merely by looking at the hydrophobic character and/or glass transition temperature (Tg) of each polymer. In this chapter, semi-empirical modeling was applied to the Weibull parameters for water uptake, calculated in Chapter 4, using the polymers selected by the Combinatorial-Computational Method (CCM) in Chapter 5.

6.1   Methods

6.1.1   Overview

The data-mining package WEKA (Waikato Environment for Knowledge Analysis) [48] was used in this study. The methodology can be summarized in the following steps (Figure 6-1):

- Two-dimensional descriptors were previously calculated by Smith et al. [101] for the complete library of 112 polymers. Three-dimensional descriptors were calculated by Gubskaya et al. [106], for 56 polymers from the library, as described in Chapter 5.

- From those 56 polymers, 23 polymers were selected using the CCM to study water uptake, as detailed in the Chapter 5.

- Using the Weibull equation, three parameters for water uptake (WU_{eq}, b and t_{scale}) were obtained for the polymers that reached an equilibrium water uptake in the time of the study (18 polymers of the 23), as described in Chapter 4. They were used for training and test set of the model, while the 5 remaining were used for external validation of the model.

- Using all 18 equilibrated polymers, a small set of descriptors were selected to build the model.

- The subset of 18 polymers was divided into 16 for training and 2 for test, by all possible combinations, built for each training and test set, and used to predict for the rest of the 56 polymers of the library, for which descriptors were available.
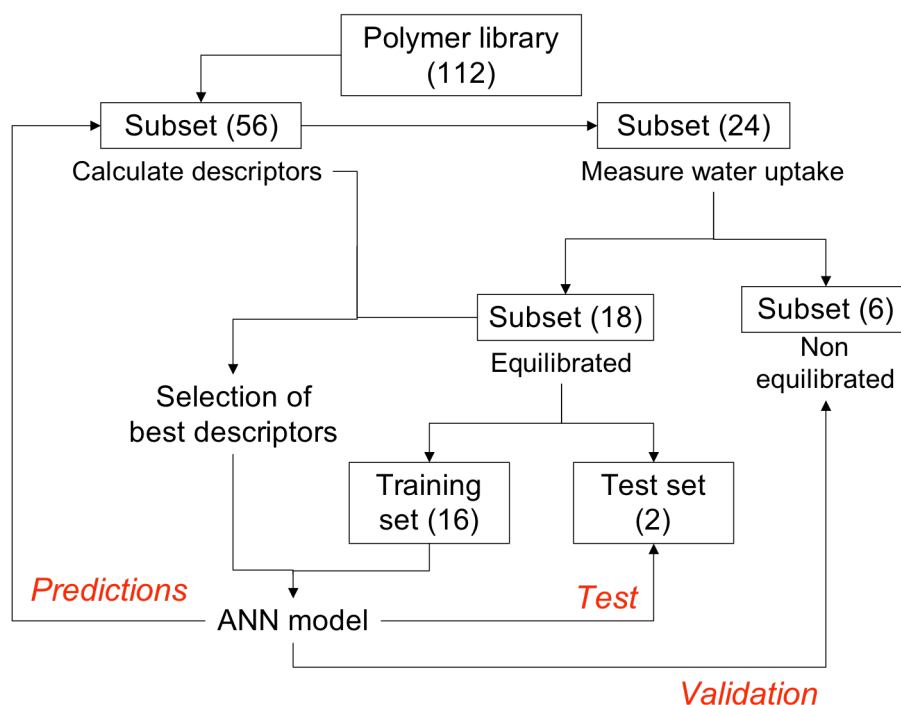
Figure 6-1: Scheme of experimental method for surrogate model of water uptake.

6.1.2 *Experimental parameters*

The three parameters of the Weibull equation described in Chapter 4 were used to build a surrogate model for water uptake (Table 6-1).

Table 6-1: Parameters for Weibull model for 18 polymers of the L-tyrosine-derived polyarylate library.

Polymer[1]	WU_{eq} (%)	b	t_{scale} (days)	relative absolute error
poly(DTB adipate) 111kDa	18.2 ± 1.2	0.42	9.18	16%
poly(DTB succinate) 145kDa	4.0 ± 0.3	0.45	0.24	3%
poly(DTBn adipate) 69kDa	32.2 ± 7.2	0.67	8.76	12%
poly(DTE adipate) 126kDa	36.2 ± 3.2	0.54	5.79	5%
poly(DTE glutarate) 80kDa	29.6 ± 3.4	0.49	12.66	7%
poly(DTiP adipate) 144kDa	27.6 ± 1.0	0.51	4.60	5%
poly(DTM adipate) 99kDa	14.5 ± 3.5	0.42	2.21	8%
poly(DTM sebacate) 126kDa	12.3 ± 2.7	0.47	0.82	7%
poly(DTO adipate) 132kDa	6.1 ± 0.3	0.24	2.79	9%
poly(DTO sebacate) 123kDa	2.7 ± 0.4	0.25	0.05	5%
poly(DTO succinate) 84kDa	3.5 ± 0.6	1.00	0.01	9%
poly(HTE adipate)	7.8 ± 1.1	0.25	0.26	6%
poly(HTE succinate)	43.1 ± 10.6	0.40	3.42	16%
poly(HTH adipate) 87kDa	18.0 ± 2.1	0.45	3.06	5%
poly(HTH sebacate) 64kDa	2.3 ± 0.4	0.53	0.08	7%
poly(DTM (R)(+) methyladipate) 68kDa	90.1 ± 8.8	0.91	3.74	12%
poly(DTsB glutarate) 86kDa	97.4 ± 4.1	0.78	10.72	11%
poly(DTsB (R)(+) methyladipate) 79kDa	136.5 ± 10.0	0.79	7.22	4%

[1] Polymers are ordered by name used in the descriptor set.

6.1.3   Descriptor selection

Starting from 2,272 descriptors (2D, 3D in vacuum and 3D in water for the 18 polymers with experimental data), useless descriptors (i.e., constant and highly variable ones) were eliminated.

A correlation based feature selection (CFS) was used to reduce the dimensionality of the descriptors for each parameter in study. CFS is a function available in WEKA that evaluates the worth of a subset of attributes (descriptors) by considering the individual predictive ability of each feature along with the degree of redundancy between them. With that, it selects a subset of attributes that are highly correlated with the parameter while removing irrelevant, redundant and noise attributes [212]. A genetic search algorithm was used in conjunction with the CFS, allowing a parallel search of the attribute space, and avoiding local optima.

Expectation-maximization (EM) [48] cluster analysis was employed to categorize the parameters of the Weibull equation for the polymers into three classes (i.e., low, medium, high).

From the descriptors pre-selected and the parameters classification, two descriptors were selected by J48 decision tree [47] with full training set, as the most significant ones with respect to the set of Weibull parameters according to the classes identified by the cluster analysis. A linear regression with all pre-selected descriptors was used to select another two descriptors, i.e., the highest positive and negative weight on the linear regression. For details on the cluster and decision tree methods, see the introduction and Chapter 5.

Three models were considered: *Model 1* was built with three descriptors selected by decision tree and linear regression; *Model 2* was built with four descriptors selected by decision tree and linear regression; and *Model 3* was built with four descriptors selected by trial and error.

6.1.4 *Artificial Neural Networks*

Using a similar approach to that in Chapter 5, a multilayer perceptron was used to build Artificial Neural Networks (ANN) models for each parameter with the four descriptors selected previously. All input variables were scaled to the unit interval while the learning rate and the momentum applied for updating the weights were 0.3 and 0.2, respectively. Randomization of the initial weights and shuffling of the training data were performed by varying the seed for the random number generator. The model obtained with each seed represents a local optimum, based on the initial weights. Thus, running enough seeds and selecting the best model among them, would allow finding the global

optimum. For the present models, a hundred ANN models were obtained with different seeds, from which the best model in terms of root mean squared (rms) error for the training set was selected.

Each model was built considering 16 polymers as training set and 2 polymers as test set, in all possible combinations. Model accuracy was evaluated by the Pearson coefficient (r) over the polymers when part of either the training or the test set, as defined in the introduction.

6.1.5   Sensitivity of the model

To evaluate the sensitivity of the model to different parameters, models were repeated with different descriptors, different number of descriptors (2, 3 and 4) and for different number of seeds.

6.2   Results and Discussion

6.2.1   Descriptors selection

6.2.1.1   Cluster analysis

Table 6-2 shows the classification obtained for each parameter by EM cluster analysis of the 18 polymers.

6.2.1.2   Descriptor dimension reduction

After removing useless descriptors, 1,912 descriptors were selected from the original 2,272 ones. CFS was used to select the descriptors that were highly correlated with the parameter of study, finishing with 475, 604 and 592 descriptors for WU_{eq}, b, and t_{scale}, respectively.

Table 6-2: Classification of polymers from EM cluster analysis of the three parameters of the Weibull equation for water uptake for the subset of the L-tyrosine-derived polyarylate library.

Polymer[1]	WU_{eq}	b	t_{scale}
poly(DTB adipate) 111kDa	LOW	MEDIUM	HIGH
poly(DTB succinate) 145kDa	LOW	MEDIUM	LOW
poly(DTBn adipate) 69kDa	MEDIUM	HIGH	HIGH
poly(DTE adipate) 126kDa	MEDIUM	MEDIUM	HIGH
poly(DTE glutarate) 80kDa	MEDIUM	MEDIUM	HIGH
poly(DTiP adipate) 144kDa	MEDIUM	MEDIUM	MEDIUM
poly(DTM adipate) 99kDa	LOW	MEDIUM	MEDIUM
poly(DTM sebacate) 126kDa	LOW	MEDIUM	LOW
poly(DTO adipate) 132kDa	LOW	LOW	MEDIUM
poly(DTO sebacate) 123kDa	LOW	LOW	LOW
poly(DTO succinate) 84kDa	LOW	HIGH	LOW
poly(HTE adipate)	LOW	LOW	LOW
poly(HTE succinate)	MEDIUM	MEDIUM	MEDIUM
poly(HTH adipate) 87kDa	LOW	MEDIUM	MEDIUM
poly(HTH sebacate) 64kDa	LOW	MEDIUM	LOW
poly(DTM (R)(+) methyladipate) 68kDa	HIGH	HIGH	MEDIUM
poly(DTsB glutarate) 86kDa	HIGH	HIGH	HIGH
poly(DTsB (R)(+) methyladipate) 79kDa	HIGH	HIGH	HIGH

[1] Polymers are ordered by name used in the descriptor set.

6.2.1.3 Decision tree analysis

Two descriptors for each parameter were selected by decision tree analysis, using those pre-selected descriptors, and the classes for each parameter (Table 6-3). For WU_{eq}, the decision tree built with the 2D descriptor nCt (number of tertiary carbon atoms (sp3)) and the 3D descriptor Mor25m in water, classified correctly 17 of the 18 polymers (Figure 6-2). Only one polymer was wrongly classified as "High" when it was "Medium". The decision tree for b, with the 2D descriptor BEHv2 and the 3D descriptors Mor27e and P2m in water, classified correctly 17 of the 18 polymers (Figure 6-3). Only one polymer was wrongly classified as "Low" when it was "Medium". Since three descriptors appeared in this tree, only the highest two (i.e., BEHv2 and MOR27e in water) were used in the ANN model. The decision tree for t_{scale}, with the 3D descriptors L3u in water and HATS5e in vacuum. classified correctly 16 of the 18 polymers. Only two polymers were

wrongly classified, one as "Low" when it was "High", and the other as "Medium" when it was "Low". Further analysis of the descriptors is included at the end of this chapter.

Table 6-3: Summary of descriptors selected by decision tree analysis.

Parameter	Descriptor	Type
WU_{eq}	nCt (2D)	Atom counts
	Mor25m (3D water)	3D-MoRSE
b	BEHv2 (2D)	BCUT
	Mor27e (3D water)	3D-MoRSE
	P2m (3D water)	WHIM
t_{scale}	L3u (3D water)	WHIM
	HATS5e	H-GETAWAY
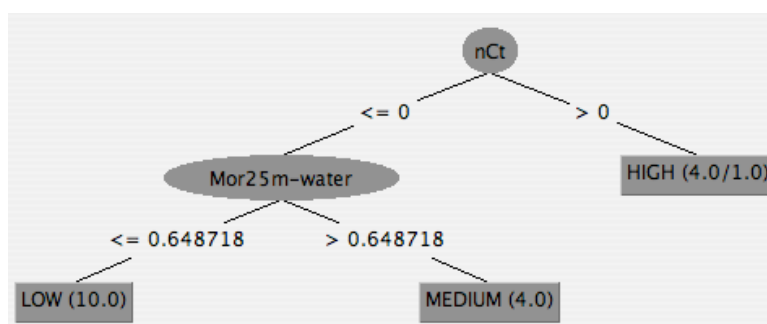
Figure 6-2: Decision tree for WU_{eq} by J48. The values in parentheses after the classes represent the correct/incorrect classification of each class.
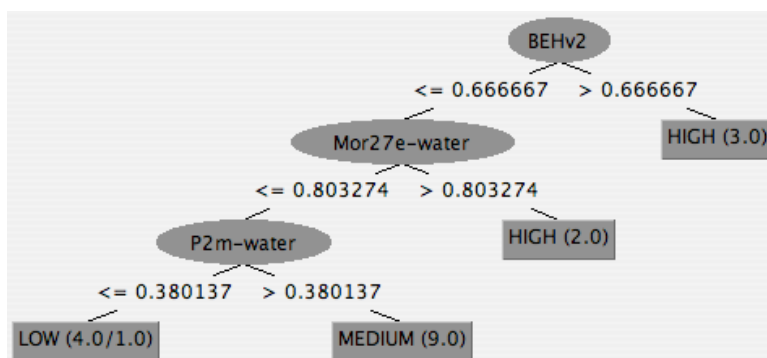
Figure 6-3: Decision tree for b by J48. The values in parentheses after the classes represent the correct/incorrect classification of each class.
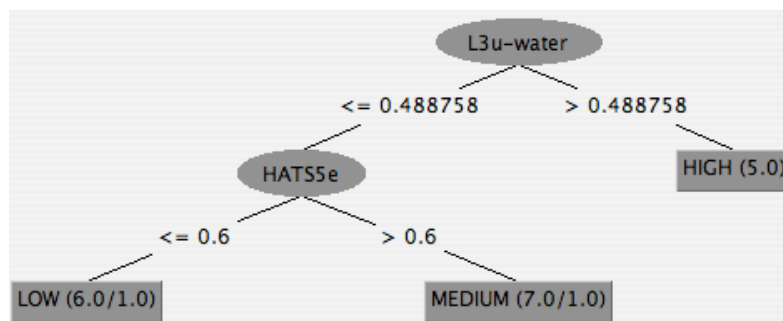
Figure 6-4: Decision tree for t_{scale} by J48.

6.2.1.4 <u>Linear regression</u>

A linear regression was applied to correlate the parameter's values and the descriptors pre-selected (Section 6.2.1.2). The two descriptors with higher weights in the linear regression were selected to build the surrogate models (Table 6-4). R8p+ in vacuum and Mor25e in vacuum were selected for WU_{eq}; Mor09p in vacuum and Mor18p in water were selected for $b;$ and R8u+ and R6e+ in vacuum were selected for t_{scale}. Further analysis of the descriptors is included at the end of this chapter.

Table 6-4: Summary of descriptors selected by linear regression.

Parameter	Descriptor	Type
WU_{eq}	R8p+ (3D vacuum)	R-GETAWAY
	Mor25e (3D vacuum)	3D-MoRSE
b	Mor09p (3D in vacuum)	3D-MoRSE
	Mor18p (3D water)	3D-MoRSE
t_{scale}	R8u+ (3D vacuum)	R-GETAWAY
	R6e+ (3D vacuum)	R-GETAWAY

6.2.2 Model 1 (3 descriptors)

Model 1 was built using three descriptors for each parameter of the Weibull equation. They correspond to the two descriptors selected by the decision tree analysis

and one descriptor selected as the most correlated with each parameter by the linear regression.

6.2.2.1 ANN model

An ANN model was built for all combinations of 16 polymers as training set and 2 as test set. Pearson correlation coefficients for training and test sets were calculated for the average prediction of each parameter for each polymer as part of either training or test set, respectively (Table 6-5). The model obtained for the equilibrium water uptake (WU_{eq}), the most important parameter of the Weibull equation, is very accurate (r = 0.89). Predictions accurately represent the relative order in water uptake of the polymers studied (Figure 6-5). Figure 6-6 and Figure 6-7 show that the accuracy of the predictions of the other two parameters (b and tscale) is inaccurate for the test set (r = 0.45 and 0.42, respectively).

Table 6-5: ANN results for the parameters of the Weibull equation, evaluated as the Pearson coefficient for training and test sets.

Parameter	Descriptors Model 1	Pearson coefficient of training sets[1]	Pearson coefficient of test sets[1]
WU_{eq}	nCt Mor25m water R8p+ vacuum	0.99	0.89
b	BEHv2 Mor27e water Mor09p vacuum	0.95	0.45
t_{scale}	L3u water HATS5e vacuum R8u+ vacuum	0.98	0.42

[1]average over all combinations of training/test sets.

Figure 6-5: Prediction versus experimental values for WU_{eq} (Model 1) for polymers as part of training (blue) and test (red) sets. Black line represents x=y. Values are presented as mean value ± SD of predictions (y-error) ± SD of experimental values (x-error).

Figure 6-6: Prediction versus experimental values for b (Model 1) for polymers as part of training (blue) and test (red) sets. Black line represents x=y. Values are presented as mean value ± SD of predictions (y-error).

Figure 6-7: Prediction versus experimental values for t_{scale} (Model 1) for polymers as part of training (blue) and test (red) sets. Black line represents x=y. Values are presented as mean value ± SD of predictions (y-error).

6.2.2.2 Predictions over test and training sets

Water uptake for each polymer was calculated from the predicted values of WU_{eq}, b and t_{scale} for each combination of training and test sets. When the predicted value of WU_{eq} or b was a negative value, it was considered 0 water uptake. When the predicted value of t_{scale} was a negative value, it was considered 10^{-10} days.

Predictions of water uptake for ten polymers were accurate, with respect to the experimental values (Figure 6-8 and Figure 6-9). The water uptake profiles of those polymers ranges from low (poly(DTO adipate), poly(HTE adipate), poly(DTM adipate), and (poly(DTB adipate)), medium (poly(DTE adipate), poly(DTE glutarate), and poly(DTBn adipate)), and high values of water uptake (poly(DTsB glutarate), poly(DTM methyladipate), and poly(DTsB methyladipate)), showing that the model can accurately predict the three classes of water uptake in this polymer library.
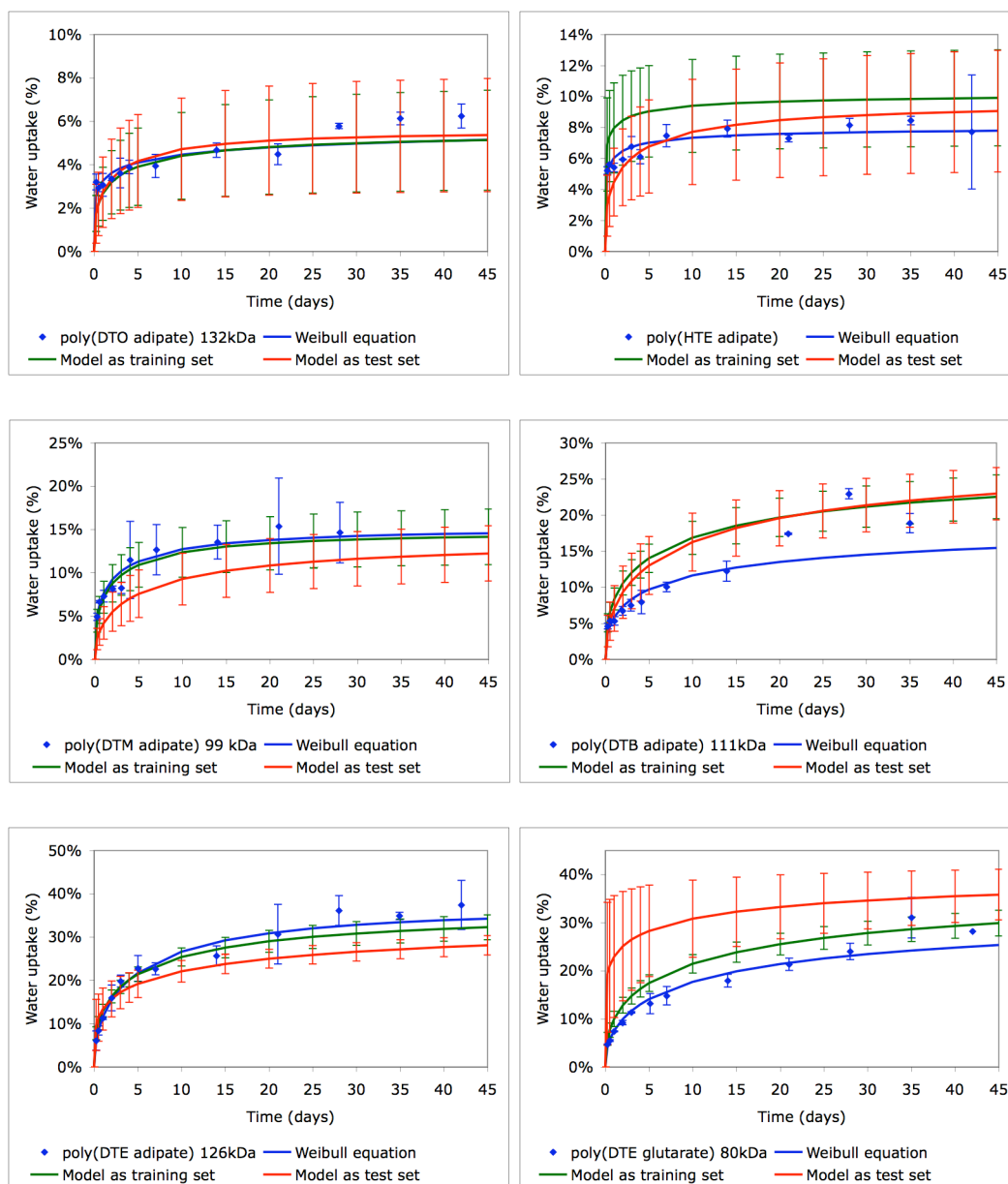
Figure 6-8: Accurate predictions of water uptake (Model 1 with 3 descriptors). Experimental values are presented as mean ± SD over three samples from separated films. Predicted values are presented as mean ± SD over the different selection of training/test sets (part 1).
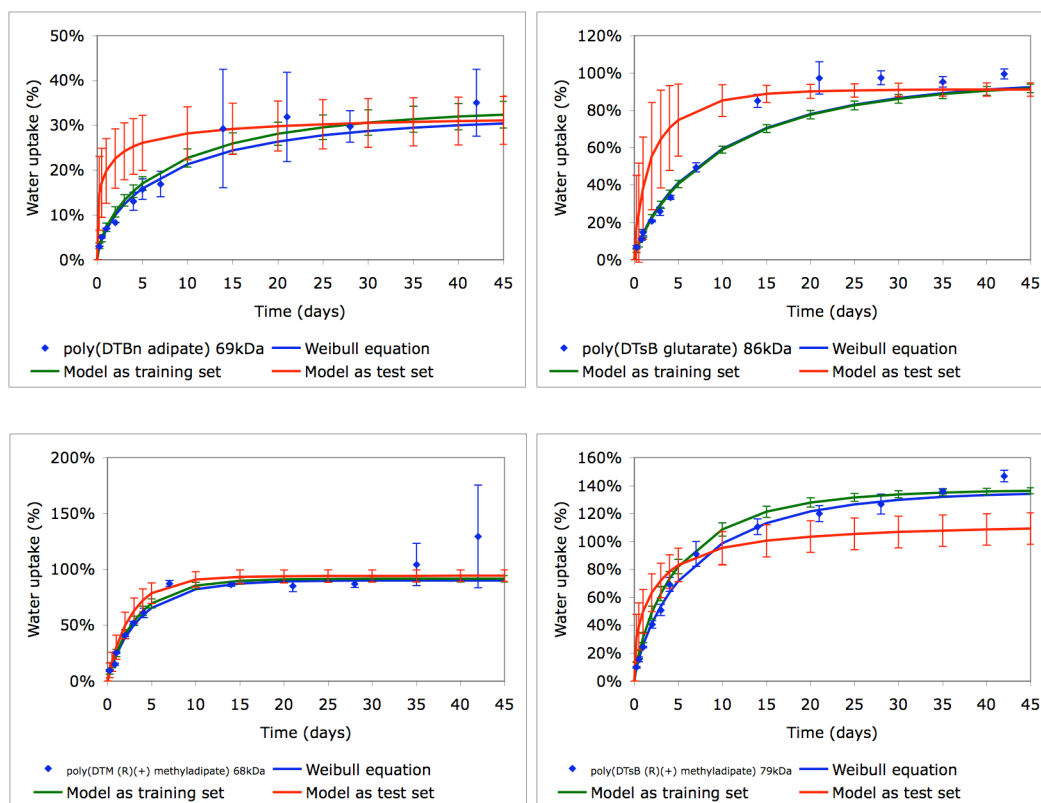
Figure 6-9: Accurate predictions of water uptake (Model 1 with 3 descriptors). Experimental values are presented as mean ± SD over three samples from separated films. Predicted values are presented as mean ± SD over the different selection of training/test sets (part 2).

Predictions of water uptake for two polymers were accurate for training set, but inaccurate for test set. Predictions overestimate water uptake for poly(DTiP adipate) (Figure 6-10), and they underestimate water uptake for poly(HTH adipate) (Figure 6-11).
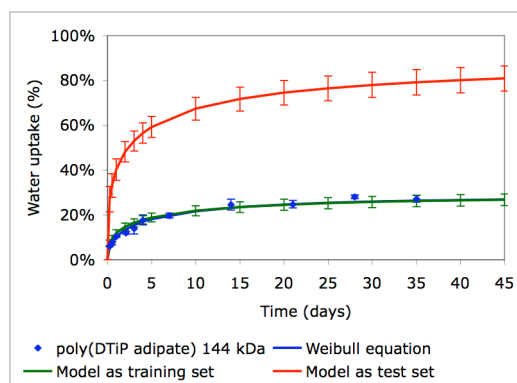
Figure 6-10: Overestimated predictions for test sets of water uptake (Model 1 with 3 descriptors). Experimental values are presented as mean ± SD over three samples from separated films. Predicted values are presented as mean ± SD over the different selection of training/test sets.
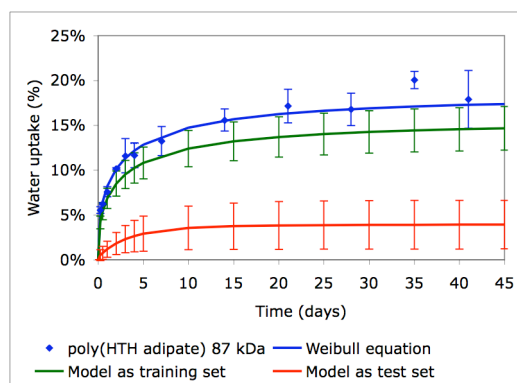
Figure 6-11: Underestimated predictions for test sets of water uptake (Model 1 with 3 descriptors). Experimental values are presented as mean ± SD over three samples from separated films. Predicted values are presented as mean ± SD over the different selection of training/test sets.

Predictions of water uptake for six polymers were inaccurate for both training and test set. Predictions overestimate water uptake for poly(DTB succinate), poly(DTO sebacate), poly(DTO succinate) and poly(HTH sebacate) (Figure 6-12). Predictions underestimate water uptake for poly(DTM sebacate) and poly(HTE succinate) (Figure 6-13).
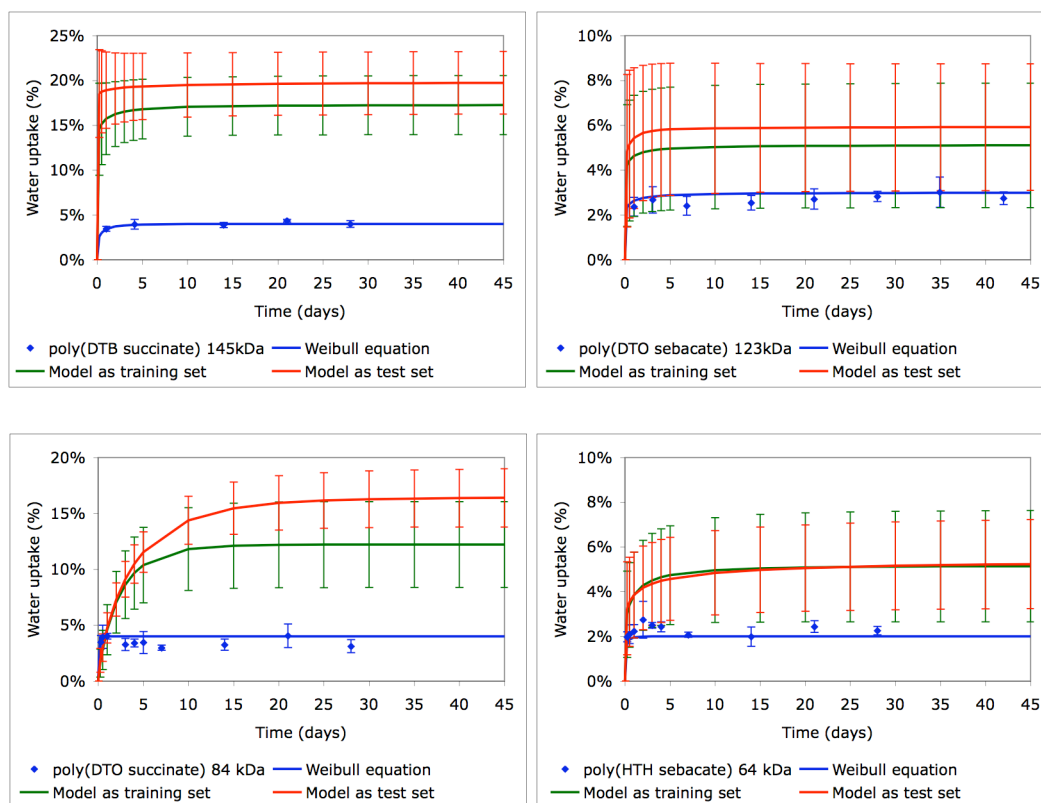
Figure 6-12: Overestimated predictions of water uptake for both training and test set (Model 1 with 3 descriptors). Experimental values are presented as mean ± SD over three samples from separated films. Predicted values are presented as mean ± SD over the different selection of training/test sets.
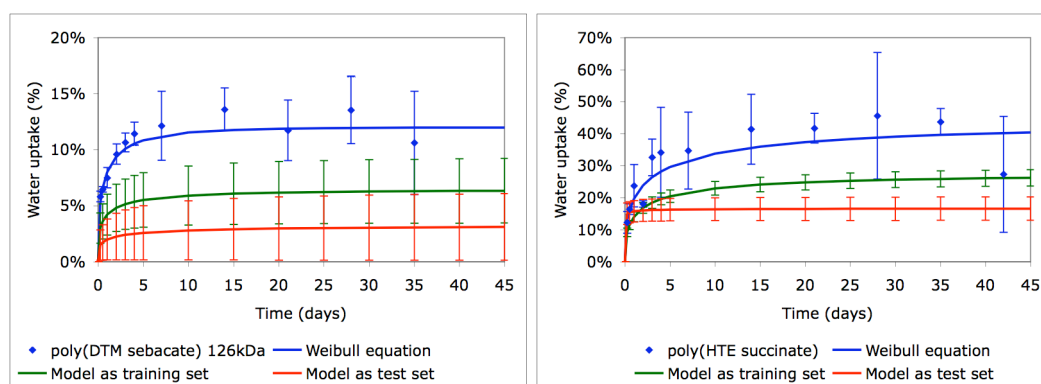
Figure 6-13: Underestimated predictions of water uptake for both training and test sets (Model 1 with 3 descriptors). Experimental values are presented as mean ± SD over three samples from separated films. Predicted values are presented as mean ± SD over the different selection of training/test sets.

6.2.3   Model 2 - 4 descriptors

Model 2 was built using four descriptors for each parameter of the Weibull equation. They correspond to the two descriptors selected by the decision tree analysis and two descriptor selected as the two most correlated with each parameter by the linear regression.

6.2.3.1   <u>ANN model</u>

An ANN model was built for all combinations of 16 polymers as training set and 2 as test set, using four descriptors obtained by decision tree and linear regression. the Pearson correlation coefficients for the training and test sets were calculated for the average prediction of each parameter for each polymer as part of either training or test set, respectively (Table 6-6). The model obtained for the equilibrium water uptake (WU_{eq}), is very accurate (r = 0.83), but less than the previous model with 3 descriptors. In general, predictions accurately represent the relative order in water uptake of the polymers studied (Figure 6-14). Predictions for the other two parameters (*b* and t_{scale}) were very inaccurate and highly variable as the selection of training and test sets were modified (Figure 6-15 and Figure 6-16).

Table 6-6: ANN results for the parameters of the Weibull equation, evaluated as the Pearson coefficient for training and test sets.

Parameter	Descriptors Model 2	Pearson coefficient of training sets[1]	Pearson coefficient of test sets[1]
WU_{eq}	nCt Mor25m water R8p+ vacuum Mor25e vacuum	0.99	0.83
b	BEHv2 Mor27e water Mor09p vacuum Mor18p water	0.99	0.45
t_{scale}	L3u water HATS5e vacuum R8u+ vacuum R6e+ vacuum	0.98	0.37

[1]Average over all combinations of training/test sets.

Figure 6-14: Prediction versus experimental values for WU_{eq} (Model 2) for polymers as part of training (blue) and test (red) sets. Black line represents x=y. Values are presented as mean value ± SD of predictions (y-error) ± SD of experimental values (x-error).
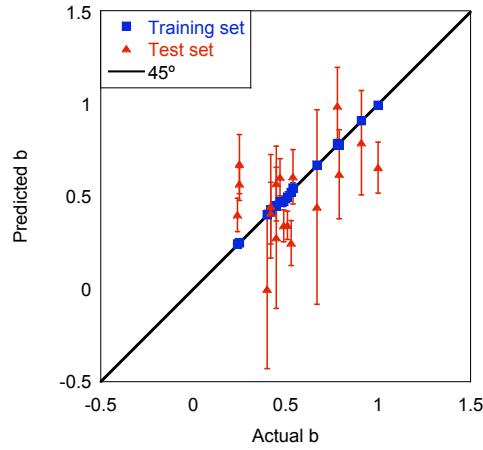
Figure 6-15: Prediction versus experimental values for *b* (Model 2) for polymers as part of training (blue) and test (red) sets. Black line represents x=y. Values are presented as mean value ± SD of predictions.
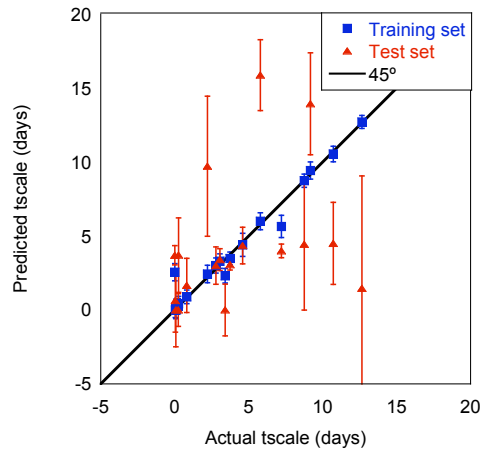
Figure 6-16: Prediction versus experimental values for t_{scale} (Model 2) for polymers as part of training (blue) and test (red) sets. Black line represents x=y. Values are presented as mean value ± SD of predictions.

6.2.3.2 Predictions over test and training sets

Water uptake for each polymer was calculated from the predicted values of WU_{eq}, *b* and t_{scale} for each combination of training and test sets. When the predicted value of WU_{eq} or *b* was a negative value, it was considered 0 water uptake. When the predicted value of t_{scale} was a negative value, it was considered 10^{-10} days.

Predictions of water uptake for six polymers (poly(DTB adipate), poly(DTBn adipate), poly(DTO adipate), poly(DTM methyladipate), poly(DTsB glutarate), and poly(DTsB methyladipate)) were accurate, with respect to the experimental values.

Predictions of water uptake for four polymers were accurate for training set, but inaccurate for test set. Predictions overestimate water uptake for poly(DTE glutarate) and poly(DTiP adipate). Predictions underestimate water uptake for poly(DTE adipate) and poly(HTE succinate).

Predictions of water uptake for eight polymers were inaccurate for both training and test set. Predictions overestimate water uptake for poly(DTB succinate), poly(DTO sebacate), poly(DTO succinate) and poly(HTH sebacate). Predictions underestimate water uptake for poly(DTM adipate), poly(DTM sebacate), poly(HTE adipate) and poly(HTH adipate).

6.2.4 *Model 3 - trial and error*

Ten other combinations of four descriptors were used to build models for the three parameters of the Weibull equation. The following represent the best models obtained for each parameter, in terms of the Pearson coefficient for the test sets.

6.2.4.1 ANN model

Table 6-7 shows the combined best predictions over test sets for each parameter. Predictions for WU_{eq} did not improve significantly, while those for b and t_{scale} improved significantly from the two previous models.

Table 6-7: ANN results for the parameters of the Weibull equation, evaluated as the Pearson coefficient for training and test sets (Model 3).

Parameter	Descriptors for Model 3	Pearson coefficient of training sets[1]	Pearson coefficient of test sets[1]
WU_{eq}	number of primary C (sp3) R8m water C-003 C-008	0.99	0.84
b	HATS7m vacuum Mor14p water MATS2e MATS5m	0.99	0.75
t_{scale}	MATS2e R2u vacuum HATS7m vacuum R4m water	0.99	0.61

[1]Average over all combinations of training/test sets.
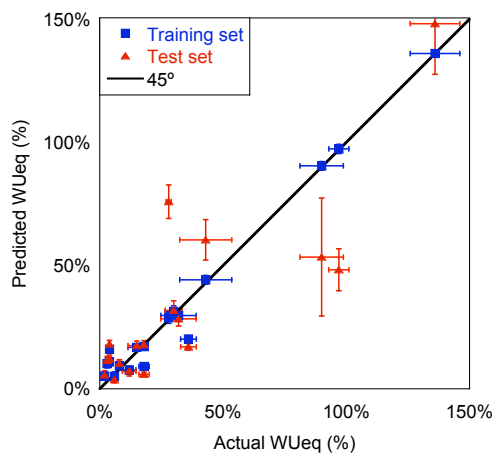
Figure 6-17: Prediction versus experimental values for WU_{eq} (Model 3) for polymers as part of training (blue) and test (red) sets. Black line represents x=y. Values are presented as mean value ± SD of predictions (y-error) ± SD of experimental values (x-error).
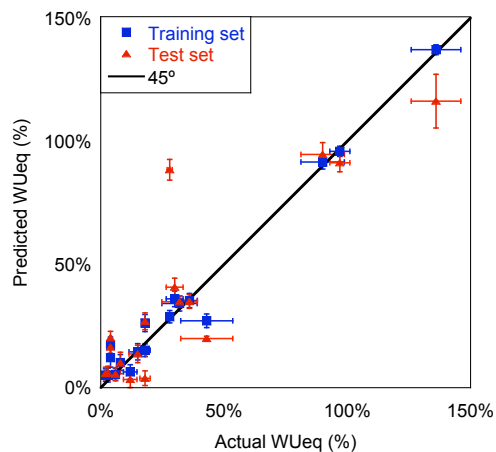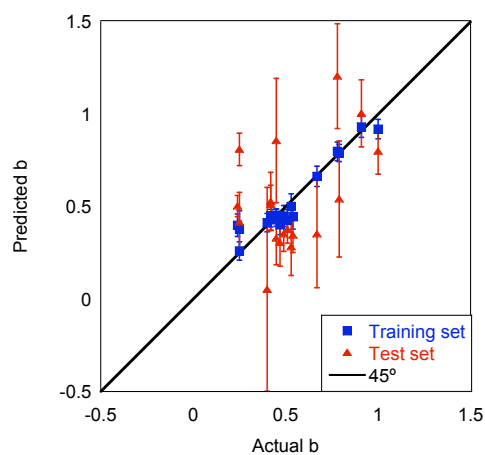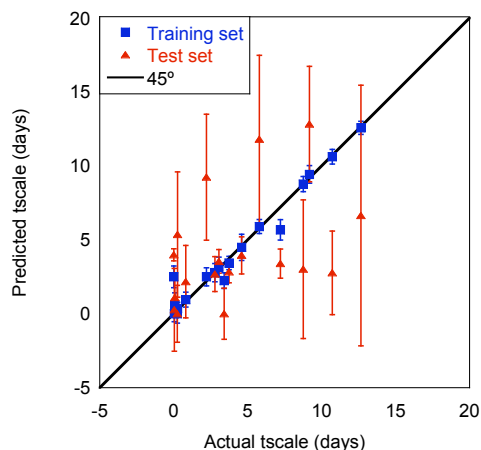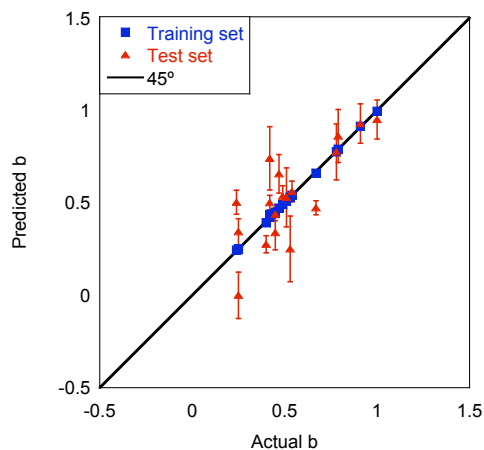
Figure 6-18: Prediction versus experimental values for *b* (Model 3) for polymers as part of training (blue) and test (red) sets. Black line represents x=y. Values are presented as mean value ± SD of predictions.
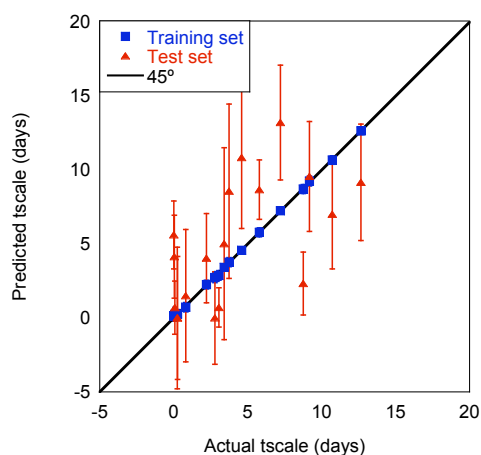
Figure 6-19: Prediction versus experimental values for t_{scale} (Model 3) for polymers as part of training (blue) and test (red) sets. Black line represents x=y. Values are presented as mean value ± SD of predictions.

6.2.4.2 Predictions over test and training sets

Predictions of water uptake for eight polymers (poly(DTB adipate), poly(DTBn adipate), poly(DTE glutarate), poly(DTM adipate), poly(DTO adipate), poly(HTE adipate), poly(HTE succinate) and poly(DTsB methyladipate)) were accurate, respect to the experimental values.

Predictions of water uptake for four polymers were accurate for training set, but inaccurate for test set. Predictions overestimate water uptake for poly(DTiP adipate), and they underestimate for poly(HTH sebacate), poly(DTM methyladipate) and poly(DTsB glutarate).

Predictions of water uptake for six polymers were inaccurate for both training and they test set. Predictions overestimate water uptake for poly(DTB succinate), poly(DTO sebacate) and poly(DTO succinate), and they underestimate for poly(DTE adipate), poly(DTM sebacate) and poly(HTH adipate).

6.2.5   *Analysis of descriptors*

Table 6-8 summarizes the descriptors used in Models 1, 2, and 3 for the three parameters of the Weibull equation. All descriptors are different from those used in the CCM to select the final subset of polymers (Chapter 5).

2D descriptors that appear in those models are functional group counts (nCt or number of tertiary carbon atoms (sp3) and number of primary carbon atoms (sp3)), atom centered fragments (C-003 and C-008), BCUT descriptors (BEHv2) and Moran 2D autocorrelations (MATS2e and MATS5m).

C-003 corresponds to the number of CHR_3 molecular subfragments, or tertiary carbon atoms, and C-008 correspond to the CHR_2X subfragments. BCUT descriptors are obtained from the positive and negative eigenvalues of the adjacency matrix, weighting the diagonal elements with atom weights [213]. 2D autocorrelations are calculated from molecular graph by summing the products of atom weights of the terminal atoms of all the paths of the considered path length (the lag) for different weighting schemes [214].

Table 6-8: Summary of descriptors used in models for parameters of the Weibull equation

Descriptor	Type	WU_{eq} M1[1]	WU_{eq} M2[1]	WU_{eq} M3[1]	b M1[1]	b M2[1]	b M3[1]	t_{scale} M1[1]	t_{scale} M2[1]	t_{scale} M3[1]
nCt	Atom counts	●	●							
number of	Atom counts			●						
primary C (sp3)										
C-003	Atom centered			●						
C-008	fragments			●						
BEHv2	BCUT				●	●				
MATS2e	2D autocorrelation						●			●
MATS5m	2D autocorrelation						●			
Mor25m	3D-MoRSE	●	●							
Mor25e	3D-MoRSE		●							
Mor27e	3D-MoRSE				●	●				
Mor09p	3D-MoRSE				●	●				
Mor14p	3D-MoRSE						●			
Mor18p	3D-MoRSE					●				
L3u	WHIM							●	●	
HATS5e	H-GETAWAY							●	●	
HATS7m	H-GETAWAY						●			●
R8p+	R-GETAWAY	●	●							●
R4m	R-GETAWAY									
R8m	R-GETAWAY			●						
R2u	R-GETAWAY									●
R8u+	R-GETAWAY							●	●	
R6e+	R-GETAWAY								●	

[1]M1, M2, and M3 represent Models 1, 2 and 3, respectively.

3D descriptors correspond to 3D-MoRSE descriptors (Mor25m, Mor27e, Mor14p and Mor18p in water, Mor25e and Mor09p in vacuum), WHIM descriptors (L3u in water), H-GETAWAY descriptors (HATS7m and HATS5e in vacuum), and R-GETAWAY descriptors (R4m and R8m in water, R2u, R8p+, R8u+ and R6e+ in vacuum).

3D-MoRSE (MOlecule Representation of Structures based on Electron diffraction) descriptors are calculated by summing atom weights viewed by a different angular scattering function. They provide 3D information from the 3D coordinates by using the same transform as in electron diffraction (which uses it to prepare theoretical scattering curves) [215].

WHIM (Weighted Holistic Invariant Molecular descriptors) descriptors are based on the projections of the atoms along principal axes. They capture relevant 3D information regarding molecular size, shape, symmetry, and atom distribution with respect to invariant reference frames. Depending on the weighting scheme, different covariance matrices and different principal axes are obtained [211].

H-GETAWAY (GEometry, Topology, and Atom-Weights AssemblY) descriptors are calculated from the molecular influence matrix H. The diagonal elements (leverages) of H encode atomic information and represent the influence of each atom in determining the whole shape of the molecule. They account only implicitly for chemical properties of molecular atoms. They allow consideration of chemical information provided by leverages with atomic weightings that account for specific physicochemical properties on the atomistic level [201].

R-GETAWAY descriptors combine the information of the H matrix with geometric interatomic distances in the molecule, accounting for the local aspects of the molecule such as branching, cyclicity and conformational changes [201].

6.2.6   Sensitivity of models

6.2.6.1   <u>Sensitivity to descriptors</u>

Using ten different sets of four descriptors, different ANN models were built, with very different results depending on which descriptors were selected (Table 6-9). This result shows that the accuracy of the predictions over test sets for any of the Weibull parameters is highly dependent on the selection of descriptors, while the accuracy over training sets is not affected.

6.2.6.2   Sensitivity to number of descriptors

Model 2 and Model 3 were repeated with the first two and three descriptors, with very different results (Table 6-10, Table 6-11, Table 6-12, Table 6-13, Table 6-14 and Table 6-15). For both sets, the use of only two descriptors resulted in less accurate models. For Model 2, the use of three descriptors resulted in better accuracy on the predictions of test sets (Model 1), in particular for $WUeq$ (Figure 6-5). In contrast, Model 3 required the fourth descriptor to obtain accurate predictions for b and t_{scale}.

Table 6-9: Pearson coefficient for training and test sets for ANN models for WU_{eq}, b, and t_{scale} using different groups of four descriptors.

Parameter		Pearson coefficient of Training set	Pearson coefficient of Test set
WU_{eq}	Minimum	0.93	0.22
	Maximum	0.99	0.84
	Average	0.98	0.54
	SD	0.02	0.22
	n	10	10
b	Minimum	0.95	-0.16
	Maximum	0.99	0.75
	Average	0.98	0.34
	SD	0.01	0.30
	n	10	10
t_{scale}	Minimum	0.82	-0.05
	Maximum	0.99	0.61
	Average	0.97	0.35
	SD	0.06	0.25
	n	9	9

Table 6-10: ANN results for WU_{eq}. Effect of number of descriptors for Model 2.

Descriptors	Pearson coefficient of training sets	Pearson coefficient of test sets
nCt Mor25m water	0.97	0.74
nCt Mor25m water R8p+ vacuum	0.99[1]	0.89[1]
nCt Mor25m water R8p+ vacuum Mor25e vacuum	0.99	0.83

[1]Correspond to model 1.

Table 6-11: ANN results for b. Effect of number of descriptors for Model 2

Descriptors	Pearson coefficient of training sets	Pearson coefficient of test sets
BEHv2 Mor27e water	0.84	0.44
BEHv2 Mor27e water Mor09p vacuum	0.95[1]	0.45[1]
BEHv2 Mor27e water Mor09p vacuum Mor18p water	0.99	0.45

[1]Correspond to model 1.

Table 6-12: ANN results for t_{scale}. Effect of number of descriptors for Model 2

Descriptors	Pearson coefficient of training sets	Pearson coefficient of test sets
L3u water HATS5e vacuum	0.89	0.19
L3u water HATS5e vacuum R8u+ vacuum	0.98[1]	0.42[1]
L3u water HATS5e vacuum R8u+ vacuum R6e+ vacuum	0.98	0.37

[1]Correspond to model 1.

Table 6-13: ANN results for WU_{eq}. Effect of number of descriptors for Model 3.

Descriptors	Pearson coefficient of training sets	Pearson coefficient of test sets
number of primary C (sp3) R8m water	0.95	0.76
number of primary C (sp3) R8m water C-003	0.99	0.85
number of primary C (sp3) R8m water C-003 C-008	0.99	0.84

Table 6-14: ANN results for b. Effect of number of descriptors for Model 3.

Descriptors	Pearson coefficient of training sets	Pearson coefficient of test sets
HATS7m vacuum Mor14p water	0.73	-0.02
HATS7m vacuum Mor14p water MATS2e	0.91	-0.11
HATS7m vacuum Mor14p water MATS2e MATS5m	0.99	0.75

Table 6-15: ANN results for t_{scale}. Effect of number of descriptors for Model 3.

Descriptors	Pearson coefficient of training sets	Pearson coefficient of test sets
MATS2e R2u vacuum	0.64	-0.07
MATS2e R2u vacuum HATS7m vacuum	0.86	0.05
MATS2e R2u vacuum HATS7m vacuum R4m water	0.99	0.61

6.2.6.3   <u>Sensitivity to selection of test set</u>

As previous results showed, predictions may be very sensitive to the selection of training and test sets. Table 6-16 summarizes these results in terms of variability of predictions over different test sets. Depending on the polymer, the standard deviation of the predictions can be as low as 4%, and as big as 1600% of the predicted value. This result shows that the predicted values must be used as a reference and experiments are always needed for validation.

6.2.6.4   <u>Sensitivity to number of seeds</u>

As mentioned in Section 6.1.4, the initial weights are determined by the random seed number. Using descriptors selected in Model 2, and only one selection of training (16 polymers) and test set (2 polymers), an ANN model was built for 200 different random seeds. Figure 6-20, Figure 6-21 and Figure 6-22 show the rms error for predictions with different seed numbers, for WU_{eq}, b and t_{scale}, respectively. The average error of training set was lower than the test set, while the lowest error for test set was lower than for training set. The model is not trained with the test set, and thus it is not possible to select the best seed for the test seed until the test set is measured. For this reason, the best seed in terms of training set error was used to build the previously discussed models, after running 100 seeds, which showed to be enough to converge the lowest error for training set.
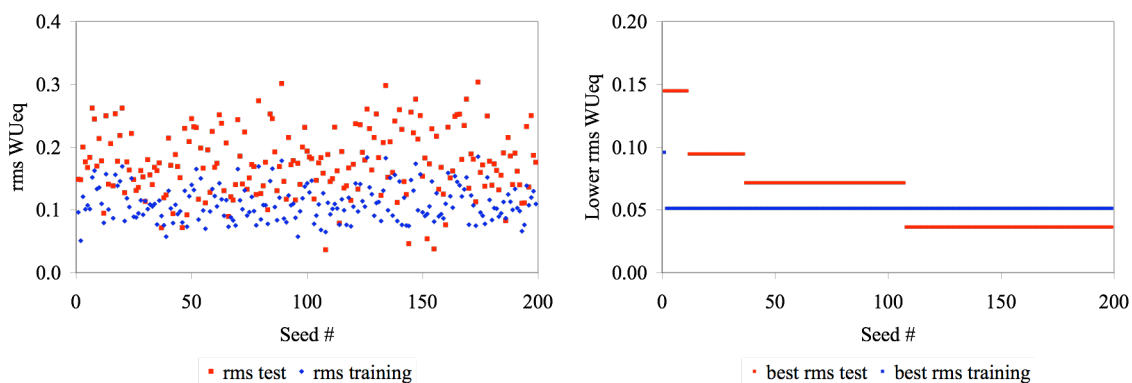
Figure 6-20: Left: Root mean squared error for predictions for WU_{eq} over training and test sets with different seeds. Right: Cumulative best rms for training and test sets.

Table 6-16: Sensitivity of training-test set selection, in term of SD over average of predicted value for each polymer as part of the test set.

Parameter	SD /average of predictions (%)	Model 1	Model 2	Model 3
WU_{eq}	Minimum	4%	4%	6%
	Maximum	97%	1629%	54%
	Average	26%	160%	20%
	SD	27%	397%	15%
	n	18	18	18
b	Minimum	11%	16%	8%
	Maximum	1035%	336%	71%
	Average	89%	58%	21%
	SD	237%	77%	17%
	n	18	18	18
t_{scale}	Minimum	10%	12%	23%
	Maximum	1033%	521%	545%
	Average	123%	107%	127%
	SD	232%	139%	131%
	n	18	18	18
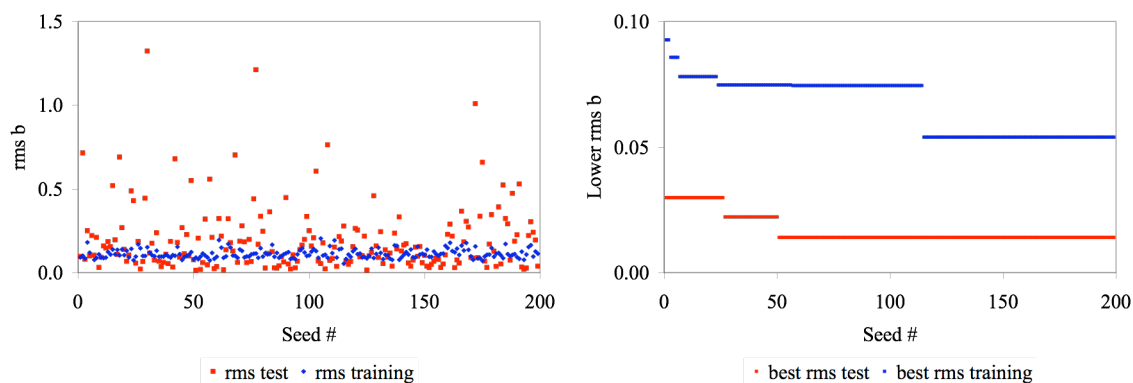
Figure 6-21: Left: Root mean squared error for predictions for *b* over training and test sets with different seeds. Right: Cumulative best rms for training and test sets.
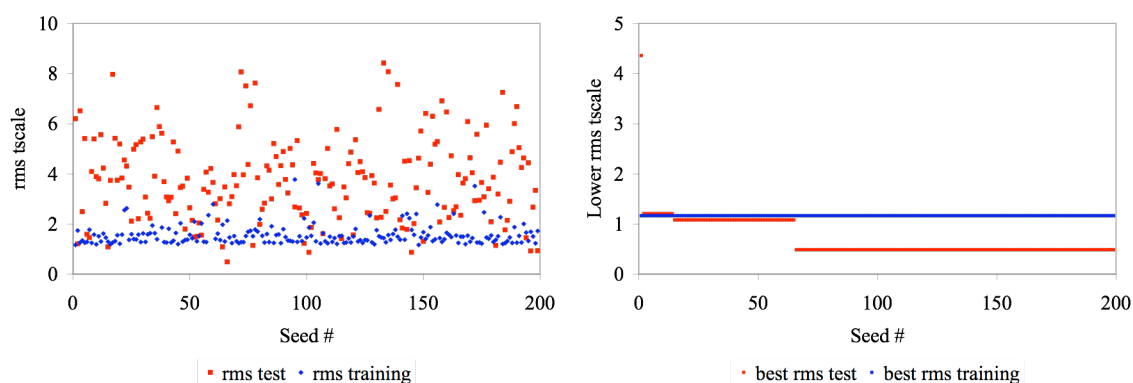
Figure 6-22: Left: Root mean squared error for predictions for t_{scale} over training and test sets with different seeds. Right: Cumulative best rms for training and test sets.

6.2.7 Comparison of models

6.2.7.1 Predictions

The outcomes of the three models do not show any correlations with polymer structure (i.e., no dependence on identity of either the alkyl ester or diacid component). Predictions of water uptake of four polymers were accurate using all models: poly(DTB adipate), poly(DTBn adipate), poly(DTO adipate), and poly(DTsB methyladipate). Predictions overestimate the water uptake of four polymers using all models: poly(DTB succinate), poly(DTiP adipate), poly(DTO sebacate), and poly(DTO succinate).

Predictions underestimate the water uptake of two polymers using all models: poly(DTM sebacate and poly(HTH adipate). For all other polymers, the accuracy on the predictions of water uptake depended on the model used.

6.2.7.2   Validation set

Using the three previous models, predictions were made for the 5 polymers that were left out of the training and test sets because their water uptake did not equilibrate and thus, the Weibull equation could not be used. For four of the five polymers, Model 3 accurately predicts water uptake profiles for the beginning of the water uptake process (until 21 days for poly(DTH suberate), until 7 days for poly(DTB (R) methyladipate), poly(DTH adipate) and poly(DTB glutarate)) (Figure 6-23).

Predictions for the fifth polymer, poly(DTBn methyladipate) are shown in Figure 6-24). This polymer has a chiral center, and predictions were obtained for the option R and L isomers, separated or averaged. Accurate predictions were obtained with Model 1 and 2, particularly for the L isomers.

6.2.7.3   Predictions over rest of the library

For each training and test set selection, predictions of each of the three Weibull parameters were made for the rest of the library (56 polymers for which descriptors were available), using each of the three models discussed previously. Water uptake for each polymer was then calculated from the predicted values of WU_{eq}, b and t_{scale} for each combination of training and test sets. When the predicted value of WU_{eq} or b was a negative value, it was considered 0 water uptake. When the predicted value of t_{scale} was a negative value, it was considered 10^{-10} days.
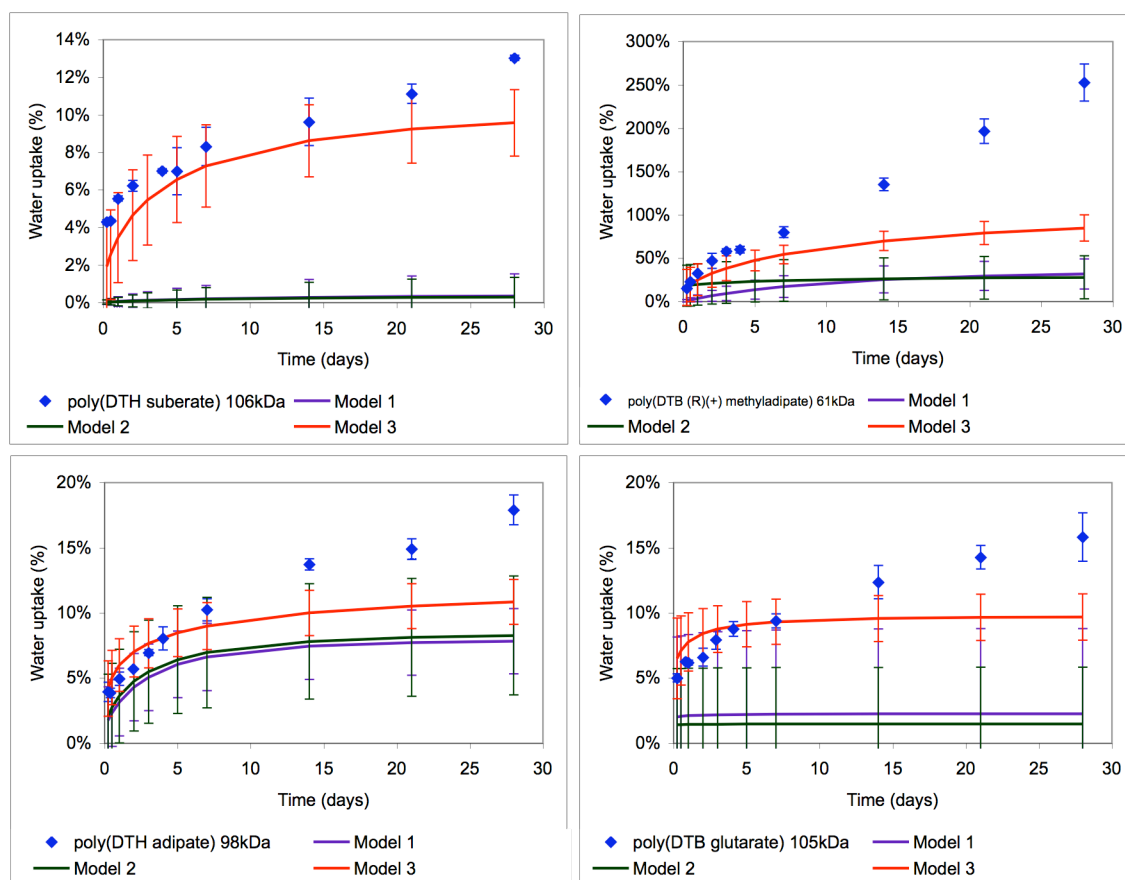
Figure 6-23: Predictions of water uptake for validation set (Models 1, 2 and 3). Experimental values are presented as mean ± SD over three samples from separate films. Predicted values are presented as mean ± SD over the different selection of training/test sets.
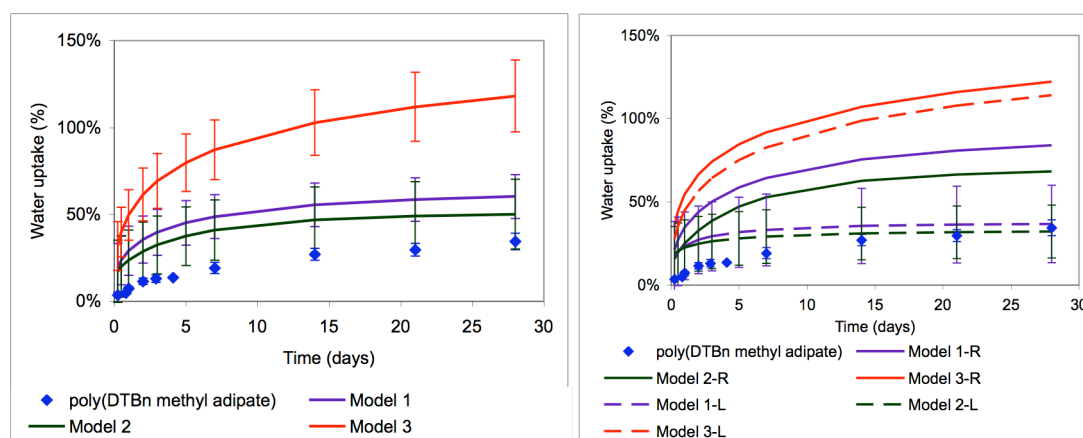
Figure 6-24: Predictions of water uptake for poly(DTBn methyladipate) (Models 1, 2 and 3). Experimental values are presented as mean ± SD over three samples from separate films. Predicted values are presented as mean ± SD over the different selection of training/test sets. Left figure represents average predictions considering R and L isomers. Right figure represents independent predictions for R or L isomers.

Comparing predictions of water uptake after 28 days of models 1 and 2 (Figure 6-25 and Figure 6-26, respectively), there are important differences in the predictions of five polymers (poly(DTBn (R) methyladipate) poly(DTE (L) methyladipate), poly(DTH (L) methyladipate), poly(DTsB (L) adipate), and poly(DTsB (R) suberate)). Even with those differences, those polymers belong to the same class of water uptake (i.e., low, medium, and high) in both predictions.

Comparing model 3 (Figure 6-27) and model 1 or 2, there are more differences. Predictions for nine polymers were higher in model 3 than in the other two models (poly(DTB (L) methyladipate), poly (DTB diglycolate), poly(DTBn (L) methyladipate), poly(DTBn (R) methyladipate), poly(DTH diglycolate), poly(DTiB adipate), poly(DTiB succinate), poly(DTM (L) methyladipate) and poly(HTE succinate)). Predictions for ten polymers were lower in Model 3 than in the other two models (poly(DTE (R) methyladipate, poly(DTH succinate), poly(DTiB sebacate), poly(DTsB (R) adipate), poly(DTsB (L) adipate), poly(DTsB (L) suberate), poly(DTsB (R) suberate), poly (HTE (L) methyladipate), poly(HTE (R) methyladipate), and poly(HTE suberate)).

Both models 1 and 3 predict low levels of water uptake for DTM (1-16%), DTO (1-21%) and HTH (5-13%) polymers (with the exception of methyladipates); low to intermediate levels of water uptake for DTBn (15-30%) and DTE (19-30%) polymers (with the exception of methyladipates), glutarate (2-29%) and suberate (1-30%) polymers (with the exception of DTsB), and sebacate (2-31%) polymers (with the exception of DTiB); intermediate levels of water uptake for succinate (11-64%) polymers (with the exception of DTiB in Model 3); medium to high levels of water uptake for DTiB (42 to

159%) polymers; high levels of water uptake for DTiP methyladipates (103-139%); and different levels of water uptake for DTH (1-87%), adipate (4-121%), and methyladipate (12-128%) polymers.

The main differences in predictions of model 1 and 3 are that only model 1 predicts that all DTB polymers have low values of water uptake (less than 35%), while model 3 predicts values for DTB polymers up to 98%. Model 1 predicts only high values of water uptake for DTsB polymers (86-130%), while model 3 has predictions from 8% for that type of polymer. Model 1 predicts low values of water uptake (10-25%) for HTE polymers (with the exception of methyladipate), while Model 3 has higher predictions for some polymers (up to 44%). Model 1 predicts low levels of water uptake for diglycolate polymers (1-15%), while model 3 predicts higher values (11-63%) for those polymers. Finally, each model predicts a different order of DTiB polymers: succinate < adipate < sebacate for model 1, and sebacate < adipate < succinate for model 3.

Figure 6-28 shows the overall profiles of water uptake predicted with model 3. It shows that different polymers show not only different values at 28 days, but also different profiles and times of equilibration.
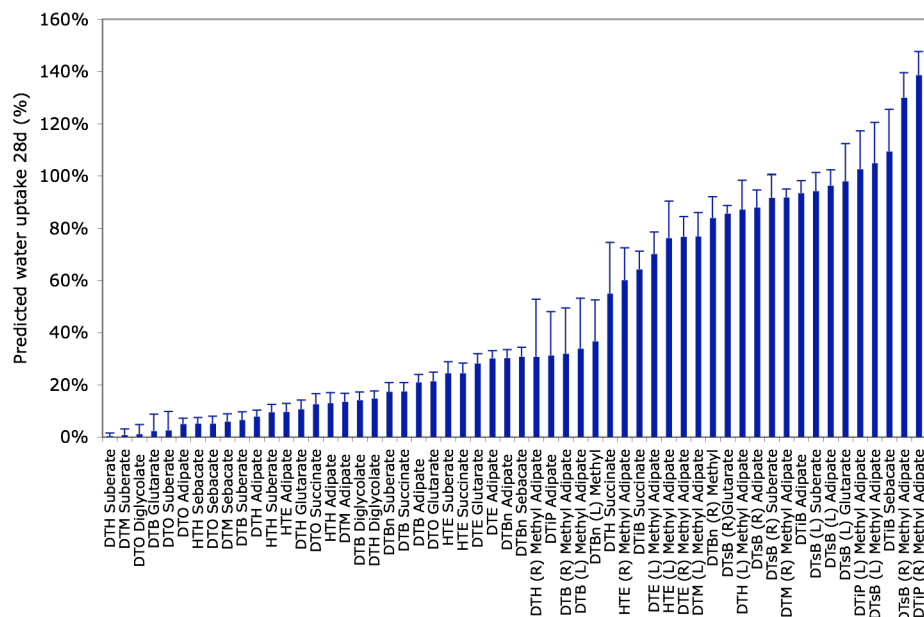
Figure 6-25: Predictions of the water uptake at 28 days over 56 polymers of the polymer library (Model 1).

Values are presented as mean value ± SD of the predicted value for each training/test set combination.

Polymers are ordered from lowest to highest water uptake predicted values.
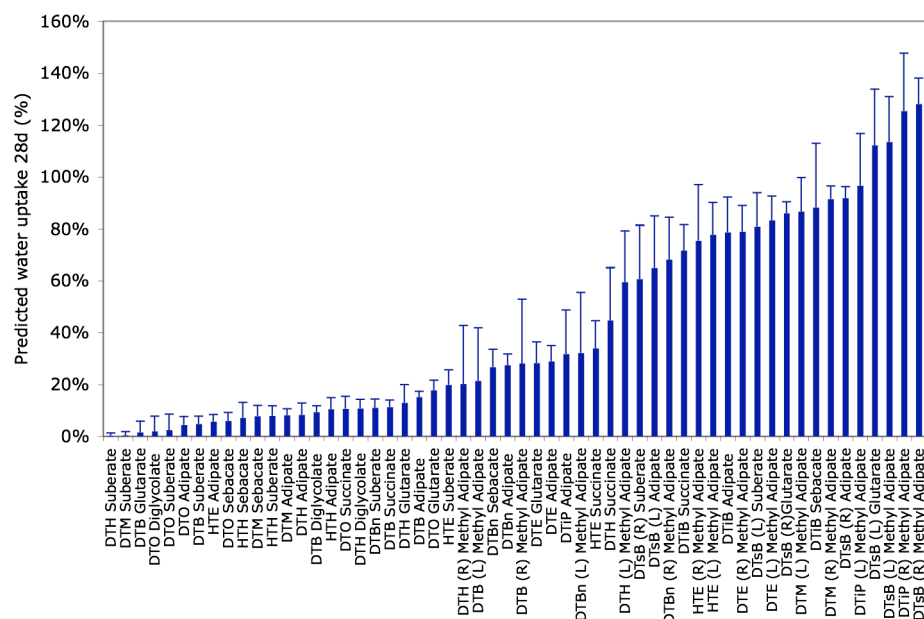
Figure 6-26: Predictions of the water uptake at 28 days over 56 polymers of the polymer library (Model 2).

Values are presented as mean value ± SD of the predicted value for each training/test set combination.

Polymers are ordered from lowest to highest water uptake predicted values.

Figure 6-27: Predictions of the water uptake at 28 days over 56 polymers of the polymer library (Model 3). Values are presented as mean value ± SD of the predicted value for each training/test set combination. Polymers are ordered from lowest to highest water uptake predicted values.

The predictions obtained can be used as a guideline for which polymers present low, medium and high levels of water uptake. If one application requires one of those levels of water in the polymer matrix, a subset can be selected from the prediction, and validated experimentally. The need for experiments does not disappear with modeling, it only allows a more focused design and more chances to find the right polymer with fewer experiments.
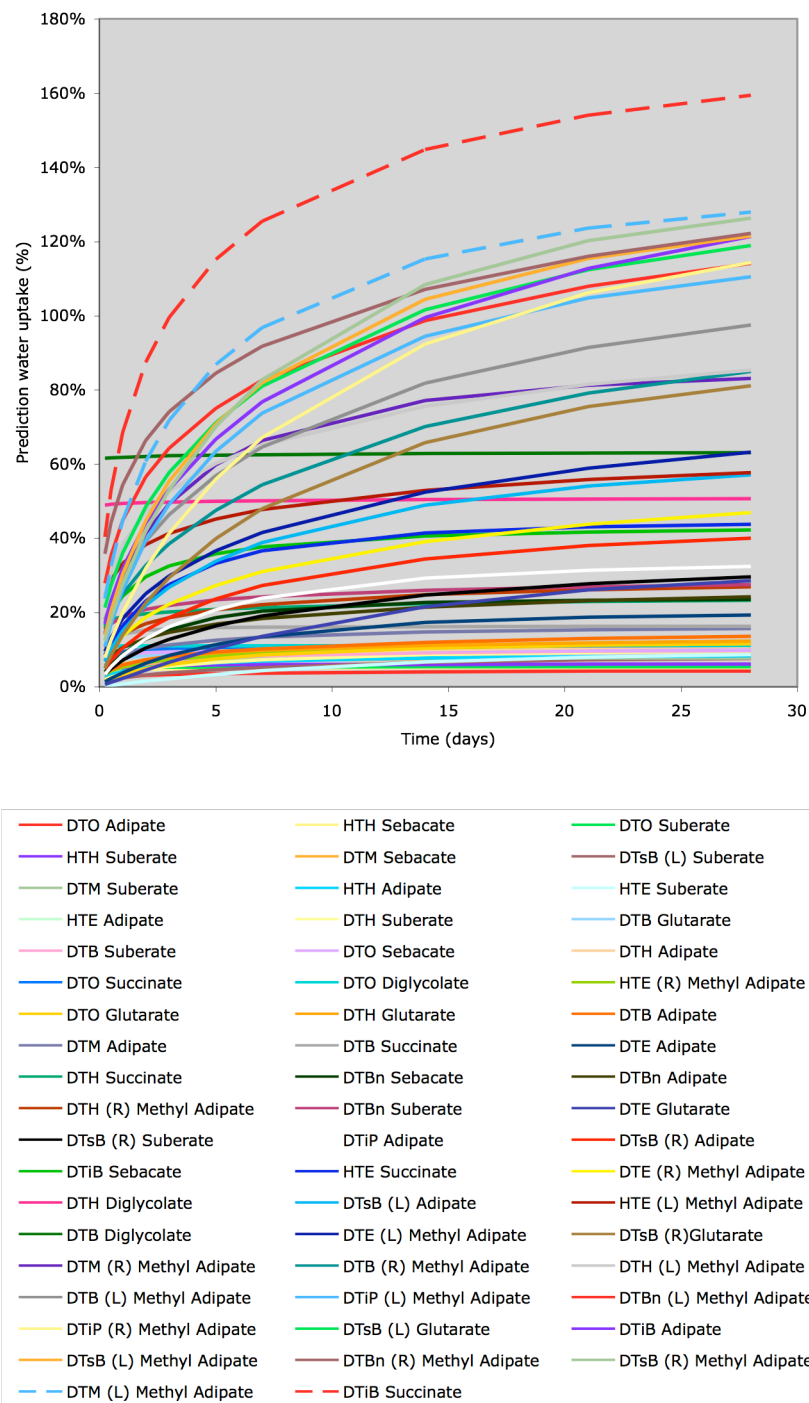
Figure 6-28: Predictions over 56 polymers of the polymer library (Model 3). Values are presented as mean value of the predicted value for each training/test set combination. Polymers are ordered from lowest to highest water uptake predicted values.

6.3 Conclusions

A surrogate model was built to predict water uptake of a polymer sub-library of 56 L-tyrosine-derived polyarylates using only 18 polymers for training (32% of the sub-library) and either three or four descriptors selected from a large set descriptors, calculated from either 2D or 3D structures. Those descriptors included atom counts; 3D information about electron diffraction (3D-MoRSE); molecular size, shape, symmetry and atom distribution (WHIM); and chemical properties of molecular atoms, branching, cyclicity and conformational changes (GETAWAY).

Three models were built using different number of descriptors (3 or 4). Accuracy depended on the descriptors used, considering 2 of the 18 polymers as test set, in all possible combinations. All models were able to accurately predict low, intermediate and high levels of water uptake for up 10 of the 18 polymers. Some models were able to predict water uptake for five polymers of the validation set that were not used in the descriptor selection.

Using those models, predictions were obtained for the rest of the sub-library. Those predictions must be used as a reference of order of magnitude and ranking of polymers in terms of water uptake, and not in terms of absolute values.

Limitations of this model include: (i) it needs experimental data to train the model; (ii) the descriptors give a reference of relevant parameters to the target property, but they cannot explain the mechanism; (iii) experimental measurements must be performed to validate the predictions; (iv) for new polymers outside of the sub-library, new descriptors must be generated, which is time consuming due to the need for molecular dynamics simulations.

The obtained models for water uptake can be improved by increasing the size of training set, by improving the descriptor selection algorithm, and by identifying other surrogate methods.

Suggested future studies include: (i) use this method to build models for other properties, such as degradation (see Chapter 7); (ii) export the model to polymers outside the library; (iii) explore the design space for target properties (e.g., water uptake, Tg, contact angle, fibrinogen adsorption, and cell response).

7 Degradation studies

A one year-degradation study was conducted in parallel to the water uptake study for a subset of the library of L-tyrosine-derived polyarylates. Samples were incubated in phosphate buffer saline (PBS) at 37ºC, and molecular weight (Mw) was measured every 30 days. Different kinetic equations (zero, first and second order) were used to fit the experimental results. A surrogate model was built to model the kinetic parameters of degradation, and to predict them for the rest of the polymer library.

7.1 Degradation kinetic studies

Different hydrolytic polymer degradation kinetics have been reported in the literature. First order kinetics has been observed for poly(lactic-co-glycolic acid) (PLGA) [27, 216, 217], poly(lactic acid) (PLA) [218], polyglyconate B [219], multiblock poly(ester urethane)s [220], poly(ε-caprolactone) (PCL) [221], poly(1,3-trimethylene carbonate) (PTMC) [221], poly(vinyl acetate) (PVA) [222], poly(m-phenylenediamineisophthyl)amide (MPD-I) [223], and L-tyrosine-derived polycarbonates [14, 15]. A first order degradation equation can be written as:

$$Mw = Mw_0 \cdot \exp(-k_1 t),$$

(7-1)

where Mw and Mw_0 are the molecular weight of the polymer at time t and time 0, respectively, and k_1 is the degradation coefficient.

A second order reaction has been observed for PLGA sponges without autocatalysis [217] and polysaccharides [224]. A second order degradation equation can be written as:

$$\frac{1}{Mw} = \frac{1}{Mw_0} + k_2 t,$$

(7-2)

where k_2 represents the degradation coefficient.

Several studies have shown multiple stages (two, three or four) of degradation of poly(glycolic acid) (PGA) [225], PLA [21, 225], PLGA [21, 225], and polymandelide [226]. The first stage is controlled by water diffusion and saturation. The second stage generally presents a slow degradation, with first or second order kinetics, followed by a reduction of the mechanical properties, and the final weight loss and scaffold disruption. Some polymers present also an intermediate stage of accelerated degradation, in general associated with autocatalysis.

7.2   Materials and methods

7.2.1   Materials

A degradation study was performed for 26 polymers of the library of L-tyrosine-derived polyarylates (Table 3-1). Three films of each polymer were pressed using the previously described protocol in Chapter 3, and annealed for at least 20 h at 5 to 10 ºC above their Tg.

7.2.2   Experimental methods

7.2.2.1   Molecular weight measurements

Mw was measured by a gel permeation chromatography (GPC) system consisting of two PL-gel columns (10^5 - 10^3 Å pore size and 30 cm in length, Polymer Laboratories LTD) connected to a Waters 717 autosampler and a Waters 2489 detector (Waters Corp., MA). The mobile phase was tetrahydroduran (THF) at a flow rate of 1 mL/min. The Mw

was calculated relative to a set of commercially available monodispersed polystyrene standards (Waters Corp., MA).

7.2.2.2 Degradation studies

Twelve samples per each film (one for each month) and three films per polymer were taken. Samples of 7 mm in diameter were incubated in separated vials with 10 mL of PBS and stored them at 37 ºC. PBS was replaced every 15 days. Samples were removed from the incubator every 30 days, blotted dry and frozen before Mw measurement as described above.

7.2.3 Computational methods

A surrogate model was built for several kinetic parameters of degradation of 21 polymers of the L-tyrosine-derived polyarylate library (Table 3-1), using the same methodology as described Chapter 6 and the data-mining package WEKA (Waikato Environment for Knowledge Analysis) [48].

7.2.3.1 Descriptor selection

Starting from the 2,272 descriptors described in Chapter 5 (2D, 3D in vacuum and 3D in water for the 18 polymers with experimental data), useless descriptors (i.e., constant and highly variable ones) were eliminated. Then, a correlation based feature selection (CFS) was used to reduce the dimensionality of the descriptors for each parameter in study. Expectation-maximization (EM) [48] cluster analysis was employed to categorize the degradation parameters (i.e., kinetic parameters of zero, first and second order degradation) for the polymers into three classes (i.e., low, medium, high).

Table 7-1: Subset of the library of L-tyrosine-derived polyarylates used for the degradation study.

Polymer[1,2]	Initial Molecular Weight (Mw, kDa)[3,4,5]	Glass transition temperature (Tg, ºC)[5]
poly(DTO sebacate)	123 ± 1	16
poly(HTH sebacate)	43 ± 1 *	23
poly(HTH sebacate)	64 ± 5	23
poly(DTH suberate)	106 ± 2	24
poly(DTO adipate)	132 ± 2	26
poly(DTH adipate)	98 ± 1	34
poly(DTB (R)(+) methyladipate)	61 ± 1	35
poly(DTsB sebacate) **	116 ± 3	36
poly(DTBn suberate)	34 ± 1 *	38
poly(HTH adipate)	87 ± 2	40
poly(DTB adipate)	111 ± 3	42
poly(DTO succinate)	84 ± 6	43
poly(DTM sebacate)	126 ± 4	45
poly(DTsB (R)(+) methyladipate)	79 ± 3	45
poly(DTsB glutarate)	86 ± 3	46
poly(DTBn adipate)	69 ± 8	48
poly(DTB glutarate)	105 ± 1	50
poly(DTM (R)(+) methyladipate)	68 ± 1	53
poly(DTBn methyladipate)	90 ± 1	55
poly(DTiP adipate)	40 ± 1 *	55
poly(DTiP adipate)	144 ± 2	55
poly(DTE adipate)	126 ± 7	59
poly(HTE adipate)	37 ± 4 *	61
poly(DTE glutarate)	80 ± 1	64
poly(DTB succinate)	145 ± 11	67
poly(DTM adipate)	99 ± 3	67

[1]Polymers are ordered by Tg values.

[2]The '**' symbol represent a polymer for which no 3D descriptors are available, and thus it was not used in the surrogate model for degradation.

[3]Each value of Mw is the mean value of three different films ± SD.

[4]The '*' symbol represent the polymers with very low Mw < 60kDa. They were not used in build the surrogate model for degradation.

[5]Tg's are single measurements of polymer before pressing ± 1ºC.

From the pre-selected descriptors and the parameter classification, two descriptors were selected by J48 decision tree [47] with full training set, and two by linear regression. For details on the cluster and decision tree methods, refer to Chapters 2 and 5.

7.2.4 Artificial Neural Networks

Using the same approach as in Chapter 6, a multilayer perceptron was used to build Artificial Neural Networks (ANN) models for each parameter with the four descriptors selected previously. All input variables were scaled to the unit interval while the learning rate and the momentum applied for updating the weights were 0.3 and 0.2, respectively. Randomization of the initial weights and shuffling of the training data were performed by varying the seed for the random number generator 100 times.

Each model was built considering 18 polymers as training set and 3 polymers as test set, in all possible combinations. Model accuracy was evaluated by the Pearson coefficient (r) over each training set and over all the polymers when part of the test set.

Predictions were obtained for the rest of the 56 polymers of the library, for which 3D descriptors were available (see Chapters 5 and 6).

7.3 Results and Discussion

7.3.1 Experimental measurements of degradation

Mw's were measured monthly for the subset of 26 polymers. Measurements were completed for 5 months for all polymers, and for 12 months for some of the polymers.

Degradation results were expressed as the Mw measured at time t with respect to the original Mw (Table 7-2 and Table 7-3). The results were highly dependent on the polymer, i.e., by 5 months, the relative Mw ranges between 10% and 88% of the original

Mw. After 12 months, Mw's were less than 30% of the initial value for all polymers for which the study was completed.

7.3.2 *Kinetic analysis of degradation*

The degradation data (Table 7-2 and Table 7-3) were used to build three different kinetic models: Zero order, first order and second order. The equation for a zero order degradation is given by:

$$Mw = Mw_0 - k_0 t, \qquad\qquad (7\text{-}3)$$

where k_0 represent the kinetic coefficient of this equation. Table 7-4 shows the obtained values for k_0 for all polymers, as calculated from minimizing the root square error. The zero order kinetic model was in general applicable during the first part of the degradation curves (e.g., Figure 7-3, Figure 7-4, and Figure 7-5). For two polymers, poly(DTBn adipate) and poly(DTO succinate), zero order kinetics were applicable for the complete degradation curve (e.g., Figure 7-5).

The fit of the data to a first order kinetic model (eq. 7-1) is shown in Table 7-5. For some polymers, first order kinetics were applicable to the complete experimental time (e.g., Figure 7-2, Figure 7-3, and Figure 7-5), while for other polymers, it was applicable only for the first part of the degradation curves (e.g., Figure 7-1, Figure 7-3, and Figure 7-4).

Table 7-2: Degradation profiles (first 6 months) for a subset of polymers from the library of tyrosine-derived polyarylates.

Polymer[1]	Initial Mw (kDa)[2]	1 mo[3]	2 mo[3]	3 mo[3]	4 mo[3]	5 mo[3]	6 mo[3,4]
poly(DTO sebacate)	123 ± 1	100 ± 5%	84 ± 2%	71 ± 2%	57 ± 1%	45 ± 2%	35 ± 2%
poly(HTH sebacate)	43 ± 1	97 ± 30%	92 ± 22%	98 ± 2%	-	88 ± 1%	82 ± 1%
poly(HTH sebacate)	64 ± 5	79 ± 8%	65 ± 10%	59 ± 7%	43 ± 4%	44 ± 4%	33 ± 4%
poly(DTH suberate)	106 ± 2	94 ± 3%	89 ± 2%	81 ± 3%	73 ± 2%	64 ± 4%	54 ± 3%
poly(DTO adipate)	132 ± 2	93 ± 1%	72 ± 2%	58 ± 2%	39 ± 4%	25 ± 3%	16 ± 2%
poly(DTH adipate)	98 ± 1	96 ± 1%	90 ± 1%	82 ± 2%	71 ± 3%	57 ± 4%	41 ± 5%
poly(DTB (R)(+) methyladipate)	61 ± 1	94 ± 1%	85 ± 1%	74 ± 2%	59 ± 1%	42 ± 3%	34 ± 1%
poly(DTsB sebacate)	116 ± 3	83 ± 2%	73 ± 2%	65 ± 3%	54 ± 1%	46 ± 2%	39 ± 2%
poly(DTBn suberate)	33 ± 1	84 ± 3%	69 ± 3%	3%	36 ± 2%	26 ± 2%	26 ± 2%
poly(HTH adipate)	87 ± 2	68 ± 3%	51 ± 2%	38 ± 2%	26 ± 2%	16 ± 1%	12 ± 2%
poly(DTB adipate)	111 ± 3	104 ± 3%	100 ± 13%	69 ± 3%	61 ± 3%	42 ± 2%	27 ± 1%
poly(DTO succinate)	84 ± 6	71 ± 6%	72 ± 6%	71 ± 11%	54 ± 6%	54 ± 4%	48 ± 5%
poly(DTM sebacate)	126 ± 4	90 ± 3%	78 ± 3%	69 ± 3%	58 ± 3%	46 ± 2%	36 ± 2%
poly(DTsB (R)(+) methyladipate)	79 ± 3	94 ± 5%	80 ± 4%	73 ± 4%	62 ± 6%	51 ± 3%	40 ± 5%
poly(DTsB glutarate)	86 ± 3	83 ± 5%	67 ± 5%	54 ± 4%	37 ± 2%	22 ± 2%	**
poly(DTBn adipate)	69 ± 8	81 ± 10%	92 ± 11%	83 ± 11%	70 ± 9%	56 ± 7%	49 ± 7%
poly(DTB glutarate)	105 ± 1	99 ± 3%	82 ± 2%	73 ± 6%	54 ± 4%	35 ± 3%	**
poly(DTM (R)(+) methyladipate)	68 ± 1	81 ± 1%	73 ± 3%	65 ± 2%	52 ± 2%	35 ± 5%	**
poly(DTBn methyladipate)	90 ± 1	107 ± 3%	95 ± 2%	91 ± 2%	88 ± 1%	78 ± 9%	**
poly(DTiP adipate)	40 ± 1	60 ± 2%	46 ± 1%	26 ± 6%	16 ± 1%	10 ± 1%	7 ± 1%
poly(DTiP adipate)	144 ± 2	81 ± 2%	71 ± 1%	61 ± 2%	51 ± 3%	39 ± 3%	30 ± 2%
poly(DTE adipate)	126 ± 7	66 ± 5%	52 ± 3%	42 ± 2%	30 ± 2%	20 ± 1%	14 ± 1%
poly(HTE adipate)	37 ± 4	72 ± 7%	48 ± 5%	36 ± 4%	26 ± 3%	18 ± 2%	14 ± 2%
poly(DTE glutarate)	80 ± 1	96 ± 11%	73 ± 3%	60 ± 4%	49 ± 2%	32 ± 1%	18 ± 1%
poly(DTB succinate)	145 ± 11	106 ± 10%	97 ± 8%	84 ± 7%	66 ± 7%	50 ± 5%	31 ± 5%
poly(DTM adipate)	99 ± 3	90 ± 11%	80 ± 3%	56 ± 3%	38 ± 6%	33 ± 3%	21 ± 3%

[1]Polymers are ordered by Tg.

[2]Each value of Mw is the mean value of three different films ± SD, measured by THF-GPC.

[3]Each value is the mean value of three samples from three different films ± SD, as a % of the initial Mw.

[4]The '**' symbol represents future measurements.

Table 7-3: Degradation profiles (from 7 to 12 months) for a subset of polymers from the library of tyrosine-derived polyarylates.

Polymer[1]	Initial Mw (kDa)[2]	7 mo[3,4]	8 mo[3,4]	9 mo[3,4]	10 mo[3,4]	11 mo[3,4,5]	12 mo[3,4,5]
poly(DTO sebacate)	123 ± 1	28 ± 5%	20 ± 1%	16 ± 2%	13 ± 1%	12 ± 2%	9 ± 2%
poly(HTH sebacate)	43 ± 1	78 ± 1%	71 ± 1%	63 ± 1%	56 ± 2%	49 ± 1%	41 ± 1%
poly(HTH sebacate)	64 ± 5	29 ± 3%	23 ± 4%	16 ± 1%	12 ± 2%	12 ± 1%	10 ± 1%
poly(DTH suberate)	106 ± 2	37 ± 2%	27 ± 4%	23 ± 1%	14 ± 2%	11 ± 1%	**
poly(DTO adipate)	132 ± 2	10 ± 2%	6 ± 1%	**	**	**	**
poly(DTH adipate)	98 ± 1	27 ± 2%	16 ± 1%	**	**	**	**
poly(DTB (R)(+) methyladipate)	61 ± 1	**	**	**	**	**	**
poly(DTsB sebacate)	116 ± 3	28 ± 4%	25 ± 1%	20 ± 1%	17 ± 1%	14 ± 1%	11 ± 1%
poly(DTBn suberate)	33 ± 1	17 ± 1%	11 ± 1%	9 ± 1%	7 ± 1%	*	*
poly(HTH adipate)	87 ± 2	7 ± 1%	6 ± 1 %	5 ± 1%	4 ± 1%	*	*
poly(DTB adipate)	111 ± 3	18 ± 1%	11 ± 1%	5 ± 1%	4 ± 1%	3 ± 1%	*
poly(DTO succinate)	84 ± 6	43 ± 4%	39 ± 3%	37 ± 2%	31 ± 3%	28 ± 3%	30 ± 3%
poly(DTM sebacate)	126 ± 4	26 ± 2%	17 ± 1%	12 ± 2%	7 ± 1%	5 ± 1%	4 ± 1%
poly(DTsB (R)(+) methyladipate)	79 ± 3	**	**	**	**	**	**
poly(DTsB glutarate)	86 ± 3	**	**	**	**	**	**
poly(DTBn adipate)	69 ± 8	38 ± 7%	27 ± 4%	22 ± 4%	15 ± 2%	11 ± 2%	8 ± 1%
poly(DTB glutarate)	105 ± 1	**	**	**	**	**	**
poly(DTM (R)(+) methyladipate)	68 ± 1	**	**	**	**	**	**
poly(DTBn methyladipate)	90 ± 1	**	**	**	**	**	**
poly(DTiP adipate)	40 ± 1	5 ± 1%	4 ± 1%	*	*	*	*
poly(DTiP adipate)	144 ± 2	23 ± 2%	15 ± 2%	9 ± 1%	6 ± 1%	3 ± 1%	2 ± 1%
poly(DTE adipate)	126 ± 7	9 ± 1%	6 ± 1%	4 ± 1%	3 ± 1%	*	*
poly(HTE adipate)	37 ± 4	**	**	**	**	**	**
poly(DTE glutarate)	80 ± 1	10 ± 2%	5 ± 1%	3 ± 1%	2 ± 1%	*	*
poly(DTB succinate)	145 ± 11	20 ± 2%	13 ± 1%	7 ± 1%	4 ± 1%	3 ± 1%	*
poly(DTM adipate)	99 ± 3	13 ± 2%	7 ± 1%	5 ± 1%	4 ± 1%	*	*

[1]Polymers are ordered by Tg

[2]Each value of Mw is the mean value of three different films ± SD, measured by THF-GPC.

[3]Each value is the mean value of three samples from three different films ± SD, as a % of the initial Mw.

[4]The '**' symbol represents future measurements.

[5]The '*' symbol represents late degradation stages where Mw was below the limit of detection of the GPC.

Table 7-4: Fitted parameter for the zero order equation for the degradation of the subset of L-tyrosine-derived polyarylates.

Polymer[1]	k_0 (slope zero order release)[2]	$(R^2)^2$	Range[2,3]
poly(DTO sebacate) 123kDa	0.137	0.997	1-5mo
poly(HTH sebacate) 43kDa	0.030	0.868	0-7mo
poly(HTH sebacate) 64kDa	0.075	0.964	1-9mo
poly(DTH suberate) 106kDa	0.076	0.984	0-6mo
poly(DTO adipate) 131kDa	0.150	0.990	0-6mo
poly(DTH adipate) 98kDa	0.130	0.992	2-8mo
poly(DTB (R) (+) methyladipate) 61kDa	0.118	0.981	0-6mo*
poly(DTsB sebacate) 116kDa	0.085	0.990	1-8mo
poly(DTBn suberate) 33kDa	0.118	0.985	0-7mo
poly(HTH adipate) 87kDa	0.116	0.976	1-6mo
poly(DTB adipate) 110kDa	0.145	0.964	2-8mo
poly(DTO succinate) 84kDa	0.047	0.959	1-11mo
poly(DTM sebacate) 126kDa	0.105	0.999	0-8mo
poly(DTsB (R) (+) methyladipate) 79kDa	0.102	0.994	0-6mo*
poly(DTsB glutarate) 86kDa	0.155	0.999	0-5mo*
poly(DTBn adipate) 69kDa	0.082	0.971	0-12mo
poly(DTB glutarate) 105kDa	0.158	0.988	1-5mo*
poly(DTM (R) (+) methyladipate) 68kDa	0.120	0.981	0-5mo*
poly(DTBn methyladipate) 90kDa	0.042	0.899	0-5mo*
poly(DTiP adipate) 40kDa	0.154	0.982	1-4mo
poly(DTiP adipate) 144kDa	0.093	0.991	1-9mo
poly(DTE adipate) 126kDa	0.104	0.984	1-6mo
poly(HTE adipate) 37kDa	0.185	0.955	0-4mo
poly(DTE glutarate) 80kDa	0.137	0.988	0-7mo
poly(DTB succinate) 145kDa	0.152	0.991	1-7mo
poly(DTM adipate) 99kDa	0.141	0.975	0-6mo

[1]Polymers are ordered by Tg values.

[2]Slope was calculated from the Mw data in the time range in the table. R^2 is the correlation coefficient of the linear fit.

[3]The '*' symbol represent the polymers for which data is still being recollected and thus, the slope is calculated with partial data.

Table 7-5: Fitted parameter for the first order equation for the degradation of the subset of L-tyrosine-derived polyarylates.

Polymer[1]	k_1 (slope first order release)[2]	(R^2)[2]	Range[2,3]
poly(DTO sebacate) 123kDa	0.228	0.997	1-12mo
poly(HTH sebacate) 43kDa	0.077	0.892	0-12mo
poly(HTH sebacate) 64kDa	0.195	0.987	0-12mo
poly(DTH suberate) 106kDa	0.100	0.960	0-6mo
poly(DTO adipate) 131kDa	0.422	0.992	0-8mo*
poly(DTH adipate) 98kDa	0.108	0.921	0-5mo
poly(DTB (R) (+) methyladipate) 61kDa	0.188	0.942	0-6mo*
poly(DTsB sebacate) 116kDa	0.185	0.993	0-12mo
poly(DTBn suberate) 33kDa	0.283	0.973	0-10mo
poly(HTH adipate) 87kDa	0.371	0.995	0-8mo
poly(DTB adipate) 110kDa	0.425	0.983	2-11mo
poly(DTO succinate) 84kDa	0.104	0.970	0-11mo
poly(DTM sebacate) 126kDa	0.167	0.972	0-6mo
poly(DTsB (R) (+) methyladipate) 79kDa	0.152	0.969	0-6mo*
poly(DTsB glutarate) 86kDa	0.242	0.976	0-4mo
poly(DTBn adipate) 69kDa	0.224	0.978	2-10mo
poly(DTB glutarate) 105kDa	0.154	0.908	0-4mo
poly(DTM (R) (+) methyladipate) 68kDa	0.153	0.980	0-4mo
poly(DTBn methyladipate) 90kDa	0.047	0.873	0-5mo*
poly(DTiP adipate) 40kDa	0.437	0.995	0-7mo
poly(DTiP adipate) 144kDa	0.207	0.982	0-7mo
poly(DTE adipate) 126kDa	0.342	0.994	0-11mo
poly(HTE adipate) 37kDa	0.332	0.997	0-6mo*
poly(DTE glutarate) 80kDa	0.226	0.961	0-5mo
poly(DTB succinate) 145kDa	0.445	0.983	3-10mo
poly(DTM adipate) 99kDa	0.389	0.990	2-10mo

[1]Polymers are ordered by Tg values.

[2]Slope was calculated from the Mw data in the time range in the table. R^2 is the correlation coefficient of the linear fit.

[3]The '*' symbol represent the polymers for which data is still being recollected and thus, the slope is calculated with partial data.

Table 7-6: Fitted parameter for the second order equation for the degradation of the subset of L-tyrosine-derived polyarylates.

Polymer[1]	$k_{2\text{-}BEGINNING}$ (slope second order release)[2]	$(R^2)^2$	Range[2]	$k_{2\text{-}END}$ (slope second order release)[2]	$(R^2)^2$	Range[2,3]
poly(DTO sebacate) 123kDa	0.302	0.959	1-5mo	1.456	0.989	6-12mo
poly(HTH sebacate) 43kDa	0.047	0.867	0-7mo	0.318	0.976	8-12mo
poly(HTH sebacate) 64kDa	0.349	0.953	0-7mo	1.319	0.945	8-12mo
poly(DTH suberate) 106kDa	0.135	0.924	0-6mo	1.642	0.940	7-11mo*
poly(DTO adipate) 131kDa	0.379	0.879	0-4mo	4.021	0.966	5-11mo*
poly(DTH adipate) 98kDa	0.099	0.918	0-4mo	1.535	0.923	5-8mo*
poly(DTB (R) (+) methyladipate) 61kDa	0.115	0.968	0-3mo	0.635	0.998	4-6mo*
poly(DTsB sebacate) 116kDa	0.257	0.962	0-6mo	1.356	0.966	8-12mo
poly(DTBn suberate) 33kDa	0.328	0.876	0-5mo	2.556	0.997	6-10mo
poly(HTH adipate) 87kDa	0.675	0.959	0-4mo	3.539	0.980	5-10mo
poly(DTB adipate) 110kDa	0.629	0.904	2-6mo	8.068	0.984	7-11mo
poly(DTO succinate) 84kDa	0.210	0.955	0-12mo	0.232	0.961	3-12mo
poly(DTM sebacate) 126kDa	0.219	0.941	0-5mo	5.153	0.983	8-12mo
poly(DTsB (R) (+) methyladipate) 79kDa	0.129	0.967	0-3mo	0.445	0.979	4-6mo*
poly(DTsB glutarate) 86kDa	0.280	0.967	0-3mo	1.353	0.958	3-5mo*
poly(DTBn adipate) 69kDa	0.164	0.847	0-6mo	1.564	0.958	7-11mo
poly(DTB glutarate) 105kDa	0.131	0.967	0-3mo	*	*	*
poly(DTM (R) (+) methyladipate) 68kDa	0.215	0.963	0-4mo	*	*	*
poly(DTBn methyladipate) 90kDa	0.034	0.983	0-4mo	*	*	*
poly(DTiP adipate) 40kDa	1.260	0.905	0-4mo	4.336	0.980	5-8mo
poly(DTiP adipate) 144kDa	0.294	0.942	0-5mo	13.908	0.945	9-12mo
poly(DTE adipate) 126kDa	0.754	0.918	0-5mo	6.104	0.993	6-11mo
poly(HTE adipate) 37kDa	0.719	0.969	0-4mo	*	*	*
poly(DTE glutarate) 80kDa	0.395	0.886	0-5mo	12.198	0.993	7-10mo
poly(DTB succinate) 145kDa	0.260	0.906	1-5mo	8.405	0.991	8-12mo
poly(DTM adipate) 99kDa	0.437	0.917	0-5mo	5.453	0.971	6-10mo

[1]Polymers are ordered by Tg values.

[2]Slope was calculated from the Mw data in the time range in the table. R^2 is the correlation coefficient of the linear fit.

Results for the second order kinetic model (eq. 7-2) are shown in Table 7-6. Second order kinetics were in general applicable only to the first part of the degradation curves (e.g., Figure 7-3 and Figure 7-4), followed by a much faster degradation phase, characterized by a second kinetic coefficient. Only for poly(DTO succinate) was the second order kinetic applicable for the complete degradation curve (Figure 7-5).

Those results show that it is not possible to determine the degradation kinetic solely from the Mw reduction data. Further experiments must be performed with model compounds to understand the degradation mechanism for this polymer library.

7.3.3 *Effect of initial molecular weight*

As described in Chapter 3, poly(DTiP adipate) water uptake was greater for the lower initial Mw polymer. Similarly, as shown in Figure 7-1, degradation was faster to the lower Mw material.

However, the relationship between Mw and degradation is inverted for poly(HTH sebacate) (Figure 7-2), which presents very low water uptake levels. One possible explanation is the different nature of the two polymers (DTR vs HTR). Further experiments should be designed to explain those differences and how different initial Mw affects the degradation rates for different classes of polymers.
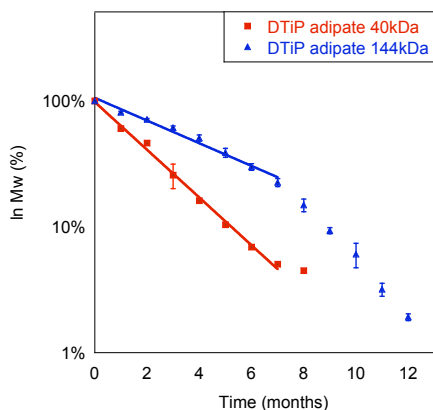
Figure 7-1: Degradation profiles of poly(DTiP adipate) of two different Mw's (40kDa and 144kDa), as modeled for first order kinetics.
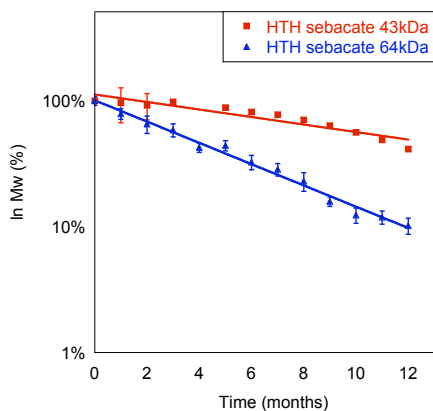
Figure 7-2: Degradation profiles of poly(HTH sebacate) of two different Mw's (44kDa and 64kDa), as modeled for first order kinetics.

7.3.4 *Effect of polymer structure*

As was the case for water uptake (Chapter 3), degradation rates also cannot be directly derived from the polymer structure. Comparing five of the adipates of the study that have different number of carbons in the pendant chain (DTM:1, DTE:2, DTB:4, DTH:6, and DTO:8) (Figure 7-3), one would expect that the longer the pendant chain, the more hydrophobic the polymer, and thus the slower the degradation rate, but all of them present a very similar degradation profile.

Comparing the DTB polymers of the study that have different number of carbons in the diacid chain (succinate: 2, glutarate: 3, adipate: 4, and methyladipate: 5) (Figure 7-4), they do not present any difference in their degradation profiles.

However, comparing three of the DTO polymers with different number of carbons in the diacid chain (succinate: 2, adipate: 4, and sebacate: 8), very significant differences in degradation rates were observed. The fastest degradation was observed for poly(DTO adipate), followed by poly(DTO sebacate) and poly(DTO succinate). Again, degradation kinetics cannot be inferred by merely examining at the chemical structure of the monomers.
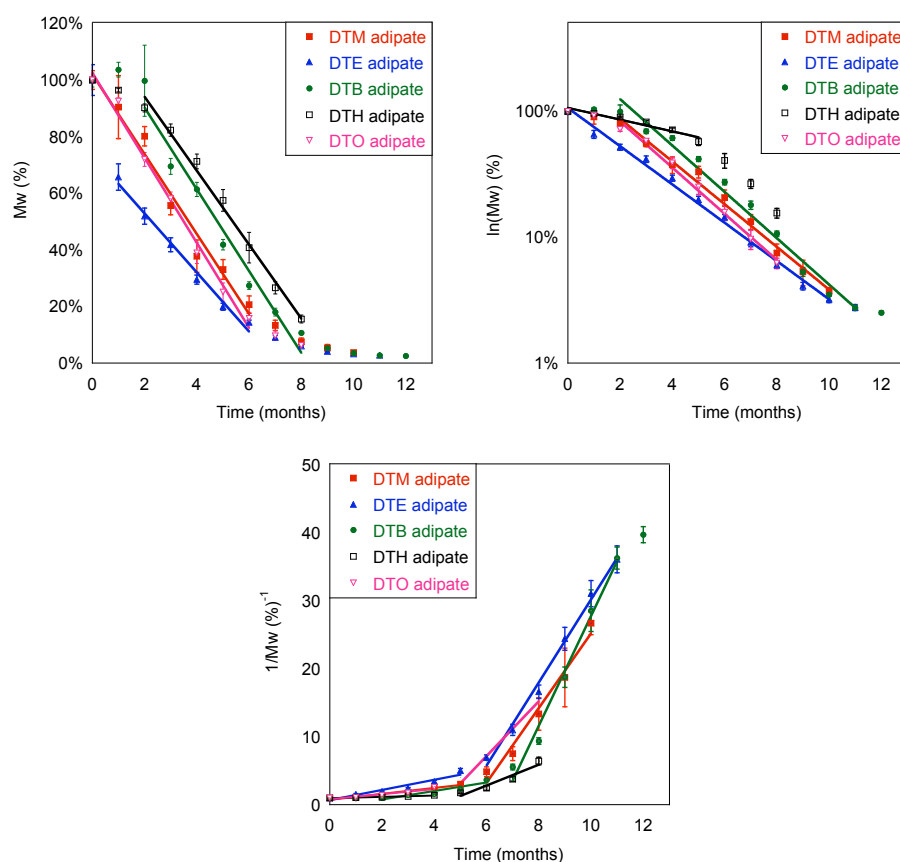
Figure 7-3: Degradation profiles of five "adipate" polymers, as modeled for zero, first or second order kinetics.
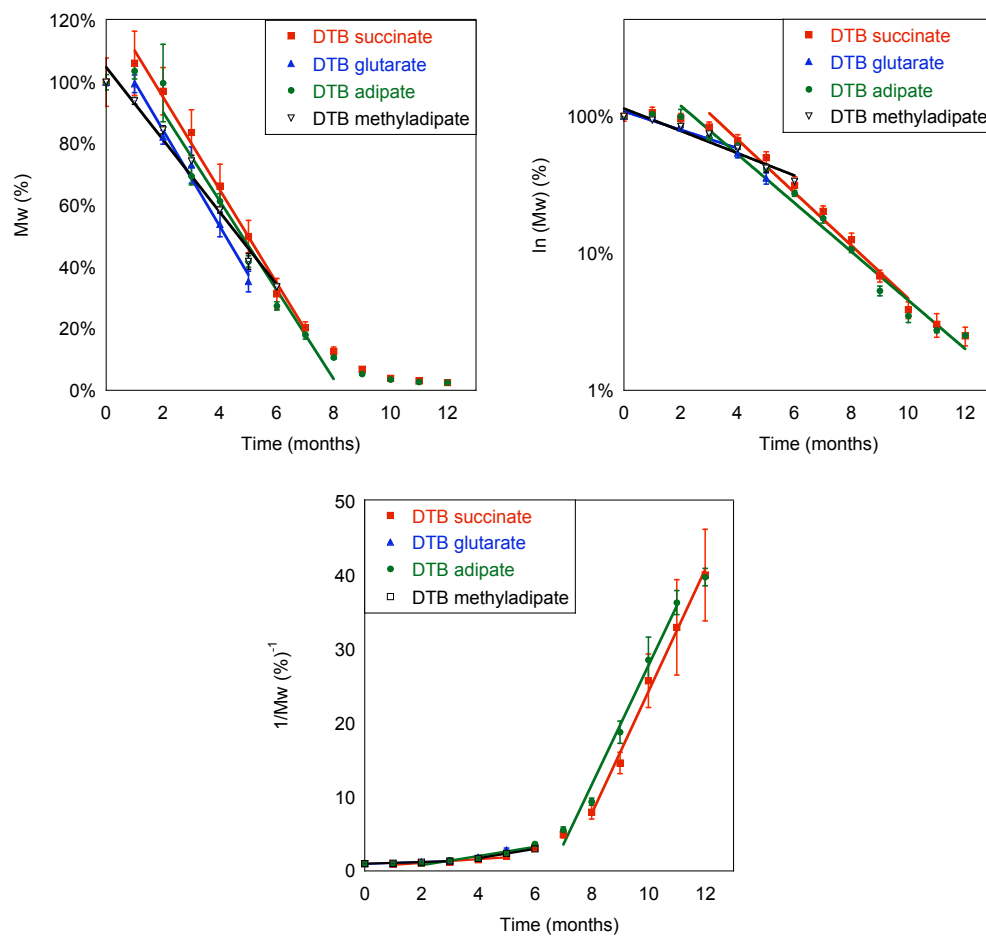
Figure 7-4: Degradation profiles of four "DTB" polymers, as modeled for zero, first or second order kinetics.
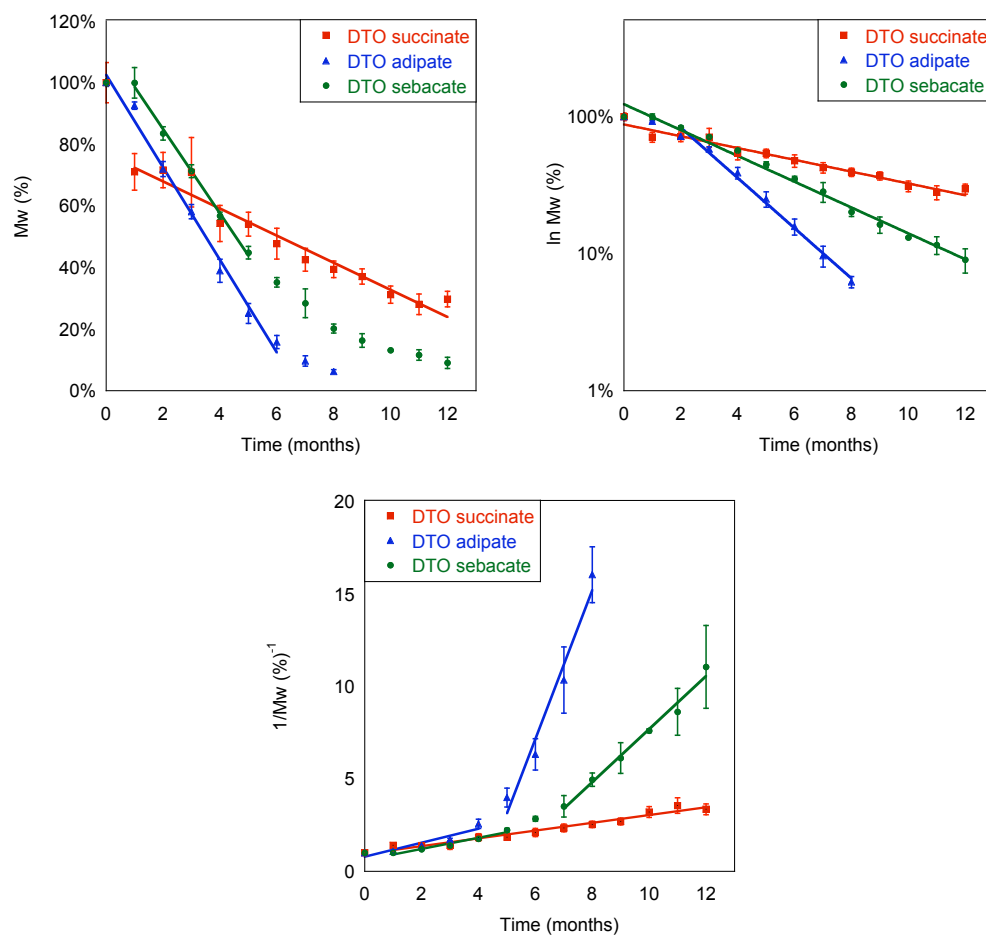
Figure 7-5: Degradation profiles of three "DTO" polymers, as modeled for zero, first or second order kinetics.

7.3.5 *Relationship between water uptake and degradation*

As shown in Figure 7-6, degradation cannot be correlated with the water uptake equilibrium levels, as calculated in Chapters 3 and 4. One would expect that the higher the water content, the faster the degradation, which is not what is observed. Only the kinetic coefficient of the zero order equation is slightly correlated with the equilibrium water uptake.
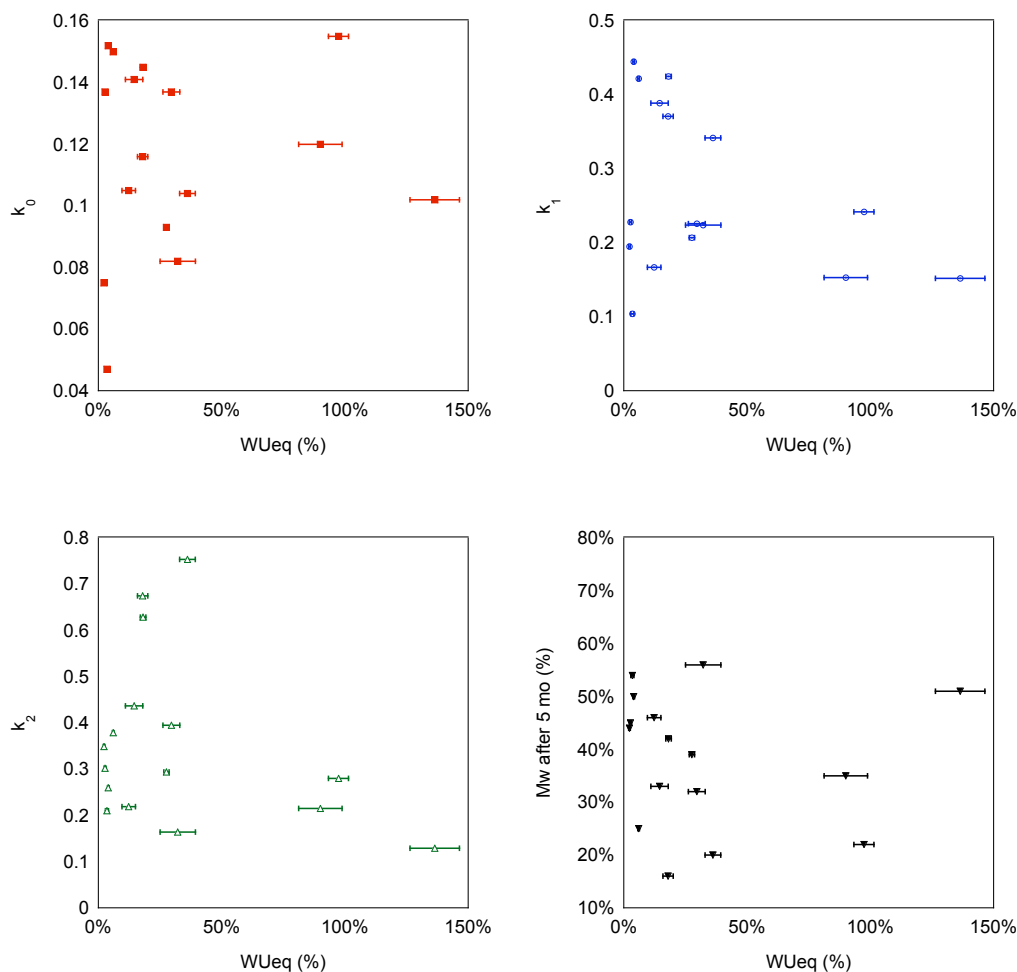
Figure 7-6: Water uptake equilibrium (WUeq, %), as calculated in Chapter 4, compared with kinetic parameters of zero order (k_0), first order (k_1), and second order kinetics (k_2), and with the Mw after 5 months of incubation, in terms if % of initial Mw.

7.3.6   Surrogate model of degradation

The previous results show the need for a different model for degradation, independent of the water uptake values and including not only the chemical structure of the polymers, but also three-dimensional features that could explain the different degradation profiles. Since there is no evidence to prefer one kinetic model over the other two, a surrogate model was built for the values of the kinetic parameters of all three

kinetic equations (k_0, k_1, and k_2), and for the Mw levels after 5 months of incubation, as compared with the initial Mw's.

7.3.6.1 Cluster analysis

Table 7-7 shows the classification obtained for each parameter by EM cluster analysis of the 21 polymers. The classification changes depending on which kinetic model is used.

Table 7-7: Classification of degradation kinetic parameters for the subset of the L-tyrosine-derived polyarylate library.

Polymer[1]	k_0	k_1	k_2	Mw 5 months (%)
poly(DTB adipate) 110kDa	HIGH	HIGH	HIGH	MEDIUM
poly(DTB glutarate) 105kDa	HIGH	LOW	LOW	MEDIUM
poly(DTB succinate) 145kDa	HIGH	HIGH	MEDIUM	MEDIUM
poly(DTBn adipate) 69kDa	LOW	MEDIUM	LOW	MEDIUM
poly(DTE adipate) 126kDa	MEDIUM	HIGH	HIGH	LOW
poly(DTE glutarate) 80kDa	HIGH	MEDIUM	MEDIUM	MEDIUM
poly(DTH adipate) 98kDa	HIGH	LOW	LOW	MEDIUM
poly(DTH suberate) 106kDa	LOW	LOW	LOW	HIGH
poly(DTiP adipate) 144kDa	LOW	LOW	MEDIUM	MEDIUM
poly(DTM adipate) 99kDa	HIGH	HIGH	MEDIUM	MEDIUM
poly(DTM sebacate) 126kDa	MEDIUM	LOW	MEDIUM	MEDIUM
poly(DTO adipate) 131kDa	HIGH	HIGH	MEDIUM	LOW
poly(DTO sebacate) 123kDa	HIGH	MEDIUM	MEDIUM	MEDIUM
poly(DTO succinate) 84kDa	LOW	LOW	MEDIUM	MEDIUM
poly(HTH adipate) 87kDa	MEDIUM	HIGH	HIGH	LOW
poly(HTH sebacate) 64kDa	LOW	LOW	MEDIUM	MEDIUM
poly(DTB methyladipate) 61kDa	MEDIUM	LOW	LOW	MEDIUM
poly(DTBn methyladipate) 90kDa	LOW	LOW	LOW	HIGH
poly(DTM methyladipate) 68kDa	MEDIUM	LOW	MEDIUM	MEDIUM
poly(DTsB glutarate) 86kDa	HIGH	MEDIUM	MEDIUM	LOW
poly(DTsB methyladipate) 79kDa	MEDIUM	LOW	LOW	MEDIUM

[1]Polymers are ordered by the order in the descriptor set (by polymer name).

7.3.6.2   Selection of descriptors

After removing useless descriptors, 1,917 descriptors were selected from the original 2,272. CFS was used to select the descriptors that were highly correlated with the parameter of study, resulting in 831, 412, 604, and 667 descriptors for k_0, k_1, k_2, and Mw, respectively, after 5 months.

Between two and four descriptors were used to build decision trees for each parameter (Table 7-8).Four descriptors were used by the decision tree for k_0 (Mor24v (3D in vacuum), Me, BELe1 and X3A (2D)). The decision tree correctly classified 20 of the 21 polymers (only one polymer was wrongly classified as "Low" when it was "Medium", Figure 7-7). Three descriptors were used for k_1 (Mor11m (3D in vacuum), nCp and JGI6 (2D)). This decision tree correctly classified 20 of the 21 polymers (only one was classified as "Low" when it was "Medium", Figure 7-8). Two descriptors were used for k_2 (R1m+ (3D in vacuum) and De (3D in water)). This decision tree correctly classified 20 of the 21 polymers (only one was classified as "Low" when it was "Medium", Figure 7-9). Two descriptors were also used for the Mw after 5 months (Mor02u and G1p (3D in water)). This decision tree correctly classified 20 of the 21 polymers (only one was classified as "Medium" when it was "Low", Figure 7-10).

Only the first 2 descriptors of each decision tree were used in the surrogate models. Other two descriptors were selected by linear regression (Table 7-9).

Table 7-8: Summary of descriptors selected by decision tree analysis.

Parameter	Descriptor	Type
k_0	Mor24v (3D vacuum)	3D-MoRSE
	Me (2D)	Topological
	BELe1 (2D)	BCUT
	X3A (2D)	Kier-Hall connectivity index
k_1	Mor11m (3D vacuum)	3D-MoRSE
	nCp (2D)	Atom counts
	JGI6 (2D)	Topological
k_2	R1m+ (3D vacuum)	R-GETAWAY
	De (3D water)	WHIM
Mw after 5mo (%)	Mor02u (3D water)	3D-MoRSE
	G1p (3D water)	WHIM
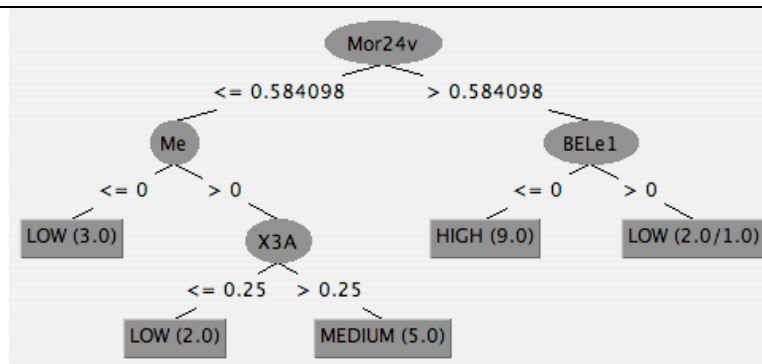
Figure 7-7: Decision tree for k_0 (zero order kinetics) of degradation. The values in parentheses after the classes represent the correct/incorrect classification of each class.
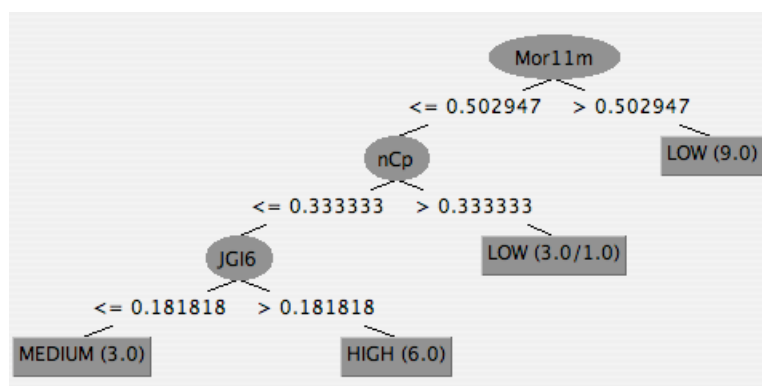
Figure 7-8: Decision tree for k_1 (first order kinetics) of degradation. The values in parentheses after the classes represent the correct/incorrect classification of each class.
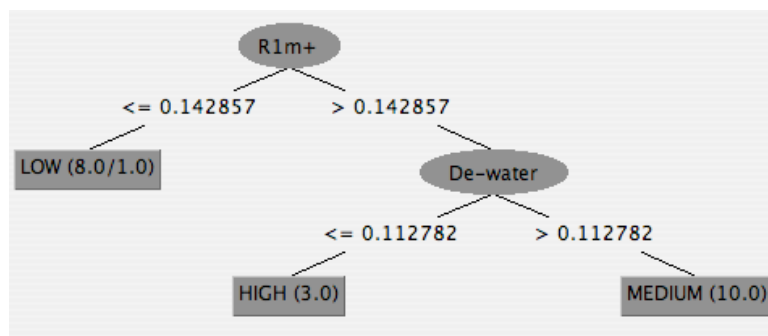
Figure 7-9: Decision tree for k_2 (second order kinetics) of degradation. The values in parentheses after the classes represent the correct/incorrect classification of each class.
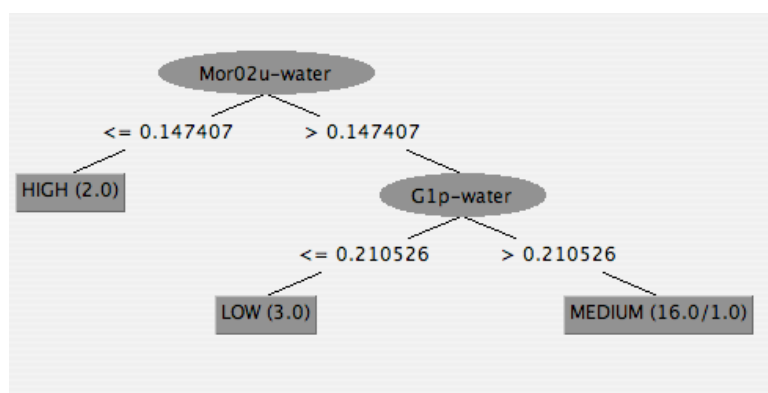
Figure 7-10: Decision tree for Mw after 5 months (%). The values in parenthesis after the classes represent the correct/incorrect classification of each class.

Table 7-9: Descriptors selected to build the surrogate model of degradation.

Parameter	Descriptors[1]	Type
k_0	Mor04m (3D vacuum)	3D-MoRSE
	Gm (3D water)	WHIM
k_1	Mor11m (3D vacuum) *	
	Mor30e (3D water)	3D-MoRSE
	Mor11p (3D vacuum)	
K_2	GATS7e (2D)	Autocorrelation
	Mor30u (3D water)	3D-MoRSE
Mw after 5mo (%)	GATS4p (2D)	Autocorrelation
	GATS7e (2D)	

[1]The '*' symbol represents a descriptor appear in both decision tree and linear regression.

All descriptors selected by this methodology were different from the previously selected descriptors for the water uptake models (Chapters 5 and 6). Among 2D descriptors, nCp represents the number of primary carbons (sp3), Me is the mean atomic Sanderson electronegativity, and the Geary autocorrelation descriptors (GATS) are topological descriptors calculated from the molecular graph [42].

Among 3D descriptors, 3D-MoRSE (MOlecule Representation of Structures based on Electron diffraction) descriptors appear for all parameters of the degradation models. They provide 3D information from the 3D coordinates by using the same transform as in electron diffraction [215]. WHIM (Weighted Holistic Invariant Molecular descriptors) descriptors (G1p, Gm, and De) capture 3D information regarding molecular size, shape, symmetry, and atom distribution [211]. R1m+ is a R-GETAWAY (GEometry, Topology, and Atom-Weights Assembly) descriptor. They capture 3D information regarding local aspects of the molecule such as branching, cyclicity and conformational changes [201].

7.3.6.3   Artificial neural network model

An ANN model was built for all combinations of 19 polymers as training and 2 as test set. Pearson correlation coefficient for training and test sets were calculated for the average prediction of each parameter for each polymer as part of either training or test set, respectively (Table 7-10, Figure 7-11). Only the model obtained for k_1, the kinetic parameter for the first order degradation, was accurate for the test set ($r = 0.70$), suggesting that this is the mechanism that governs the degradation of L-tyrosine-derived polyarylates. All other models were very inaccurate for the test set ($r < 0.4$).

Table 7-10: ANN results for the parameters of degradation, evaluated as the Pearson coefficient for training and test sets.

Parameter	Pearson coefficient of training sets[1]	Pearson coefficient of test sets[1]
k0	0.96	-0.01
k1	0.98	0.70
k2	0.98	0.17
Mw after 5mo (%)	0.98	0.38

[1]Average over all combinations of training/test sets.
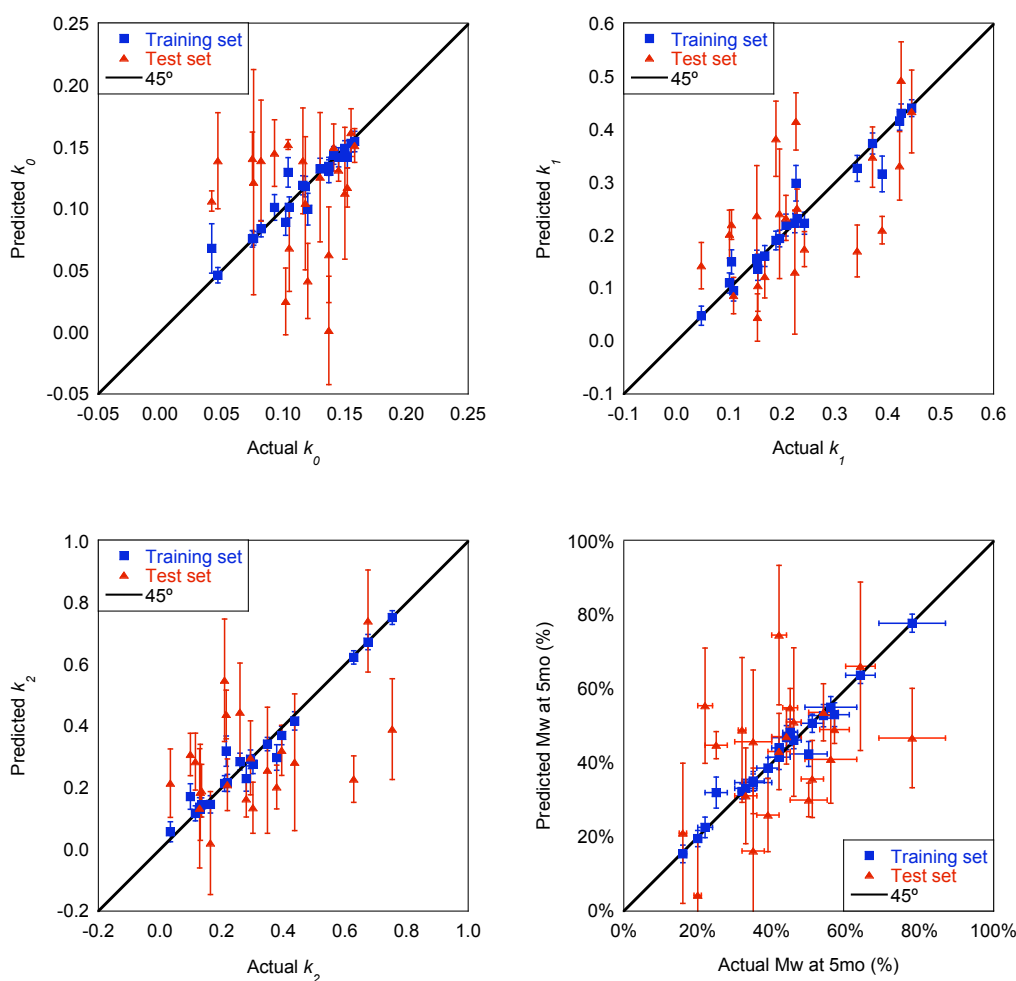
Figure 7-11: Predictions versus experimental values for k_0 (zero order kinetics), k_1 (first order kinetics), k_2 (second order kinetics), and Mw after 5mo (% of initial Mw). Blue represents the results for the polymers when they were part of the training set, while red represents when they were part of the test set. Black line represents x=y. Values are presented as mean value ± SD of predictions (y-error) ± SD of experimental values for the Mw after 5mo (x-error).

Since the model obtained for k_1 was accurate for training and test sets, predictions were obtained for the rest of the library (56 polymers for which descriptors were available) (Figure 7-12). Values of k_1 ranges from 0.06 to 0.44. For some polymers the SD of the predictions was very high (up to 120% of the predicted value), indicating that the selection of training set plays a very significant role in the predictions.
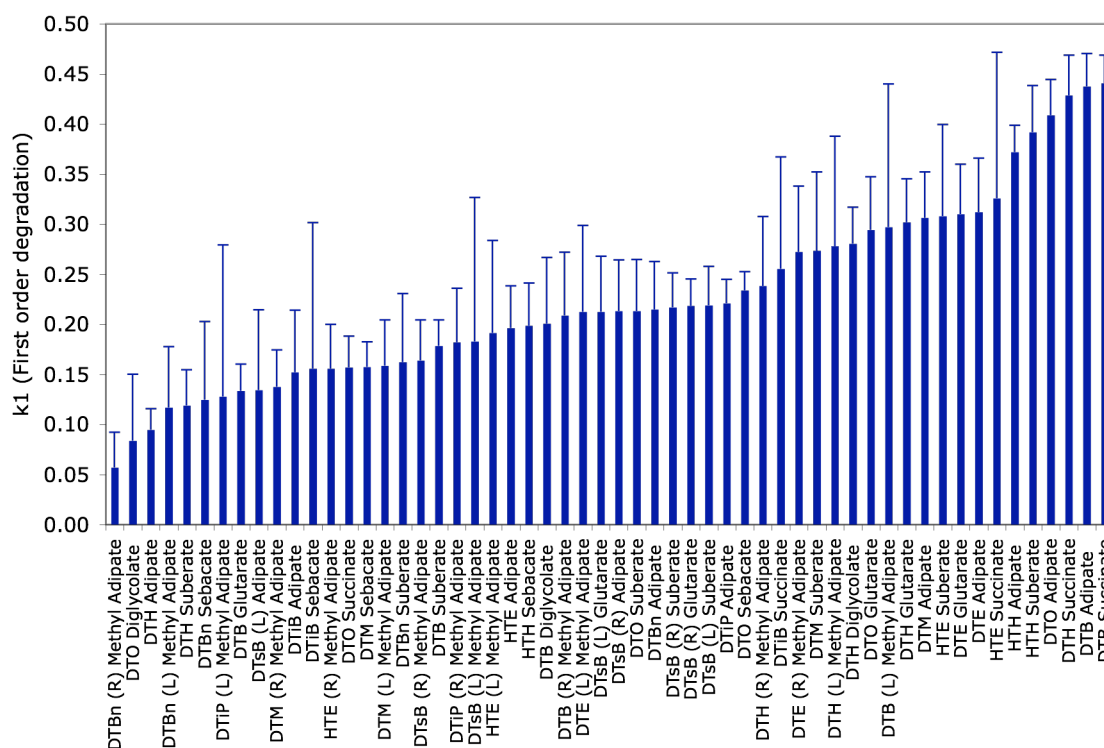
Figure 7-12: Prediction of k_1 (first order kinetics) over 56 polymers of the polymer library. Values are presented as mean value ± SD of the predicted value for each training/test set combination. Polymers are ordered from lowest to highest predicted values.

The predicted values of k_1 the first order degradation rate can serve as an indicator of which polymers may be fast, intermediate or slow degrading. However, the initial Mw also plays a fundamental role in the degradation rates, and it must be taken into account when designing a degradable system. Further experiments and models should be design

to elucidate how the initial Mw determines the overall degradation rate over the complete library.

7.4   Conclusions

The study of degradation for a subset of L-tyrosine-derived polyarylates provides some insights of the degradation behavior of this polymer family. Three different kinetic equations (zero, first and second order) were used model the degradation process. However, without a more complete study that includes model compounds and the effect of other variables such as temperature, it is not possible to define a priori which kinetic model to use.

The effect of initial Mw on the degradation rates was observed to depend on the polymer. For one polymer, poly(DTiP adipate), the lower the initial Mw, the faster the degradation, while for poly(HTH sebacate) the opposite trend was observed.

Since the degradation profiles could not be correlated to chemical structure, hydrophobicity, or water content, a surrogate model was developed to model and predict them. Descriptors were selected from 2D and 3D structures, including number of primary carbons, electronegativity, and topological descriptors; 3D information about electron diffraction (3D-MorSE); molecular size, shape, symmetry and atom distribution (WHIM); and chemical properties of molecular atoms, branching, cyclicity and conformational changes (GETAWAY).

Separated semi-empirical models were built for the kinetic parameters of degradation, considering zero, first, and second order. The high accuracy on the test sets for the first order kinetic parameter suggests that the mechanism of degradation may follow a first order equation. With this model, the kinetic parameter was predicted for the

rest of the subset of the library. Those results could be used as starting point to select a group of polymers that follow a desired degradation rate. From them, and through experiments, the best polymer from this group could then be selected.

8   Concluding Remarks and Future Work

This work demonstrates that the water uptake and degradation for a library of polymers can be accurately modeled using only a small training set and molecular descriptors for all the polymers in the library. This is the first time that a dynamic property such as water uptake, is modeled and predicted for a large library of polymers.

In the experimental part of this study, polymer processing and initial molecular weight were found to be critical to obtaining reproducible water uptake measurements. Controlling the processing techniques by incorporating an annealing step after pressing, and controlling the initial molecular weight, reproducible water uptake was obtained for a series of L-tyrosine-derived polyarylates.

Initial correlation with intuitive parameters such as glass transition temperature or hydrophobicity was not sufficient to predict either water uptake nor the degradation behavior for all polymers measured, and thus, semi-empirical models needed to be built.

In the computational part of this study, the Combinatorial-Computational Method was shown to be useful in identifying key polymers to include in the training set for the water uptake studies. In only three iterations, it converged to only feasible predictions, and as result, a set of 23 polymers was selected for the water uptake study.

Using a combination of expectation-maximization cluster analysis, decision tree analysis, linear regression and artificial neural networks, accurate surrogate models were obtained for the water uptake profiles of 18 polymers from the library, as represented by three parameters of the Weibull equation. The accuracy of the models depended on the number and type of descriptors, and on the selection of the training and test set. Therefore, all possible combinations of 16 polymers as training and 2 polymers as test set

were used. Those models were able to predict the water uptake profile of 5 independent polymers that were not used in any previous step of the semi-empirical model.

A similar approach was applied to the degradation kinetic parameters for 21 of the polymers from this library. An accurate model for the test sets was obtained for the kinetic parameter of first order degradation, suggesting that this is the kinetics of degradation of those polymers.

Predictions were obtained for water uptake and degradation for 56 polymers from the L-tyrosine-derived polyarylate library. These predictions must be used as a reference of relative levels of water uptake and degradation, respectively, and experiments must be performed to validate the predictions before selecting a polymer for a determined application.

Future studies that can be derived from this study could further elucidate the mechanisms of water uptake and degradation. For water uptake, additional measurements must be obtained for early and late times of incubation. The early measurements may allow understanding the mechanism of water uptake far from the equilibrium, while the late measurements may allow finding the equilibrium water uptake for all polymers. To elucidate the mechanism of degradation, model compounds should be used to follow the products generated by the degradation.

Another study should aim at understanding of the effect of initial molecular weight and degree of polymerization on degradation, by measuring water uptake and degradation for a series of polymers with different initial molecular weights and different end groups (i.e., controlling the relative number of hydrophilic end groups).

Semi-empirical models may be improved by increasing the size of the training sets and by generating more meaningful descriptors, such as 3D descriptors in explicit water. Future studies may extend the methodology, used here for water uptake and degradation in polyarylates, to other properties and other polymer libraries.

Finally, having several semi-empirical models for different polymer properties such as glass transition temperature, contact angle, fibrinogen adsorption, cell response, water uptake and degradation for the same polymer library may be used to test the final goal of the Combinatorial-Computational Method. Having a set of required properties associated with an application to solve a medical need, a group of polymers can be selected from the mentioned models. After this selection, the actual parameters must be measured experimentally, models should be validated, and then the best polymer should be selected to begin the device development process. This will allow us to accelerate the discovery and selection of rationally designed materials having the target device application in mind.

9   References

1.   Kohn J, Welsh WJ, Knight D. A new approach to the rational discovery of polymeric biomaterials. Biomaterials 2007;28:4171-4177.

2.   Li SM, Garreau H, Vert M. Structure property relationships in the case of the degradation of massive aliphatic poly-(alpha-hydroxy acids) in aqueous-media .1. Poly(DL-lactic acid). J Mater Sci Mater Med 1990;1:123-130.

3.   Vert M, Li S, Garreau H. More about the degradation of LA/GA-derived matrices in aqueous-media. J Controlled Release 1991;16:15-26.

4.   Kranz H, Ubrich N, Maincent P, Bodmeier R. Physicomechanical properties of biodegradable poly(D,L-lactide) and poly(D,L-lactide-co-glycolide) films in the dry and wet states. J Pharm Sci 2000;89:1558-1566.

5.   Blasi P, D'Souza SS, Selmin F, DeLuca PP. Plasticizing effect of water on poly(lactide-co-glycolide). J Controlled Release 2005;108:1-9.

6.   Tanaka M, Mochizuki A. Effect of water structure on blood compatibility--thermal analysis of water in poly(meth)acrylate. J Biomed Mater Res, Part A 2004;68:684-695.

7.   Siepmann J, Peppas NA. Hydrophilic matrices for controlled drug delivery: An improved mathematical model to predict the resulting drug release kinetics (the "sequential layer" model). Pharm Res 2000;17:1290-1298.

8.   Wu N, Wang LS, Tan DCW, Moochhala SM, Yang YY. Mathematical modeling and in vitro study of controlled drug release via a highly swellable and dissoluble polymer matrix: polyethylene oxide with high molecular weights. J Controlled Release 2005;102:569-581.

9.   Bourke SL, Kohn J. Polymers derived from the amino acid L-tyrosine: Polycarbonates, polyarylates and copolymers with poly(ethylene glycol). Adv Drug Del Rev 2003;55:447-466.

10.   Brocchini S, James K, Tangpasuthadol V, Kohn J. Structure-property correlations in a combinatorial library of degradable biomaterials. J Biomed Mater Res 1998;42:66-75.

11.   Fiordeliso J, Bron S, Kohn J. Design, synthesis, and preliminary characterization of tyrosine-containing polyarylates: new biomaterials for medical applications. J Biomater Sci Polym Ed 1994;5:497-510.

12.   Hooper KA, Macon ND, Kohn J. Comparative histological evaluation of new tyrosine-derived polymers and poly (L-lactic acid) as a function of polymer degradation. J Biomed Mater Res 1998;41:443-454.

13.   Medical News Today. FDA approves first medical device for hernia repair using rutgers biomaterial. Online. 2006. Available from: http://www.medicalnewstoday.com/articles/35740.php

14.   Tangpasuthadol V, Pendharkar SM, Kohn J. Hydrolytic degradation of tyrosine-derived polycarbonates, a class of new biomaterials. Part I: Study of model compounds. Biomaterials 2000;21:2371-2378.

15.   Tangpasuthadol V, Pendharkar SM, Peterson RC, Kohn J. Hydrolytic degradation of tyrosine-derived polycarbonates, a class of new biomaterials. Part II: 3-yr study of polymeric devices. Biomaterials 2000;21:2379-2387.

16.   Grizzi I, Garreau H, Li S, Vert M. Hydrolytic degradation of devices based on poly(DL-lactic acid): Size-dependence. Biomaterials 1995;16:305-311.

17.   von Burkersroda F, Schedl L, Gopferich A. Why degradable polymers undergo surface erosion or bulk erosion. Biomaterials 2002;23:4221-4231.

18.   Small ICB, Watson TF, Chadwick AV, Sidhu SK. Water sorption in resin-modified glass-ionomer cements: An in vitro comparison with other materials. Biomaterials 1998;19:545-550.

19.   Jeong JH, Lim DW, Han DK, Park TG. Synthesis, characterization and protein adsorption behaviors of PLGA/PEG di-block co-polymer blend films. Colloids Surf, B 2000;18:371-379.

20.   Bajpai SK, Tankhiwale R. Investigation of water uptake behavior and stability of calcium alginate/chitosan bi-polymeric beads: Part-1. React Funct Polym 2006;66:645-658.

21.   Lyu S, Schley J, Loy B, Lind D, Hobot C, Sparer R, et al. Kinetics and time-temperature equivalence of polymer degradation. Biomacromolecules 2007;8:2301-2310.

22.   Akbari H, D'Emanuele A, Attwood D. Effect of fabrication technique on the erosion characteristics of polyanhydride matrices. Pharm Dev Technol 1998;3:251-259.

23.   Chung H, Jang WB, Hwang J, Han H. Analysis of dimensionally stable copolyimide with a low-level residual stress. J Polym Sci, Part B: Polym Phys 2001;39:796-810.

24.   Sancaktar E, Negandhi N, Adwani S. Evaluation of processing effects in injection-molded amorphous and crystalline thermoplastics using an excimer laser. J Appl Polym Sci 2006;101:258-268.

25.   Akele N, Thominette F, Paris D, Pays MF, Verdu J. Physical ageing and water sorption in polycarbonate. Journal of Materials Science Letters 1996;15:1001-1002.

26.   Surana R, Pyne A, Suryanarayanan R. Effect of aging on the physical properties of amorphous trehalose. Pharm Res 2004;21:867-874.

27.   Loo SCJ, Ooi CP, Wee SHE, Boey YCF. Effect of isothermal annealing on the hydrolytic degradation rate of poly(lactide-co-glycolide) (PLGA). Biomaterials 2005;26:2827-2833.

28.   Li Y, Wang F, Yang J, Liu D, Roy A, Case S, et al. Synthesis and characterization of controlled molecular weight disulfonated poly(arylene ether sulfone) copolymers and their applications to proton exchange membranes. Polymer 2006;47:4210-4217.

29.   Gao T, Uludag H. Effect of molecular weight of thermoreversible polymer on in vivo retention of rhBMP-2. J Biomed Mater Res 2001;57:92-100.

30.   Hoskins T, Roman PJ, Ludovice PJ, Henderson CL. Equilibrium water uptake and diffusion behavior in model polynorbornene photoresist polymers. Proc of SPIE 2005;5753:851-861.

31.   Singh L, Ludovice PJ, Henderson CL. Effect of nanoscale confinement on the diffusion behavior of photoresist polymer thin films. Proc of SPIE 2004;5376:369-378.

32.   D570-98: Standard test method for water absorption of plastics. 1998.

33.   Park ES, Maniar M, Shah J. Water uptake in to polyanhydride devices: kinetics of uptake and effects of model compounds incorporated, and device geometry on water uptake. J Controlled Release 1996;40:55-65.

34.   Takata H, Furuichi K, Nishikawa M, Fukada S, Katayama K, Takeishi T, et al. Concentration profiles of tritium penetrated into concrete. Fusion Sci Technol 2008;54:223-226.

35.   Takata H, Nishikawa M, Arimura Y, Egawa T, Fukada S, Yoshitake M. Study on water uptake of proton exchange membrane by using tritiated water sorption method. Int J Hydrogen Energy 2005;30:1017-1025.

36.   Theis DL, Rohrs BR, Stodola JD, Borchert SJ. A rapid, sensitive, radiotracer technique for the determination of water uptake of packaged dosage formulations. Pharm Technol 2005:126-134.

37.   Brocchini S, James K, Tangpasuthadol V, Kohn J. A combinatorial approach for polymer design. J Am Chem Soc 1997;119:4553-4554.

38.   Suarez N, Brocchini S, Kohn J. The study of water uptake in degradable polymers by thermally stimulated depolarization currents. Biomaterials 1998;19:2347-2356.

39.   Suarez N, Brocchini S, Kohn J. Study of relaxation mechanisms in structurally related biomaterials by thermally stimulated depolarization currents. Polymer 2001;42:8671-8680.

40.   Haykin S. Neural networks, a comprehensive foundation. Second ed. Upper Saddle River, NJ: Pearson Education, 1999.

41.   Beale R, Jackson T. Neural computing: an introduction. Great Britain: IOP Publishing Ltd., 1990.

42.   Todeschini R, Consonni V. Handbook of molecular descriptors. 1st ed. Wemheim, Germany: Wiley-VCH, 2000.

43.   Pereira JCG, Catlow CRA, Price GD. Molecular dynamics simulation of liquid H2O, MeOH, EtOH, Si(OMe)(4), and Si(OEt)(4), as a function of temperature and pressure. J Phys Chem A 2001;105:1909-1925.

44.   Tamai Y, Tanaka H, Nakanishi K. Molecular dynamics study of polymer-water interaction in hydrogels .2. Hydrogen-bond dynamics. Macromolecules 1996;29:6761-6769.

45.   Gubskaya AV, Kusalik PG. Molecular dynamics simulation study of ethylene glycol, ethylenediamine, and 2-aminoethanol. 2. Structure in aqueous solutions. J Phys Chem A 2004;108:7165-7178.

46.   Behler J, Price DW, Drew MGB. Water structuring properties of carbohydrates, molecular dynamics studies on 1,5-anhydro-D-fructose. Phys Chem Chem Phys 2001;3:588-601.

47.   Quinlan R. C4.5: Programs for machine learning. San Mateo, CA: Morgan Kaufmann Publishers, 1993.

48.   Witten IH, Frank E. Data Mining: Practical machine learning tools and techniques with JAVA implementations. 1st edition ed. San Diego: Academic Press, 2000.

49.   Gao JG, Xu J, Chen B, Zhang QJ. A quantitative structure-property relationship study for refractive indices of conjugated polymers. J Mol Model 2007;13:573-578.

50.   Afantitis A, Melagraki G, Makridima K, Alexandridis A, Sarimveis H, Iglessi-Markopoulou O. Prediction of high weight polymers glass transition temperature using RBF neural networks. J Mol Struc-Theochem 2005;716:193-198.

51.   Seyhan AT, Tayfur G, Karakurt M, Tanoglu M. Artificial neural network (ANN) prediction of compressive strength of VARTM processed polymer composites. Comp Mater Sci 2005;34:99-105.

52.   Gao JW, Wang XY, Li XB, Yu XL, Wang HL. Prediction of polyamide properties using quantum-chemical methods and BP artificial neural networks. J Mol Model 2006;12:513-520.

53.   Liu WQ, Yi PG, Tang ZL. QSPR models for various properties of polymethacrylates based on quantum chemical descriptors. QSAR Comb Sci 2006;25:936-943.

54.   Gharagheizi F. QSPR analysis for intrinsic viscosity of polymer solutions by means of GA-MLR and RBFNN. Comp Mater Sci 2007;40:159-167.

55.   Xu J, Liang H, Chen B, Xu WL, Shen XL, Liu HT. Linear and nonlinear QSPR models to predict refractive indices of polymers from cyclic dimer structures. Chemometr Intell Lab 2008;92:152-156.

56.   Jiang ZY, Zhang Z, Friedrich K. Prediction on wear properties of polymer composites with artificial neural networks. Compos Sci Technol 2007;67:168-176.

57.   Du C, Tang D, Zhou J, Wang H, Shaviv A. Prediction of nitrate release from polymer-coated fertilizers using an artificial neural network model. Biosyst Eng 2008;99:478-486.

58.   Cypcar CC, Camelio P, Lazzeri V, Mathias LJ, Waegell B. Prediction of the glass transition temperature of multicyclic and bulky substituted acrylate and methacrylate polymers using the energy, volume, mass (EVM) QSPR model. Macromolecules 1996;29:8954-8959.

59.   Katritzky AR, Rachwal P, Law KW, Karelson M, Lobanov VS. Prediction of polymer glass transition temperatures using a general quantitative structure-property relationship treatment. J Chem Inf Comp Sci 1996;36:879-884.

60.   Camelio P, Cypcar CC, Lazzeri V, Waegell B. A novel approach toward the prediction of the glass transition temperature: Application of the EVM model, a designer QSPR equation for the prediction of acrylate and methacrylate polymers. Journal of Polymer Science Part a-Polymer Chemistry 1997;35:2579-2590.

61.   Reynolds CH. Designing diverse and focused combinatorial libraries of synthetic polymers. J Comb Chem 1999;1:297-306.

62.   Carro AM, Campisi B, Camelio P, Phan-Tan-Luu R. Improving an EVM QSPR model for glass transition temperature prediction using optimal design. Chemometr Intell Lab 2002;62:79-88.

63.   Garcia-Domenech R, de Julian-Ortiz JV. Prediction of indices of refraction and glass transition temperatures of linear polymers by using graph theoretical indices. J Phys Chem B 2002;106:1501-1507.

64.   Mattioni BE, Jurs PC. Prediction of glass transition temperatures from monomer and repeat unit structure using computational neural networks. J Chem Inf Comp Sci 2002;42:232-240.

65.   Sun H, Tang YW, Wu GS, Zhang FS. Investigation of the relationship of the glass-transition temperature and the polymer structure by fuzzy set theory. Journal of Polymer Science Part B-Polymer Physics 2002;40:454-459.

66.   Cao CZ, Lin YB. Correlation between the glass transition temperatures and repeating unit structure for high molecular weight polymers. J Chem Inf Comp Sci 2003;43:643-650.

67.   Dai JF, Liu SL, Chen Y, Cao CZ. A quantitative structure-property relationship study on glass transition temperature of polyacrylates. Acta Polym Sin 2003:343-347.

68.   Morrill JA, Jensen RE, Madison PH, Chabalowski CF. Prediction of the formulation dependence of the glass transition temperatures of amine-epoxy copolymers using a QSPR based on the AM1 method. J Chem Inf Comp Sci 2004;44:912-920.

69.   Brown WM, Martin S, Rintoul MD, Faulon JL. Designing novel polymers with targeted properties using the signature molecular descriptor brown. J Chem Inf Comp Sci 2006;46:826-835.

70.   Duce C, Micheli A, Solaro R, Starita A, Tine MR. Prediction of chemical-physical properties by neural networks for structures. Macromol Symp 2006;234:13-19.

71.   Duce C, Micheli A, Starita A, Tine MR, Solaro R. Prediction of polymer properties from their structure by recursive neural networks. Macromol Rapid Comm 2006;27:711-715.

72.   Yu XL, Wang XY, Li XB, Gao JW, Wang HL. Prediction of glass transition temperatures for polystyrenes by a four-descriptors QSPR model. Macromol Theor Simul 2006;15:94-99.

73.   Yu XL, Wang XY, Wang HL, Liu AH, Zhang CL. Prediction of the glass transition temperatures of styrenic copolymers using a QSPR based on the DFT method. J Mol Struc-Theochem 2006;766:113-117.

74.   Bertinetto C, Duce C, Micheli A, Solaro R, Starita A, Tine MR. Prediction of the glass transition temperature of (meth)acrylic polymers containing phenyl groups by recursive neural network. Polymer 2007;48:7121-7129.

75.   Liu AH, Wang XY, Wang L, Wang HL, Wang HL. Prediction of dielectric constants and glass transition temperatures of polymers by quantitative structure property relationships. Eur Polym J 2007;43:989-995.

76.   Yu XL, Yi B, Wang XY, Xie ZM. Correlation between the glass transition temperatures and multipole moments for polymers. Chem Phys 2007;332:115-118.

77.   Chen X, Sztandera L, Cartwright HM. A neural network approach to prediction of glass transition temperature of polymers. Int J Intell Syst 2008;23:22-32.

78.   Schut J, Bolikal D, Khan IJ, Pesnell A, Rege A, Rojas R, et al. Glass transition temperature prediction of polymers through the mass-per-flexible-bond principle. Polymer 2007;48:6115-6124.

79.   Katritzky AR, Sild S, Lobanov V, Karelson M. Quantitative structure-property relationship (QSPR) correlation of glass transition temperatures of high molecular weight polymers. J Chem Inf Comp Sci 1998;38:300-304.

80.   Katritzky AR, Sild S, Karelson M. Correlation and prediction of the refractive indices of polymers by QSPR. J Chem Inf Comp Sci 1998;38:1171-1176.

81.   Xu J, Chen B, Zhang QJ, Guo B. Prediction of refractive indices of linear polymers by a four-descriptor QSPR model. Polymer 2004;45:8651-8659.

82.   Holder AJ, Ye L, Eick JD, Chappelow CC. A quantum-mechanical QSAR model to predict the refractive index of polymer matrices. QSAR Comb Sci 2006;25:905-911.

83.   Whittaker AK, Blakey I, Chen L, Dargaville B, Liu HP, Conley W, et al. Rational design of high-RI resists for 193nm immersion lithography. J Photopolym Sci Tec 2007;20:665-671.

84.   Melagraki G, Afantitis A, Sarimveis H, Koutentis PA, Markopoulos J, Igglessi-Markopoulou O. A novel QSPR model for predicting theta (lower critical solution temperature) in polymer solutions using molecular descriptors. J Mol Model 2007;13:55-64.

85.   Xu J, Liu L, Xu WL, Zhao SP, Zuo DY. A general QSPR model for the prediction of theta (lower critical solution temperature) in polymer solutions with topological indices. J Mol Graph Model 2007;26:352-359.

86.   Xu J, Chen B, Liang H. Accurate prediction of theta (lower critical solution temperature) in polymer solutions based on 3D descriptors and artificial neural networks. Macromol Theor Simul 2008;17:109-120.

87.   Afantitis A, Melagraki G, Sarimveis H, Koutentis PA, Markopoulos J, Igglessi-Markopoulou O. Prediction of intrinsic viscosity in polymer-solvent combinations using a QSPR model. Polymer 2006;47:3240-3248.

88.   Al-Haik MS, Hussaini MY, Garmestani H. Prediction of nonlinear viscoelastic behavior of polymeric composites using an artificial neural network. Int J Plasticity 2006;22:1367-1392.

89.   Patel HC, Tokarski JS, Hopfinger AJ. Molecular modeling of polymers .16. Gaseous diffusion in polymers: A quantitative structure-property relationship (QSPR) analysis. Pharm Res 1997;14:1349-1354.

90.   Tokarski JS, Hopfinger AJ, Hobbs JD, Ford DM, Faulon JLM. Molecular modelling of polymers 17. Simulation and QSPR analyses of transport behavior in amorphous polymeric materials. Comput Theor Polym S 1997;7:199-214.

91.   Nantasenamat C, Naenna T, Isarankura Na Ayudhya C, Prachayasittikul V. Quantitative prediction of imprinting factor of molecularly imprinted polymers by artificial neural network. J Comput Aided Mol Des 2005;19:509-524.

92.   Nantasenamat C, Sarankura-Na-Ayudhya C, Naenna T, Prachayasittikul V. Quantitative structure-imprinting factor relationship of molecularly imprinted polymers. Biosens Bioelectron 2007;22:3309-3317.

93.   Yu XL, Wang X, Li XB, Gao JW, Wang H. Quantitative structure-property relationship studies of polymeric cohesive energy by density functional theory. Journal of Polymer Science Part B-Polymer Physics 2006;44:409-415.

94.   Yu XL, Wang XY, Wang HL, Li XB, Gao JW. Prediction of solubility parameters for polymers by a QSPR model. QSAR Comb Sci 2006;25:156-161.

95.   Khajeh A, Hopfenberg HB, Frisch HL. Solubility prediction for carbon dioxide in polymers by artificial neural network. Iran Polym J 2007;16:759-768.

96.   Yu XL, Xie ZM, Yi B, Wang XY, Liu F. Prediction of the thermal decomposition property of polymers using quantum chemical descriptors. Eur Polym J 2007;43:818-823.

97.   Yu XL, Yi B, Xie ZM, Wang XE, Liu F. Prediction of the conformational property for polymers using quantum chemical descriptors. Chemometr Intell Lab 2007;87:247-251.

98.   Gubskaya AV, Kholodovych V, Knight D, Kohn J, Welsh WJ. Prediction of fibrinogen adsorption for biodegradable polymers: Integration of molecular dynamics and surrogate modeling. Polymer 2007;48:5788-5801.

99.   Kholodovych V, Smith JR, Knight D, Abramson S, Kohn J, Welsh WJ. Accurate predictions of cellular response using QSPR: a feasibility test of rational design of polymeric biomaterials. Polymer 2004;45:7367-7379.

100.   Smith JR, Kholodovych V, Knight D, Kohn J, Welsh WJ. Predicting fibrinogen adsorption to polymeric surfaces in silico: a combined method approach. Polymer 2005;46:4296-4306.

101.   Smith JR, Kholodovych V, Knight D, Welsh WJ, Kohn J. QSAR models for the analysis of bioresponse data from combinatorial libraries of biomaterials. QSAR Comb Sci 2005;24:99-113.

102.   Smith JR, Knight D, Kohn J, Rasheed K, Weber N, Kholodovych V, et al. Using surrogate modeling in the prediction of fibrinogen adsorption onto polymer surfaces. J Chem Inf Comput Sci 2004;44:1088-1097.

103.   Smith JR, Seyda A, Weber N, Knight D, Abramson S, Kohn J. Integration of combinatorial synthesis, rapid screening, and computational modeling in biomaterials development. Macromol Rapid Commun 2004;25:127–140.

104.   Kholodovych V, Gubskaya AV, Bohrer M, Harris N, Knight D, Kohn J, et al. Prediction of biological response for large combinatorial libraries of biodegradable polymers: Polymethacrylates as a test case. Polymer 2008;49:2435-2439.

105.   Ebube NK, Owusu-Ababio G, Adeyeye CM. Preformulation studies and characterization of the physicochemical properties of amorphous polymers using artificial neural networks. Int J Pharm 2000;196:27-35.

106.   Gubskaya AV, Kholodovych V, Knight D, Kohn J, Welsh WJ. Prediction of fibrinogen adsorption for biodegradable polymers: Integration of molecular dynamics and surrogate modeling. Polymer 2007;48:5788-5801.

107.   Kholodovych V, Welsh WJ, Thakur R, Michniak B, Kohn J. Molecular Modeling the Water Uptake of Biomaterials. Society for Biomaterials Annual Meeting, 2006.

108.   Hatakeyama H, Hatakeyama T. Interaction between water and hydrophilic polymers. Thermochim Acta 1998;308:3-22.

109.   Crank J, Park GS. Diffusion in polymers. 1st ed. London, Great Britain: Academic Press Inc., 1968.

110.   Correlo VM, Pinho ED, Pashkuleva I, Bhattacharya M, Neves NM, Reis RL. Water absorption and degradation characteristics of chitosan-based polyesters and hydroxyapatite composites. Macromol Biosci 2007;7:354-363.

111.   Han H, Gryte CC, Ree M. Water diffusion and sorption in films of high-performance poly(4,4'-oxydiphenylene pyromellitimide) - effects of humidity, imidization history and film thickness. Polymer 1995;36:1663-1672.

112. Sun YM. Sorption/desorption properties of water vapour in poly(2-hydroxyethyl methacrylate) .2. Two-stage sorption models. Polymer 1996;37:3921-3928.

113. Nogueira P, Ramirez C, Torres A, Abad MJ, Cano J, Lopez J, et al. Effect of water sorption on the structure and mechanical properties of an epoxy resin system. J Appl Polym Sci 2001;80:71-80.

114. Santos C, Clarke RL, Braden M, Guitian F, Davy KWM. Water absorption characteristics of dental composites incorporating hydroxyapatite filler. Biomaterials 2002;23:1897-1904.

115. Asaoka K, Hirano S. Diffusion coefficient of water through dental composite resin. Biomaterials 2003;24:975-979.

116. Sideridou I, Achilias DS, Spyroudi C, Karabela M. Water sorption characteristics of light-cured dental resins and composites based on Bis-EMA/PCDMA. Biomaterials 2004;25:367-376.

117. Chowdhury MA, Hill DJ, Whittaker AK. Mass uptake study of the diffusion of water and SBF into poly(2-hydroxyethyl methacrylate-co-tetrahydrofurfuryl methacrylate) containing aspirin or vitamin B12. J Biomater Sci Polym Ed 2005;16:1047-1061.

118. Sutandar P, Ahn DJ, Franses EI. Ftir Atr Analysis for Microstructure and Water-Uptake in Poly(Methyl Methacrylate) Spin Cast and Langmuir-Blodgett Thin-Films. Macromolecules 1994;27:7316-7328.

119. Polishchuk AY, Zaikov GE. General-Model of Transport of Water and Low-Molecular-Weight Solute in Swelling Polymer. Int J Polym Mater 1994;25:1-12.

120. Riggs PD, Parker S, Braden M, Kalachandra S. Influence of additives on the water uptake of hydrosilanized silicone rubbers. Biomaterials 1997;18:721-726.

121. Perez C, Collazo A, Izquierdo M, Merino P, Novoa XR. Characterisation of the barrier properties of different paint systems - Part I. Experimental set-up and ideal Fickian diffusion. Prog Org Coat 1999;36:102-108.

122. Palin WM, Fleming GJP, Burke FJT, Marquis PM, Randall RC. The influence of short and medium-term water immersion on the hydrolytic stability of novel low-shrink dental composites. Dent Mater 2005;21:852-863.

123.   Pitt CG, Shah SS. Manipulation of the rate of hydrolysis of polymer-drug conjugates - the degree of hydration. J Controlled Release 1995;33:397-403.

124.   Siepmann J, Kranz H, Bodmeier R, Peppas NA. HPMC-matrices for controlled drug delivery: A new model combining diffusion, swelling, and dissolution mechanisms and predicting the release kinetics. Pharm Res 1999;16:1748-1756.

125.   Bajpai AK, Bajpai J, Shukla S. Modulation of in vitro release of crystal violet from a binary polymer hydrogel system. J Macromol Sci A 2002;39:489-508.

126.   Stafford GD, Braden M. Water Absorption of Some Denture Base Polymers. J Dent Res 1968;47:341-.

127.   Miskovic-Stankovic VB, Drazic DM, Kacarevic-Popovic Z. The sorption characteristics of epoxy coatings electrodeposited on steel during exposure to different corrosive agents. Corros Sci 1996;38:1513-1523.

128.   Miskovic-stankovic VB, Drazic DM, Teodorovic MJ. Electrolyte penetration through epoxy coatings electrodeposited on steel. Corros Sci 1995;37:241-252.

129.   Chaplin A, Hamerton I, Herman H, Mudhar AK, Shaw SJ. Studying water uptake effects in resins based on cyanate ester/bismaleimide blends. Polymer 2000;41:3945-3956.

130.   Valente AJM, Polishchuk AY, Burrows HD, Lobo VMM. Permeation of water as a tool for characterizing the effect of solvent, film thickness and water solubility in cellulose acetate membranes. Eur Polym J 2005;41:275-281.

131.   Garcia-Pascual P, Sanjuan N, Bon J, Carreres JE, Mulet A. Rehydration process of Boletus edulis mushroom: characteristics and modelling. J Sci Food Agr 2005;85:1397-1404.

132.   Bagley E, Long FA. Two-stage Sorption and Desorption of Organic Vapors in Cellulose Acetate. J Am Chem Soc 1955;77:2172-2178.

133.   Parker S, Braden M. Water-absorption of methacrylate soft lining materials. Biomaterials 1989;10:91-95.

134.   Shay GD, Olesen KR, Stallings JL. Predicting the water-sensitivity of film-forming coatings additives by water vapor sorption: With application to thickeners and rheology modifiers. J Coat Technol 1996;68:51-63.

135. Thomas AG, Muniandy K. Absorption and desorption of water in rubbers. Polymer 1987;28:408-415.

136. Kochetkov VA, Maksimov RD. Water absorption and swelling of glass/epoxy syntactic foams. Mech Compos Mater 1996;32:61-70.

137. Sanjuan N, Carcel JA, Clemente G, Mulet A. Modelling of the rehydration process of brocolli florets. Eur Food Res Technol 2001;212:449-453.

138. Frisch HL. Sorption and transport in glassy polymers-a review. Polym Eng Sci 1980;20:2-13.

139. Liu W, Hoa S, Pugh M. Water uptake of epoxy-clay nanocomposites: Model development. Compos Sci Technol 2008;68:156-163.

140. Chirico S, Dalmoro A, Larnberti G, Russo G, Titomanlio G. Analysis and modeling of swelling and erosion behavior for pure HPMC tablet. J Controlled Release 2007;122:181-188.

141. Lyu S, Sparer R, Untereker D. Analytical solutions to mathematical models of the surface and bulk erosion of solid polymers. Journal of Polymer Science Part B-Polymer Physics 2005;43:383-397.

142. Milroy GE, Smith RW, Hollands R, Clough AS, Mantle MD, Gladden LF, et al. The degradation of polyglycolide in water and deuterium oxide. part II: Nuclear reaction analysis and magnetic resonance imaging of water distribution. Polymer 2003;44:1425-1435.

143. Crank J. The mathematics of diffusion. 2nd ed. Oxford, Great Britain: Clerendon Press, 1975.

144. Berens AR, Hopfenberg HB. Diffusion and relaxation in glassy polymer powders: 2. Separation of diffusion and relaxation parameters. Polymer 1978;19:489-496.

145. Ritger PL, Peppas NA. A simple equation for description of solute release II. Fickian and anomalous release from swellable devices. J Controlled Release 1987;5:37-42.

146. Wind MM, Lenderink HJW. A capacitance study of pseudo-fickian diffusion in glassy polymer coatings. Prog Org Coat 1996;28:239-250.

147. Gafourian T, Safari A, Adibkia K, Parviz F, Nokhodchi A. A drug release study from hydroxypropylmethylcellulose (HPMC) matrices using QSPR modeling. J Pharm Sci 2007;96:3334-3351.

148. Krokida MK, Marinos-Kouris D. Rehydration kinetics of dehydrated products. J Food Eng 2003;57:1-7.

149. Vieth W. Diffusion in and through polymers. Principles and applications. 1st ed. Germany: Hanser, 1991.

150. Bajpai SK, Singh S. Analysis of swelling behavior of poly(methacrylamide-co-methacrylic acid) hydrogels and effect of synthesis conditions on water uptake. React Funct Polym 2006;66:431-440.

151. Brannon-Peppas L, Peppas NA. Solute and penetrant diffusion in swellable polymers. IX. The mechanisms of drug release from ph-sensitive swelling-controlled systems. J Controlled Release 1989;8:267-274.

152. Perez C, Collazo A, Izquierdo M, Merino P, Novoa XR. Characterisation of the barrier properties of different paint systems Part II. Non-ideal diffusion and water uptake kinetics. Prog Org Coat 1999;37:169-177.

153. Riggs PD, Braden M, Tilbrook DA, Swai H, Clarke RL, Patel MP. The water uptake of poly(tetrahydrofurfurylmethacrylate). Biomaterials 1999;20:435-441.

154. Ghi P, Hill DJT, Whittaker AK. Water sorption by poly(tetrahydrofurfuryl methacrylate-co-2-hydroxyethyl methacrylate). I. A mass-uptake study. Journal of Polymer Science Part B-Polymer Physics 2000;38:1939-1946.

155. Michailova V, Titeva S, Kotsilkova R, Krusteva E, Minkov E. Water uptake and relaxation processes in mixed unlimited swelling hydrogels. Int J Pharm 2000;209:45-56.

156. Bajpai AK, Giri A. Water sorption behaviour of highly swelling (carboxy methylcellulose-g-polyacrylamide) hydrogels and release of potassium nitrate as agrochemical. Carbohyd Polym 2003;53:271-279.

157. Bajpai AK, Mishra A. Ionizable interpenetrating polymer networks of carboxymethyl cellulose and polyacrylic acid: Evaluation of water uptake. J Appl Polym Sci 2004;93:2054-2065.

158. Bajpai AK, Sharma M. Preparation and characterization of binary grafted polymeric blends of polyvinyl alcohol and gelatin and evaluation of their water uptake potential. J Macromol Sci A 2005;A42:663-682.

159. Bajpai AK, Sharma M. Preparation and characterization of novel pH-sensitive binary grafted polymeric blends of gelatin and poly(vinyl alcohol): Water sorption and blood compatibility study. J Appl Polym Sci 2006;100:599-617.

160. Reis AV, Guilherme MR, Cavalcanti OA, Rubira AF, Muniz EC. Synthesis and characterization of pH-responsive hydrogels based on chemically modified Arabic gum polysaccharide. Polymer 2006;47:2023-2029.

161. Brazel CS, Peppas NA. Dimensionless analysis of swelling of hydrophilic glassy polymers with subsequent drug release from relaxing structures. Biomaterials 1999;20:721-732.

162. Peppas NA, Brannonpeppas L. Water diffusion and sorption in amorphous macromolecular systems and foods. J Food Eng 1994;22:189-210.

163. Davidson Iii GWR, Peppas NA. Solute and penetrant diffusion in swellable polymers: V. Relaxation-controlled transport in P(HEMA-co-MMA) copolymers. J Controlled Release 1986;3:243-258.

164. Akdemir ZS, Kayaman-Apohan N. Investigation of swelling, drug release and diffusion behaviors of poly(N-isopropylacrylamide)/poly (N-vinylpyrrolidone) full-IPN hydrogels. Polym Advan Technol 2007;18:932-939.

165. Vrentas JS, Jarzebski CM, Duda JL. A Deborah number for diffusion in polymer-solvent systems. Aiche Journal 1975;21:894-901.

166. Davidson Iii GWR, Peppas NA. Solute and penetrant diffusion in swellable polymers: VI. The Deborah and swelling interface numbers as indicators of the order of biomolecular release. J Controlled Release 1986;3:259-271.

167. Bell CL, Peppas NA. Water, solute and protein diffusion in physiologically responsive hydrogels of poly(methacrylic acid-g-ethylene glycol). Biomaterials 1996;17:1203-1218.

168. Peppas NA, Sahlin JJ. A simple equation for the description of solute release .3. Coupling of diffusion and relaxation. Int J Pharm 1989;57:169-172.

169.   Weibull W. A statistical distribution of wide applicability. J Appl Mech 1951;18:293-297.

170.   Hahn GJ, Shapiro SS. Statistical models in engineering. 1st ed. New York: John Wiley & Sons, Inc., 1967.

171.   Machado MD, Oliveira FAR, Gekas V, Singh RP. Kinetics of moisture uptake and soluble-solids loss by puffed breakfast cereals immersed in water. Int J Food Sci Tech 1998;33:225-237.

172.   Marabi A, Livings S, Jacobson M, Saguy IS. Normalized Weibull distribution for modeling rehydration of food particulates. Eur Food Res Technol 2003;217:311-318.

173.   Marabi A, Jacobson M, Livings SJ, Saguy IS. Effect of mixing and viscosity on rehydration of dry food particulates. Eur Food Res Technol 2004;218:339-344.

174.   Marabi A, Saguy IS. Effect of porosity on rehydration of dry food particulates. J Sci Food Agr 2004;84:1105-1110.

175.   Marabi A, Saguy IS. Viscosity and starch particle size effects on rehydration of freeze-dried carrots. J Sci Food Agr 2005;85:700-706.

176.   Saguy IS, Marabi A, Wallach R. New approach to model rehydration of dry food particulates utilizing principles of liquid transport in porous media. Trends Food Sci Tech 2005;16:495-506.

177.   Garcia-Pascual P, Sanjuan N, Melis R, Mulet A. Morchella esculenta (morel) rehydration process modelling. J Food Eng 2006;72:346-353.

178.   Deng Y, Zhao YY. Effects of pulsed-vacuum and ultrasound on the osmodehydration kinetics and microstructure of apples (Fuji). J Food Eng 2008;85:84-93.

179.   Mahajan PV, Rodrigues FAS, Motel A, Leonhard A. Development of a moisture absorber for packaging of fresh mushrooms (Agaricus bispoirous). Postharvest Biol Tec 2008;48:408-414.

180.   Langenbucher F. Linearization of dissolution rate curves by the Weibull distribution. J Pharm Pharmacol 1972;24:979-981.

181.   Vudathala GK, Rogers JA. Dissolution of fluorocortisone from phospholipid coprecipitates. J Pharm Sci 1992;81:282-286.

182.   Schreiner T, Schaefer UF, Loth H. Immediate drug release from solid oral dosage forms. J Pharm Sci 2005;94:120-133.

183.   Muster TH, Prestidge CA. Water adsorption kinetics and contact angles of pharmaceutical powders. J Pharm Sci 2005;94:861-872.

184.   Long FA, Richman D. Concentration Gradients for Diffusion of Vapors in Glassy Polymers and their Relation to Time Dependent Diffusion Phenomena. J Am Chem Soc 1960;82:513-519.

185.   Sun YM, Lee HL. Sorption/desorption properties of water vapour in poly(2-hydroxyethyl methacrylate) .1. Experimental and preliminary analysis. Polymer 1996;37:3915-3919.

186.   Sanopoulou M, Roussis PP, Petropoulos JH. A detailed study of the viscoelastic nature of vapor sorption and transport in a cellulosic polymer. I. Origin and physical implications of deviations from Fickian sorption kinetics. J Polym Sci, Part B: Polym Phys 1995;33:993-1005.

187.   Joshi S, Astarita G. Diffusion-relaxation coupling in polymers which show two-stage sorption phenomena. Polymer 1979;20:455-458.

188.   Kang YS, Meldon JH, Sung N. Transport of hexane vapor in polystyrene at 25∞C I. Analysis of integral sorption data. J Polym Sci, Part B: Polym Phys 1990;28:1093-1103.

189.   Riggs PD, Clough AS, Jenneson PM, Drew DW, Braden M, Patel MP. He-3 ion-beam analysis of water uptake and drug delivery. J Controlled Release 1999;61:165-174.

190.   Abu-Ghannam N, McKenna B. The application of Peleg's equation to model water absorption during the soaking of red kidney beans (Phaseolus vulgaris L.). J Food Eng 1997;32:391-401.

191.   Maskan M. Effect of processing on hydration kinetics of three wheat products of the same variety. J Food Eng 2002;52:337-341.

192.   Bilbao-Sainz C, Andres A, Fito P. Hydration kinetics of dried apple as affected by drying conditions. J Food Eng 2005;68:369-376.

193.   Turhan M, Sayar S, Gunasekaran S. Application of Peleg model to study water absorption in chickpea during soaking. J Food Eng 2002;53:153-159.

194.   Johnson PNT, Brennan JG. Kinetics of moisture absorption by plantain flour. J Food Eng 2000;45:33-36.

195.   Smith JR, Kholodovych V, Knight D, Welsh WJ, Kohn J. Surrogate modeling for the analysis of bioresponse data from combinatorial libraries of polymers. QSAR Combinatorial Sci 2005;24:99-113.

196.   Chemical Computing Group Inc. MOE (The molecular operating environment). 02 ed. Montreal, Canada H3A 2R7, 2003.

197.   Todeschini R, Consonni V, Mauri A, Pavan M. Dragon Web version. v.3.0. Milano, Italy, 2003.

198.   Schrodinger L. Macromodel. v. 8.5. New York, NY, 2005.

199.   Still WC, Tempczyk A, Hawley RC, Hendrickson T. Semianalytical treatment of solvation for molecular mechanics and dynamics. J Am Chem Soc 1990;112:6127-6129.

200.   Jorgensen WL, Maxwell DS, TiradoRives J. Development and testing of the OPLS all-atom force field on conformational energetics and properties of organic liquids. J Am Chem Soc 1996;118:11225-11236.

201.   Consonni V, Todeschini R, Pavan M. Structure/response correlations and similarity/diversity analysis by GETAWAY descriptors. 1. Theory of the novel 3D molecular descriptors. J Chem Inf Comp Sci 2002;42:682-692.

202.   Barysz M, Trinajstic N. A novel-approach to the characterization of chemical structures. Int J Quantum Chem 1984:661-673.

203.   Lovasz L, Pelikan J. On the eigenvalues of trees. Periodica mathematica Hungarica 1973;3:175-182.

204.   Balaban AT, Ciubotariu D, Medeleanu M. Topological indexes and real number vertex invariants based on graph eigenvalues or eigenvectors. J Chem Inf Comp Sci 1991;31:517-523.

205.   Randic M. Novel shape descriptors for molecular graphs. J Chem Inf Comp Sci 2001;41:607-613.

206.   Petitjean M. Applications of the Radius Diameter Diagram to the Classification of Topological and Geometrical Shapes of Chemical-Compounds. J Chem Inf Comp Sci 1992;32:331-337.

207.   Galvez J, Garcia R, Salabert MT, Soler R. Charge Indexes - New Topological Descriptors. J Chem Inf Comp Sci 1994;34:520-525.

208.   Gasteiger J, Marsili M. Iterative partial equalization of orbital electronegativity: a rapid access to atomic charges. Tetrahedron 1980;36:3219-3228.

209.   Adamson GW, Lynch MF, Town WG. Analysis of structural characteristics of chemical compounds in a large computer-based file. Part II. Atom-centred fragments. J Chem Soc C 1971:3702-3706.

210.   Wildman SA, Crippen GM. Prediction of physicochemical parameters by atomic contributions. J Chem Inf Comp Sci 1999;39:868-873.

211.   Todeschini R, Gramatica P, Provenzani R, Marengo E. Weighted Holistic Invariant Molecular Descriptors .2. Theory Development and Applications on Modeling Physicochemical Properties of Polyaromatic Hydrocarbons. Chemometr Intell Lab 1995;27:221-229.

212.   Hall MA. Correlation-based feature selection for machine learning. Hamilton, New Zeland: The University of Waikato; 1999.

213.   Pearlman RS, Smith KM. Metric validation and the receptor-relevant subspace concept. J Chem Inf Comp Sci 1999;39:28-35.

214.   Moran PAP. Notes on continuous stochastic phenomena. Biometrika 1950;37:17-23.

215.   Gasteiger J, Schuur J, Selzer P, Steinhauer L, Steinhauer V. Finding the 3D structure of a molecule in its IR spectrum. Fresen J Anal Chem 1997;359:50-55.

216.   Wu LB, Ding JD. In vitro degradation of three-dimensional porous poly(D,L-lactide-co-glycolide) scaffolds for tissue engineering. Biomaterials 2004;25:5821-5830.

217.   Yoshioka T, Kawazoe N, Tateishi T, Chen G. In vitro evaluation of biodegradation of poly(lactic-co-glycolic acid) sponges. Biomaterials 2008;29:3438-3443.

218.   de Jong SJ, Arias ER, Rijkers DTS, van Nostrum CF, Kettenes-van den Bosch JJ, Hennink WE. New insights into the hydrolytic degradation of poly(lactic acid): participation of the alcohol terminus. Polymer 2001;42:2795-2802.

219.   Farrar DF, Gillson RK. Hydrolytic degradation of polyglyconate B: the relationship between degradation time, strength and molecular weight. Biomaterials 2002;23:3905-3912.

220.   Loh XJ, Tan KK, Li X, Li J. The in vitro hydrolysis of poly(ester urethane)s consisting of poly[(R)-3-hydroxybutyrate] and poly(ethylene glycol). Biomaterials 2006;27:1841-1850.

221.   Zhu KJ, Hendren RW, Jensen K, Pitt CG. Synthesis, Properties, and Biodegradation of Poly(1,3-Trimethylene Carbonate). Macromolecules 1991;24:1736-1740.

222.   Chattopadhyay S, Madras G. Degradation kinetics of poly(vinyl acetate) in the presence of aluminum chloride. Polym Degrad Stabil 2001;73:83-86.

223.   Horta A, Coca J, Diez FV. Degradation mechanism and kinetics of a high thermally stable aromatic polyamide. Adv Polym Tech 2000;19:120-131.

224.   Tayal A, Kelly RM, Khan SA. Rheology and molecular weight changes during enzymatic degradation of a water-soluble polymer. Macromolecules 1999;32:294-300.

225.   Hakkarainen M, Albertsson AC, Karlsson S. Weight losses and molecular weight changes correlated with the evolution of hydroxyacids in simulated in vivo degradation of homo- and copolymers of PLA and PGA. Polym Degrad Stabil 1996;52:283-291.

226.   Liu TQ, Simmons TL, Bohnsack DA, Mackay ME, Smith MR, Baker GL. Synthesis of polymandelide: A degradable polylactide derivative with polystyrene-like properties. Macromolecules 2007;40:6040-6047.

Curriculum Vita

LORETO M. VALENZUELA

Education

2009   PhD in Biomedical Engineering, Rutgers, The State University of New Jersey.

2002   Master of Science in Engineering, Major in Chemical Engineering, Pontificia Universidad Católica de Chile.

2000   Industrial Engineer, Major in Chemical Engineering, Pontificia Universidad Católica de Chile.

Experience

2002 – 2004   Instructor at Chemical and Bioprocess Engineering Department, Pontificia Universidad Católica de Chile.

Publications

2009   Valenzuela LM, Michniak B, Kohn J. Improving the reproducibility of water uptake studies of biomedical polymers (Submitted).